THE EFFECTS AND APPLICATIONS OF ERBIUM DOPED FIBER FABRY-PEROT INTERFEROMETERS

A Thesis

by

JUSTIN KEITH TAYLOR

Submitted to the Office of Graduate Studies of
Texas A&M University
in partial fulfillment of the requirements for the degree of

MASTER OF SCIENCE

May 2009

Major Subject: Electrical Engineering

THE EFFECTS AND APPLICATIONS OF ERBIUM DOPED FIBER FABRY-PEROT INTERFEROMETERS

A Thesis

by

JUSTIN KEITH TAYLOR

Submitted to the Office of Graduate Studies of
Texas A&M University
in partial fulfillment of the requirements for the degree of

MASTER OF SCIENCE

Approved by:

Chair of Committee,	Christi Madsen
Committee Members,	Robert Nevels
	Ohannes Eknoyan
	Edward Fry
Head of Department,	Costas Georghiades

May 2009

Major Subject: Electrical Engineering

ABSTRACT

The Effects and Applications of Erbium Doped Fiber Fabry-Perot Interferometers.

(May 2009)

Justin Keith Taylor, B.S., Texas A&M University

Chair of Advisory Committee: Dr. Christi Madsen

Fiber Fabry-Perot Interferometers (FFPI) are optical sensors which can be used to measure changes in stress or temperature, but efforts continue to improve them. Calculations show that the response can be dramatically altered with a gain inducing medium in the cavity.

In order to induce gain, a highly doped Erbium (Er) fiber is incorporated in the FFPI. A pump wavelength of 1480 nm is used with a wavelength near 1550 nm. The pump must be at a significantly higher power level than the signal for gain.

In order to correctly interpret responses, it is necessary to characterize the response of the measurement equipment. This includes everything from the laser and photodetector to system losses and the titanium oxide coated fibers.

Fabrication of FFPIs involves fusing titanium oxide coated fibers to standard single mode fibers. Directly fusing an Er - doped fiber to a titanium oxide coated fibers was not possible because of incompatible splice conditions required in each case. Instead, an intermediate standard single mode fiber was spliced between them. This lengthened the cavity.

Experimental results from the Er - doped Fiber Fabry-Perot Interferometer verified the hypothesis that improvements are obtainable. Overall, the measurements showed a 1.3 dB improvement in the maximum-to-minimum Insertion Loss Ratio.

To My Parents

ACKNOWLEDGEMENTS

I would like to thank my committee chair, Dr. Madsen, and my committee members, Dr. Eknoyan, Dr. Nevels, and Dr. Fry, for their guidance and support throughout the course of this research. Thanks also go to my friends and colleagues and the department faculty and staff for making my time at Texas A&M University a great experience. Finally, thanks to my mother and father for their encouragement.

NOMENCLATURE

FFPI	Fiber Fabry Perot Interferometer
EDFA	Erbium Doped Fiber Amplifier
EDFFPI	Erbium Doped Fiber Fabry Perot Interferometer
r_1	Electric Field Reflectivity of First Mirror of a FFPI
r_2	Electric Field Reflectivity of Second Mirror of a FFPI
R	Intensity Reflectance
$r = \frac{E_r}{E_o}$	Ratio of Reflected to Original Electric Field
$R = \frac{I_r}{I_o}$	Ratio of Reflected to Original Intensity
FSR	Free Spectral Range
$\mathcal{F}$	Finesse
FWHM	Full Width Half Max
g	Electric Field Single Pass Linear Gain
V_a	Anode Voltage
V_{in}	Input Voltage to the Laser Driver
V_d	Display or Monitor Voltage (in Volts unless otherwise specified)
V_{PD}	Photodetector Output Voltage
dB	Decibel
dBm	Decibel Milliwatts
P_{dBm}	Power in Decibel Milliwatts

P_{mW}	Power in Milliwatts
NF	Noise Figure
WDM	Wave Division Multiplexer
IL	Insertion Loss
SMF	Single Mode Fiber
5E-2	Shorthand for Scientific Notation for $5*10^{-2}$

TABLE OF CONTENTS

CHAPTER Page

LIST OF FIGURES

FIGURE Page

FIGURE Page

FIGURE Page

FIGURE Page

CHAPTER I

INTRODUCTION: THEORY AND BACKGROUND INFORMATION

Optical technology has become the new standard in the communication industry. Optics offers many advantages such as higher bandwidths over traditional electronics, but due to a lack of optical sensor technology, bandwidth and other advantages are lost converting to and from electronic sensors [1]. One promising technology is the Fiber Fabry- Perot Interferometer, or FFPI, which can detect changes in temperature or strain on the fiber. It has the potential for many applications; however, in its current form, it is limited by low signal-to-noise ratio, or in optical terms Finesse, and low reflected intensity. It is hoped that inserting an optical amplifier, Erbium doped fiber, within the sensor can raise the finesse and reflection intensity. Additionally, by changing the roundtrip loss in the FFPI by controlling the pump power, it is possible to tune the filter response remotely, without having to locally change the cavity (e.g. through heat or strain). This provides modulation opportunities which were not previously available[2].

The FFPI is based on the Fabry-Perot Interferometer invented by Charles Fabry and Alfred Perot in 1889 [3]. Figure 1 displays a fiber based Fabry-Perot Interferometer, which consists of two mirrors spaced a certain distance apart with a light source.

This thesis follows the style of *Journal of Lightwave Technology*.

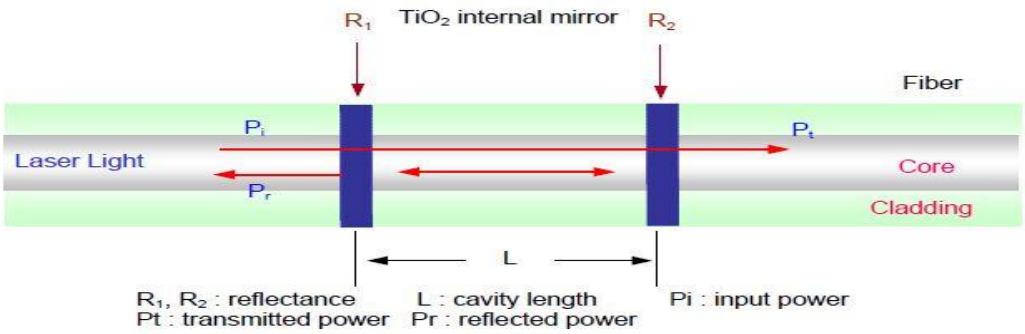

Fig. 1 Fiber Fabry-Perot Interferometer

The reflected light intensity from a FFPI is governed by the equation:

$$\frac{I_r}{I_o} = \frac{2r^2\,(1-cos\;\theta)}{1-2\,r^2\;cos\;\theta + r^4} \tag{1}$$

Where r is the electric field reflectivity and θ is the electric field phase difference accrued in successive round trips:

$$\theta = 2\pi f * \frac{2nL}{c} \tag{2}$$

From this equation it is possible to graph the reflection as a function of frequency.

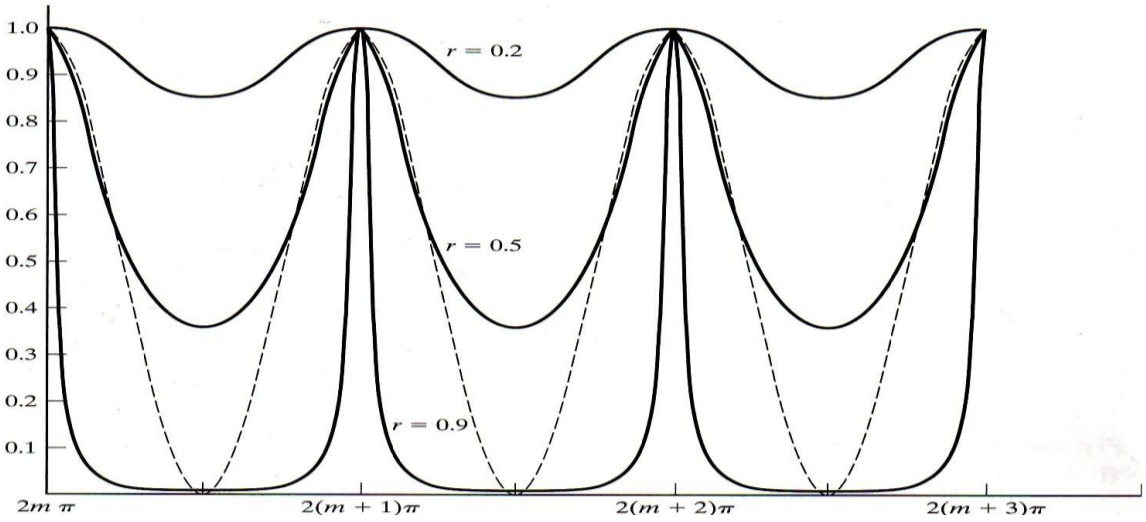

Fig. 2 Transmission Response of Fabry-Perot Interferometer

Figure 2 shows that the response is periodic as a function of frequency [4]. This is referred to as the free spectral range (FSR), where $FSR = \frac{c}{2nL}$. Additionally, the reflection (or conversely transmission) can be measured by the Finesse, which is $\mathcal{F} = \frac{\pi\, r}{1-r^2}$. The peak width is measured by a coefficient known as the Full Width Half Maximum, which is a ratio of $\frac{FSR}{\mathcal{F}}$.

However, all of this is based on a few basic assumptions. First, the reflection of both mirrors needs to be identical. Additionally, the medium must be neutral, having neither gain nor loss. Factoring in these complications alters the calculations:

$$\frac{E_r}{E_o} = r_1 + t_1 g r_2 g t_1 e^{j\theta} + t_1 g r_2 g r_1 g r_2 g t_1 e^{j2\theta} + t_1 g r_2 g r_1 g r_2 g r_1 g r_2 g t_1 e^{j3\theta} + \cdots \quad (3)$$

$$\frac{E_r}{E_o} = r_1 + t_1 g r_2 g t_1 e^{j\theta} \times \sum_{n=0}^{\infty} \left(g^2 r_1 r_2 e^{j\theta}\right)^n \quad (4)$$

Where g is the electric field single pass linear gain. Note that using the properties of infinite sums, $\sum_{n=0}^{\infty}(g^2 r_1 r_2 e^{j\theta})^n = \frac{1}{1-g^2 r_1 r_2 e^{j\theta}}$

$$\frac{E_r}{E_o} = r_1 + \frac{t_1 g r_2 g t_1 e^{j\theta}}{1-g^2 r_1 r_2 e^{j\theta}} \quad (5)$$

$$\frac{E_r}{E_o} = \frac{r_1 - r_1 g^2 r_2 r_1 e^{j\theta} + t_1 g r_2 g t_1 e^{j\theta}}{1-g^2 r_1 r_2 e^{j\theta}} \quad (6)$$

$$\frac{E_r}{E_o} = \frac{r_1 - r_2 g^2 e^{j\theta} (r_1^2 + 1 - r_1^2)}{1-g^2 r_1 r_2 e^{j\theta}} \quad (7)$$

$$\frac{E_r}{E_o} = \frac{r_1 - r_2 g^2 e^{j\theta}}{1-g^2 r_1 r_2 e^{j\theta}} \quad (8)$$

The intensity output is

$$\frac{I_r}{I_o} = \frac{r_1^2 - r_2^2 g^4 - 2\, r_1 r_2 g^2 \cos\theta}{1-2g^2 r_1 r_2 \cos\theta + r_1^2 r_2^2 g^4} \quad (9)$$

Similarly, the transmission intensity can be derived as

$$\frac{I_t}{I_o} = \frac{g^2 (1-r_1^2)(1-r_2^2)}{1-2g^2 r_1 r_2 \cos\theta + r_1^2 r_2^2 g^4} \quad (10)$$

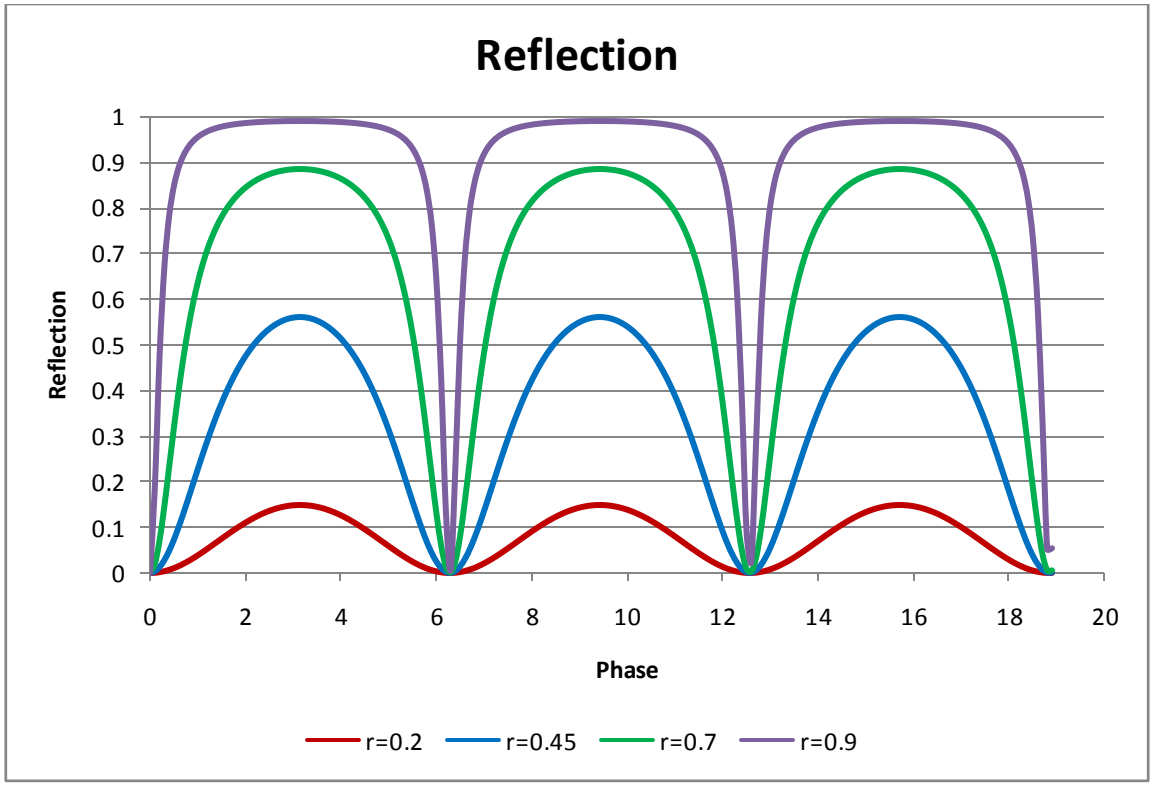

Fig. 3 Reflection Response of FFPI

Figure 3 shows how the reflection response of a FFPI varies with reflectivity values. Note how the response changes from a sinusoidal response for low reflections to a near squarewave for high reflection values [5]. TiO_2, the material used as mirrors in the FFPIs described in this paper, has an intensity reflectance ($R=r^2$) of 0.2, or an electric field reflectivity (r) of 0.45 [6].

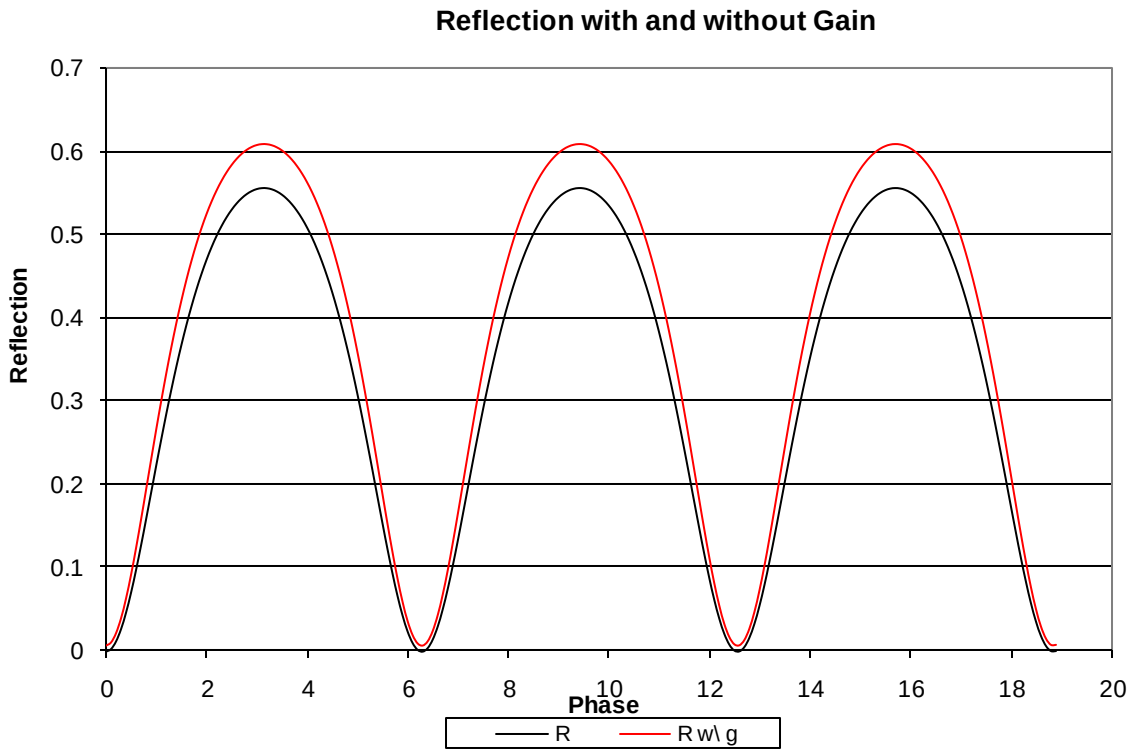

Fig. 4 Reflection with and without Gain

Figure 4 demonstrates the ability to increase maximum reflection while keeping the minimum essentially unchanged. This simulation was run with the nominal scenario of $r_1^2=r_2^2=0.2$ and g=1.04, where gain was estimated for a 1 cm length of Er-doped fiber. By inspection, the minima and maxima of the reflection equation occurs when $\theta=2\pi n$ and $2\pi n + \pi$, which makes $\cos\theta = 1$ and -1 respectively. Specifically, at $\theta=2\pi n$ the maximum reflection becomes:

$$Max\ \frac{I_r}{I_o} = \frac{(r_1+r_2g^2)^2}{(1+r_1r_2g^2)^2} \quad (11)$$

Similarly, at $\theta=2\pi n+\pi$, the minimum reflection becomes:

$$Min\ \frac{I_r}{I_o} = \frac{(r_1-r_2g^2)^2}{(1-r_1r_2g^2)^2} \quad (12)$$

Numerical analysis reveals that, in the limit as gain approaches infinity both the minimum and maximum reflections simplify to $\frac{1}{r_1r_2}$. Of course, infinite gain is not physically possible. Likewise both the minimum and maximum transmission approach zero [7]. However, these occur in regions beyond the amount of gain expected with an Erbium doped cavity [8]. Therefore, it is important to simulate the effects of gain within the expected gain regions. This was done by plotting Equations 11 and 12 versus nominal gain. Figure 5 displays the results. For calculation purposes, r_1= 0.4898 and r_2=0.4228, the measured reflection on a glass-TiO_2 interface.

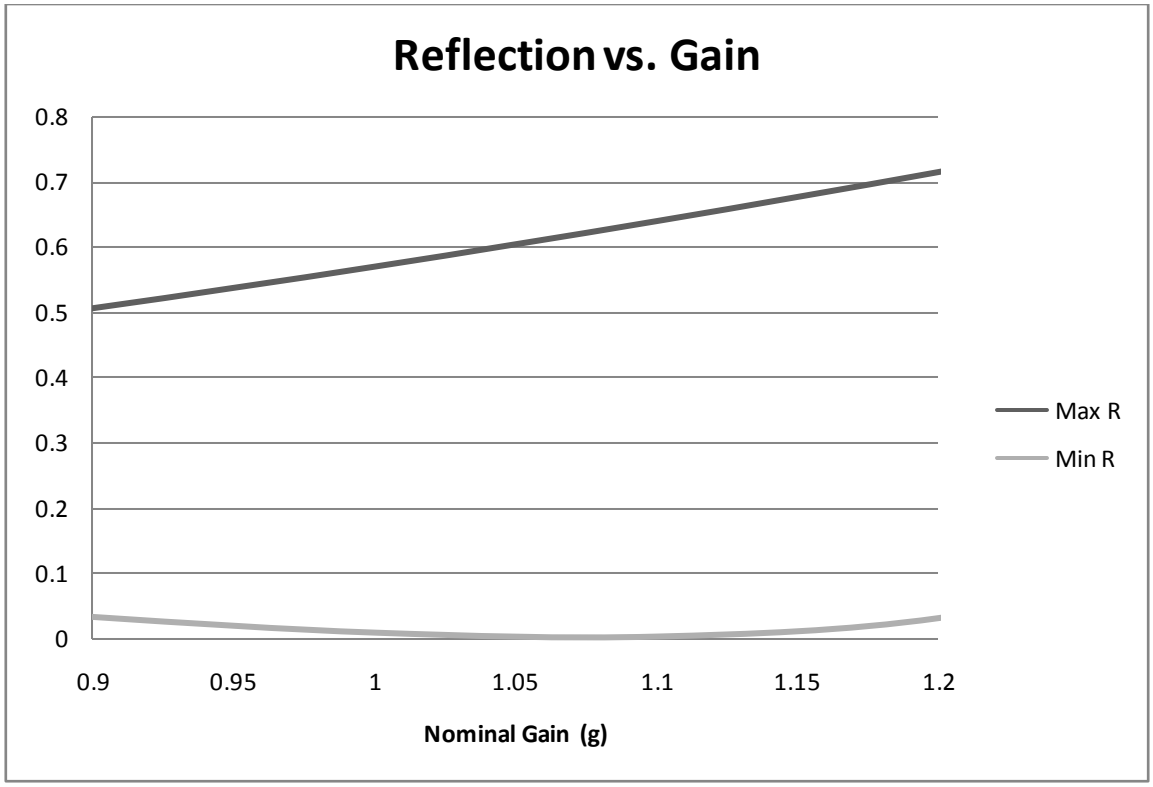

Fig. 5 Simulated Gain Response of an EDFFPI

Figure 5 shows the minimum and maximum reflection with respect to g from 0.9 to 1.2. Within this range, maximum reflection value increases with gain, however the minimum reflection reaches a minimum near g=1.08 but begins increasing afterwards. This would decrease the ratio of maximum to minimum reflections. It is noteworthy that this is graphed versus gain in linear units, not a logarithmic or decibel scale as gain is typically measured.

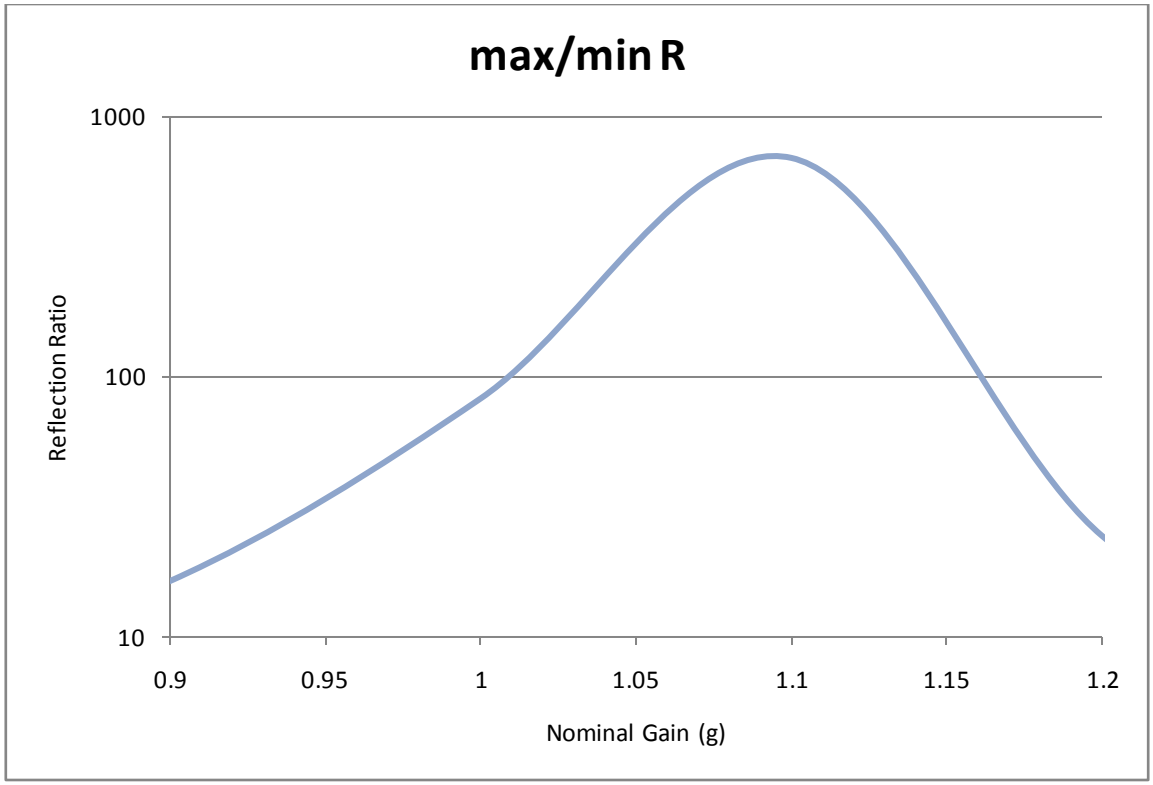

Fig. 6 Reflection Ratio of Simulated Gain Response

Figure 6 displays a ratio of maximum to minimum reflectance on a logarithmic scale versus gain. It is clearly observed on the reflection chart that it peaks near g=1.08. At this point, the gain compensates for losses and the lower reflectivity of r_2, thus balancing the FFPI mirrors and maximizing the reflection response.

CHAPTER II

DEFINING GAIN

The scope of this chapter is to model an EDFA based on the Thorlabs catalog description for 80 dB/m pump absorption, to determine the pump parameters, gain and noise figure versus input signal power, and to simulate the wavelength dependent gain. From this the goals were derived to simulate gain as function of both power and wavelength by performing experiments on a variety of signal and power levels [9]. Ultimately, the objective is to derive relationships to predict noise as gain as a function of pump and signal power and wavelength.

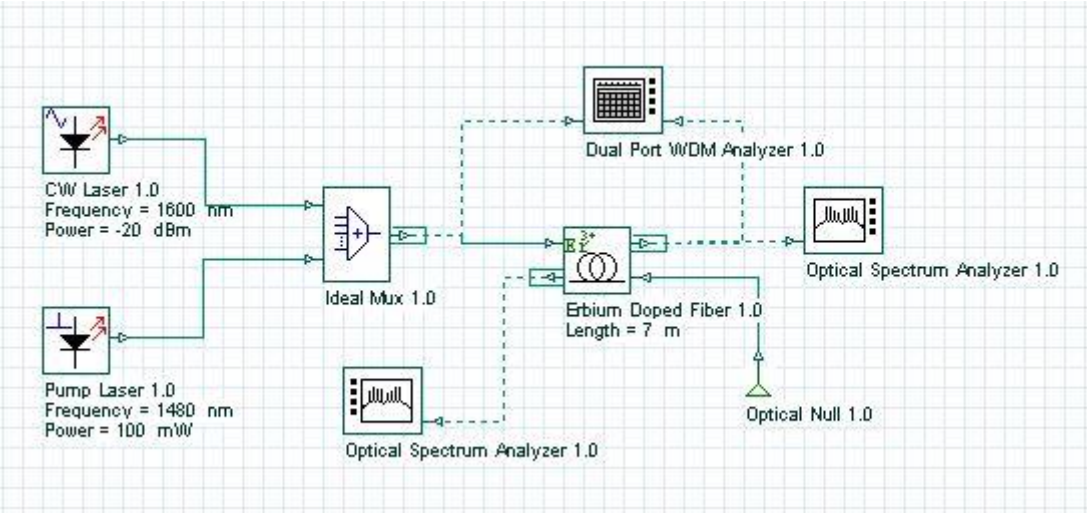

Fig. 7 EDFA Characterization Setup

The setup, seen in Figure 7, was fairly straightforward. Two lasers, a signal and a pump, were multiplexed together and sent through an erbium-doped fiber to a null to prevent any reflection. The signal and pump were measured on both sides to calculate the gain (or loss) and noise figure. Measurements were taken everywhere within the range of 1420 to 1620 nm and -60 to 30 dBm [9].

Absorption

The first objective is to compare the characteristics of the built-in Optisystem EDFA with data collected from Thorlabs, which included the wavelength dependant emission and absorption spectrum, Figure 8 [10]. Although the core size of the EDFA is the same as that of a single mode fiber, the refractive index is 1.45150 as opposed to 1.45000 for SMF, thus slightly extending the optical path length of the EDFA [11]. The emissions of the Optisystem EDFA is measured by pumping at high power but turning the signal to very low power and sweeping gain measurements. The absorption is measured by turning both the pump and signal down low and taking a sweeping measurement of the loss, which corresponds to absorption [12]. The Absorption test is performed at 1480 and 980 nm. The results are the same, so the scope is simplified to omit 980 from simulations. Plotting them together gives a graph that resembles the Absorption and Emission data received from Thorlabs. The graphs of Figure 9 confirms that Optisystem EDFA is an adequate model of the Thorlabs fiber. The difference between the absorption and emission is plotted to calculate the ideal placement of pump and signal wavelengths.

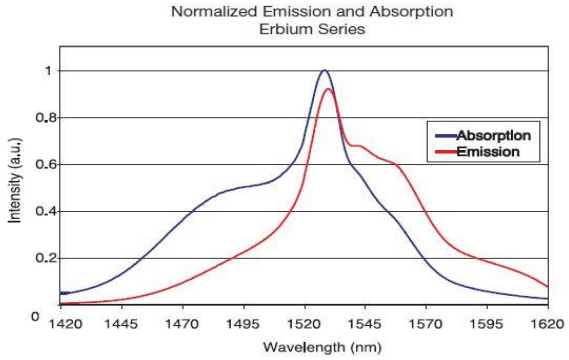

Fig. 8 Thorlabs Characterization

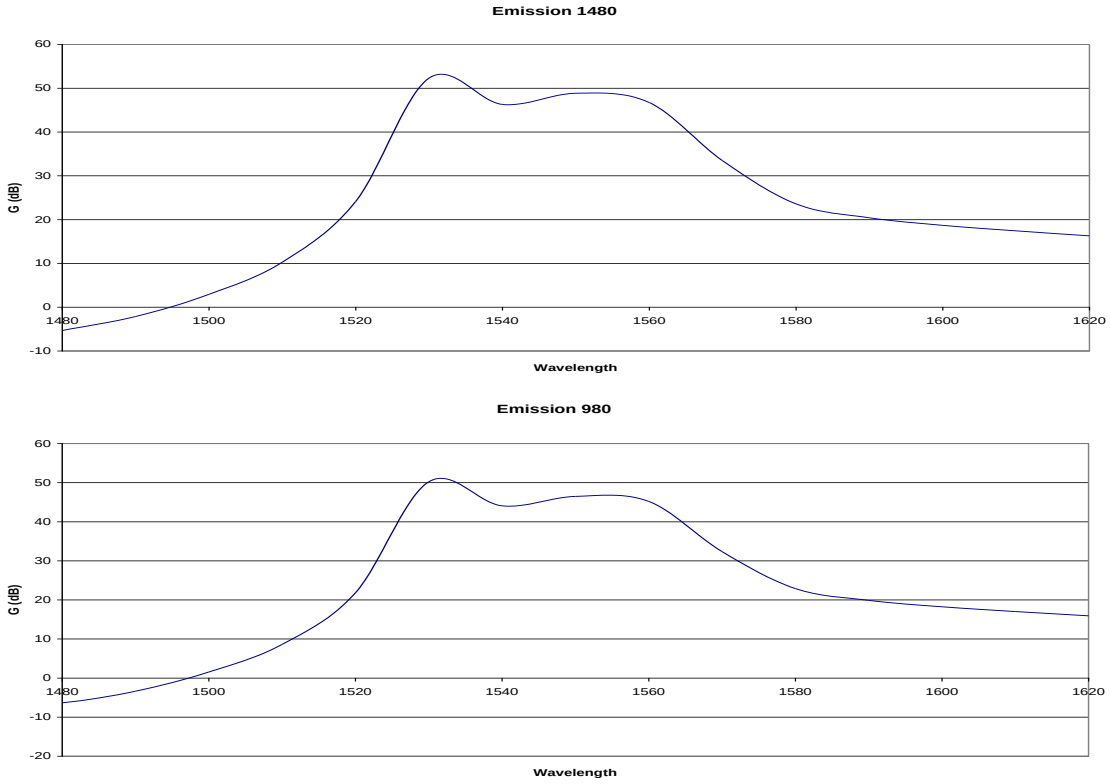

Fig. 9 Simulated Emission, Absorption, Gain and Loss of EDFA Pumped at 1480 and 980 nm

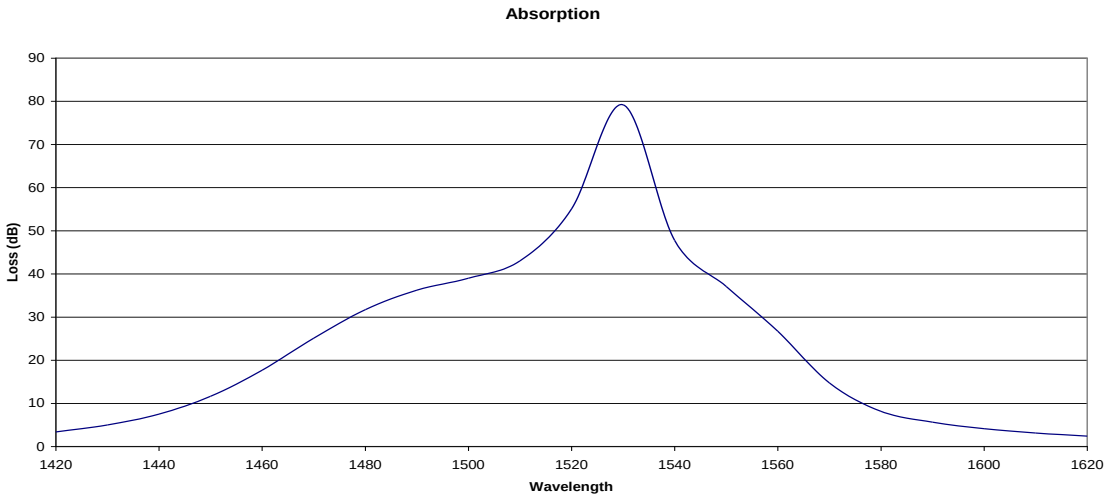

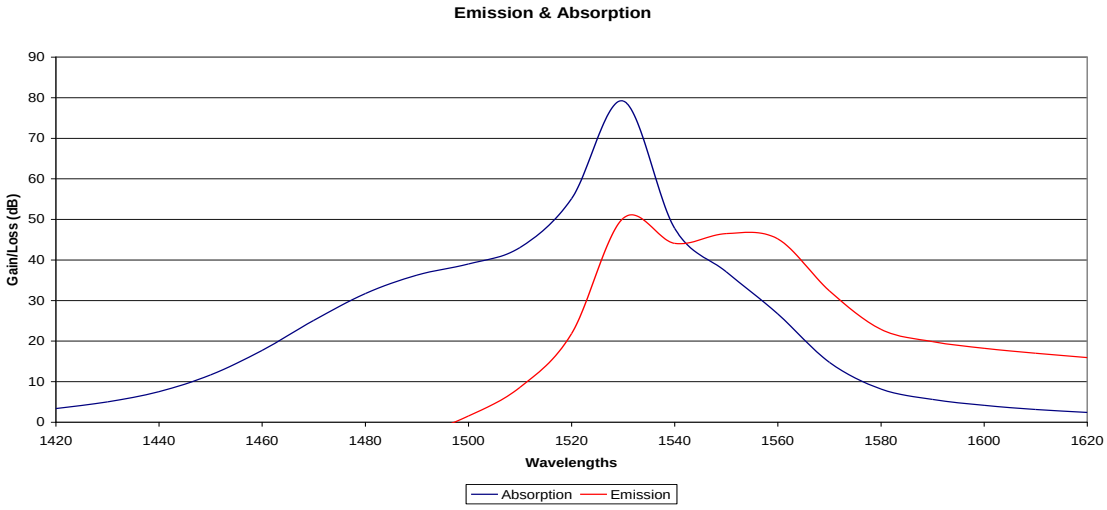

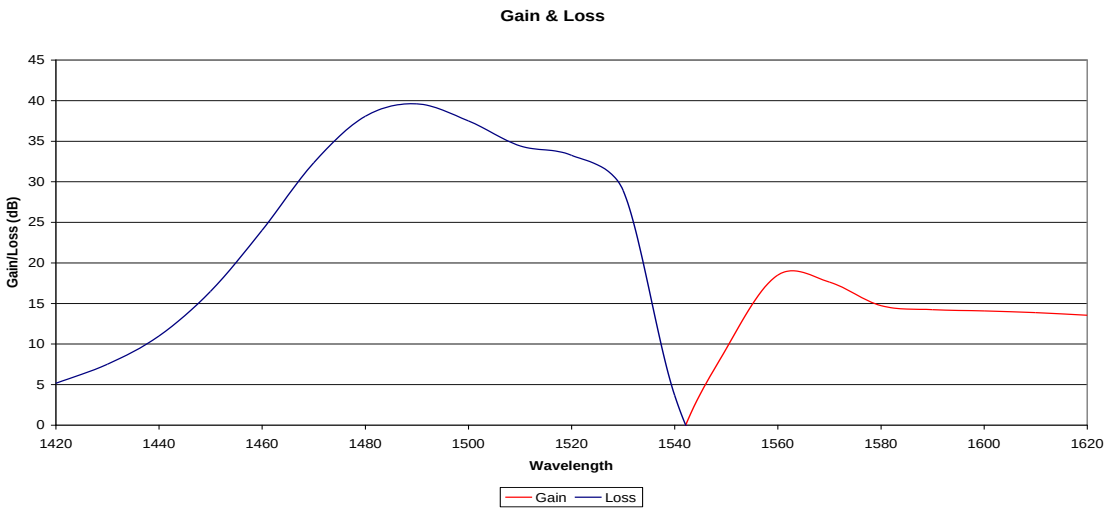

Fig. 9 continued

Power

Next, the power dependant gain is investigated. For these the pump is set at 1480nm and signal at 1550nm. In Figure 10, by holding the signal power constant at -60 dBm and sweeping the pump power level, it is determined that the signal gain is negative until around 17 dBm. In Figure 11, by raising the signal power to 20 dBm and repeating the simulation, it demonstrates that signal power level raises the gain level, but it is still negative until the pump power level is raised. Here the blue line "Signal Gain" demonstrates how much gain the signal receives. Similarly, the orange line "Pump Gain" is the absorption of the pump power.

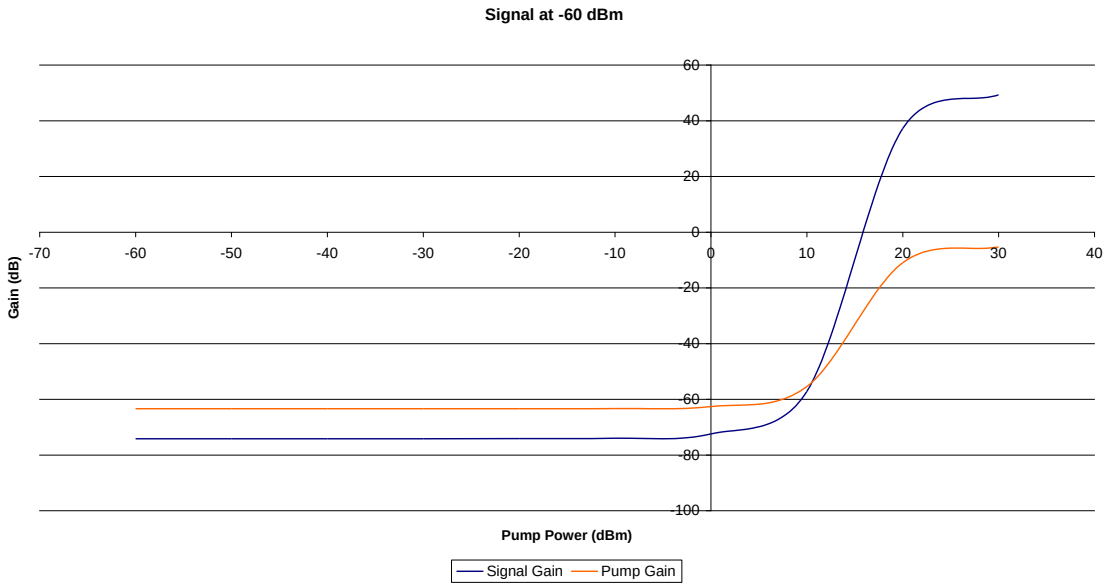

Fig. 10 Simulated Gain for Signal at -60 dBm with a Swept Pump Power

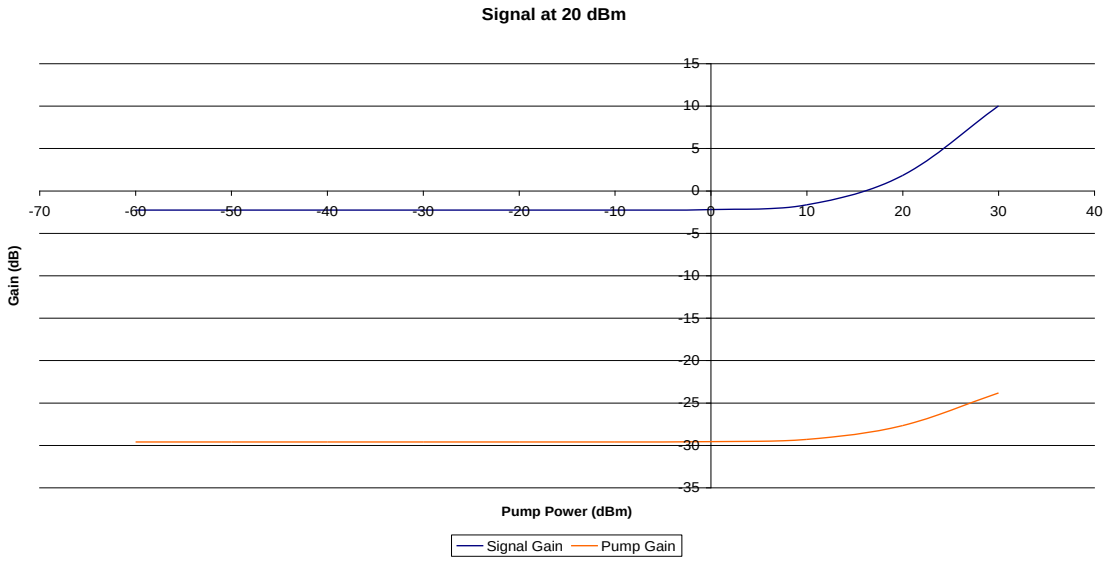

Fig. 11 Simulated Gain for Signal at 20 dBm with a Swept Pump Power

The pump power is raised to 30 dBm and sweeps the signal, then repeats with a low pump power level at -60 dBm. Figure 12 with the pump at 30 dBm shows the gain rolling off as the signal power increases to reach a saturation level. Figure 13 shows that it is possible to induce gain by increasing the signal power.

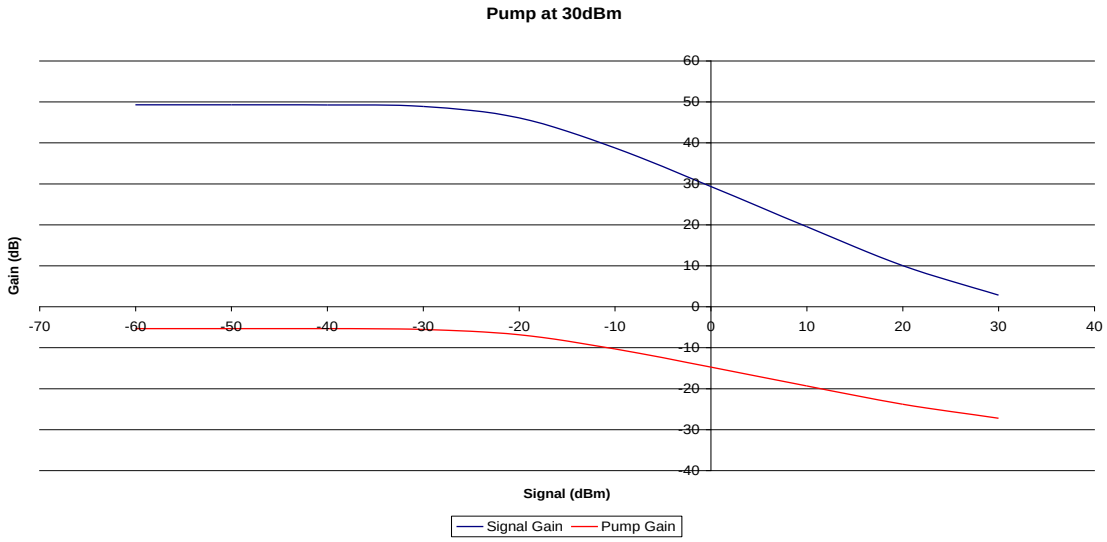

Fig. 12 Simulated Gain for Pump at 30 dBm with a Swept Signal Power

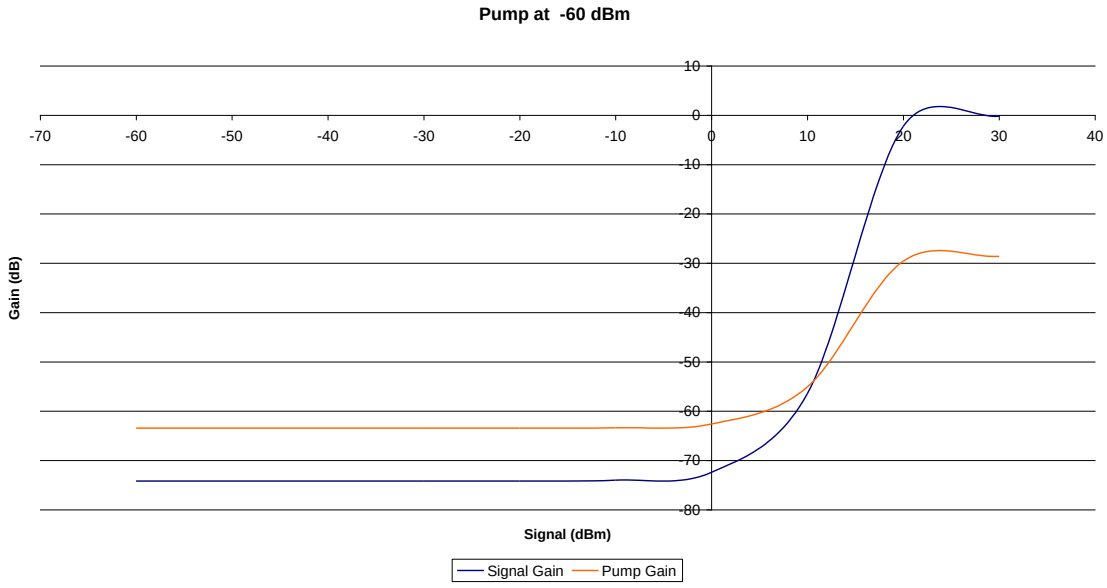

Fig. 13 Simulated Gain for Pump at -60 dBm with a Swept Signal Power

Additionally, both the pump and signal are powered at -100 dBm and sweep the wavelengths, to obtain the following loss spectrum. Similar results are derived at any pump power level up to 10 dBm, thus showing that the EDFA starts inducing positive gain around 20 dBm (at approximately 17 dBm).

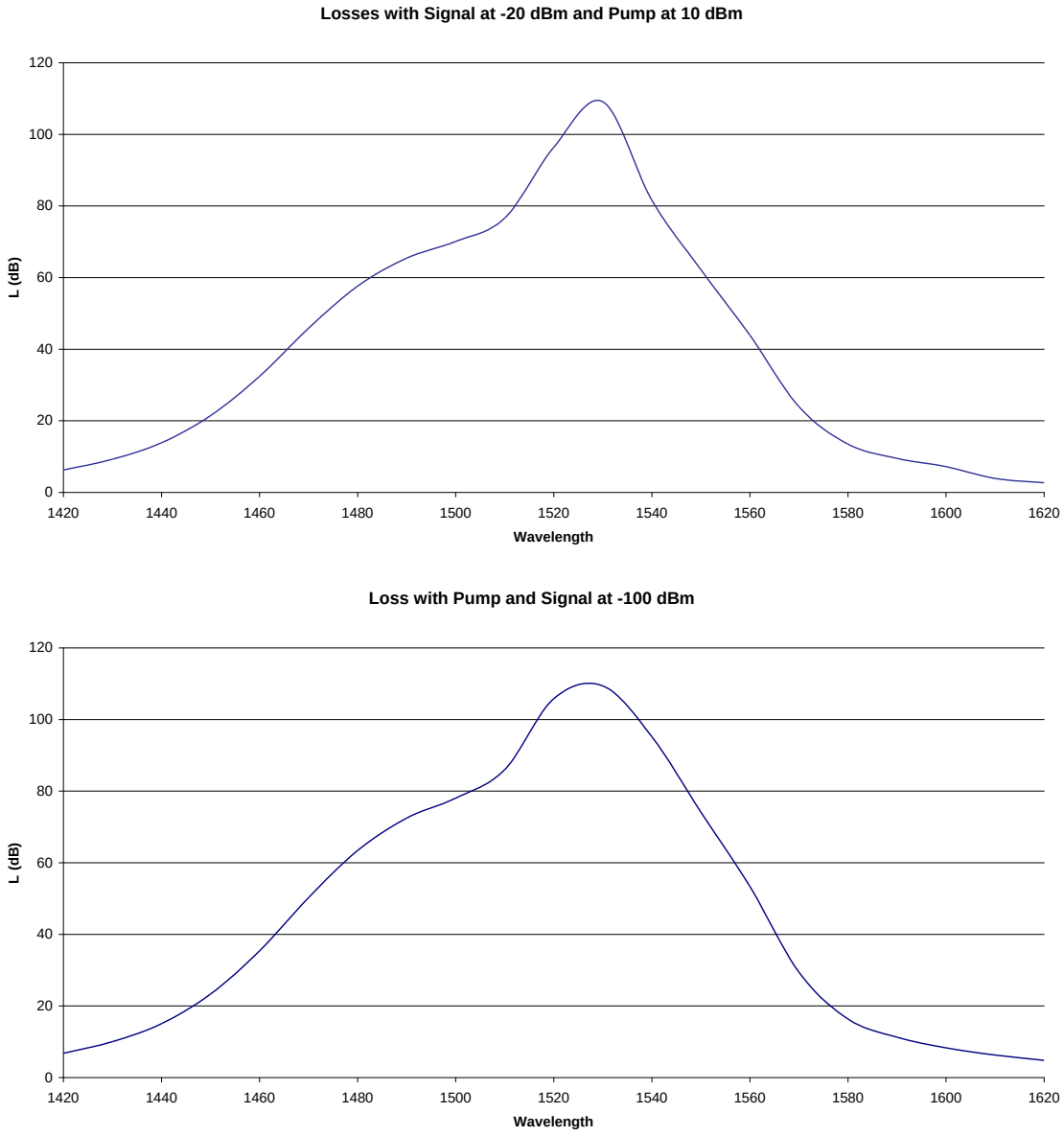

Fig. 14 Simulated Losses at Low Power

By sweeping the signal and pumps independently (every combination of 1420-1620 nm pump and signal at three different power levels), Figure 14 shows that gain peak depends on pump wavelength near 30 dBm, bandwidth from 1530 to 1580 nm. The absorption has a wide bandwidth from 1430 to 1530 nm but a peak of -80 dB at 1480. As is to be expected, gain only occurs when pumped at lower wavelength or higher frequency. However, the higher the pump wavelength, the lower the peak gain and the narrower the gain bandwidth.

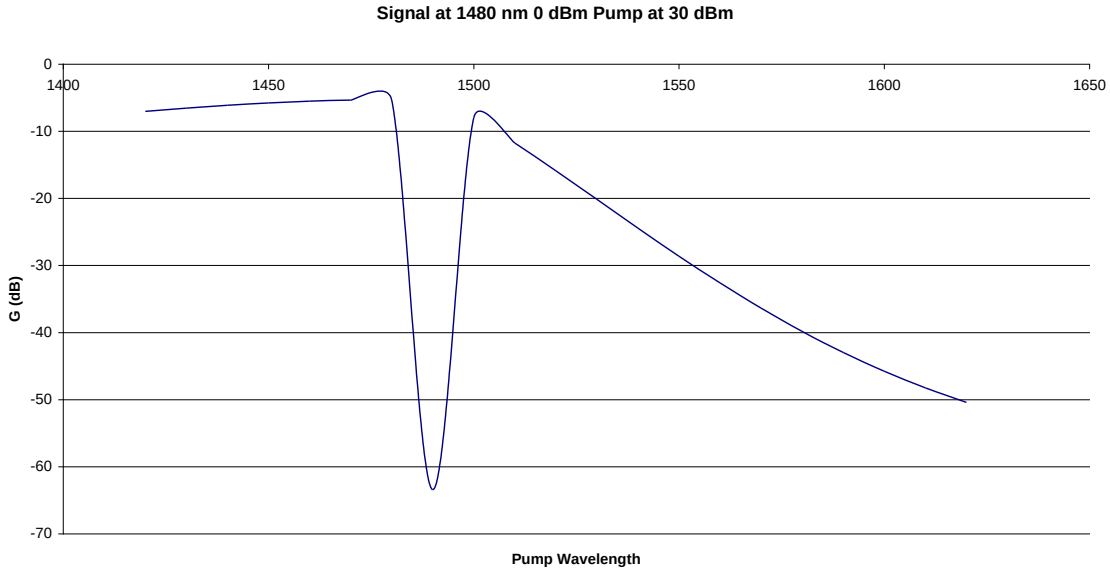

Fig. 15 Simulated Losses for Signal at 1480 nm with a Swept Pump Wavelength

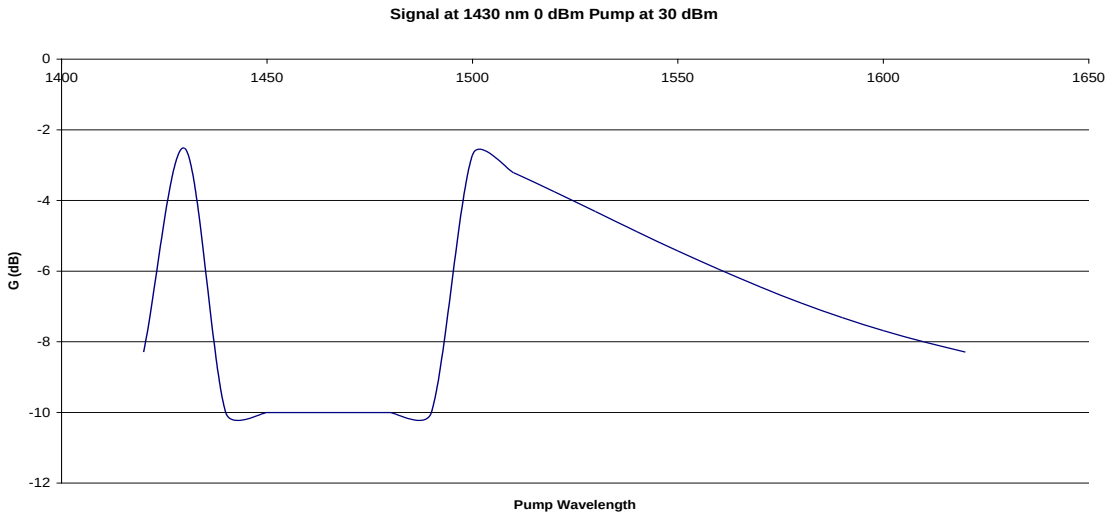

Fig. 16 Simulated Losses for Signal at 1430 nm with a Swept Pump Wavelength

Figure 15 shows peak absorption of -80 dB at 1480 nm. Figure 16 shows the wide absorption bandwidth.

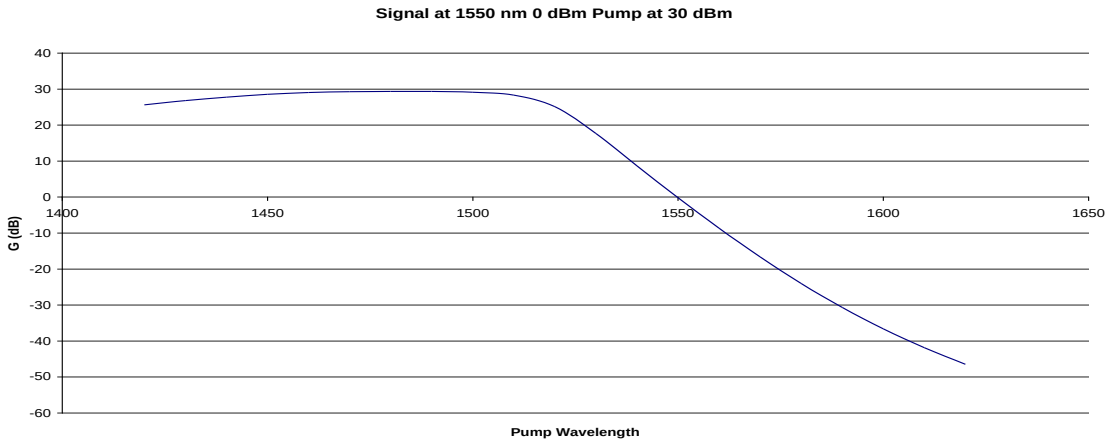

Fig. 17 Simulated Signal Gain at Swept Pump Wavelengths

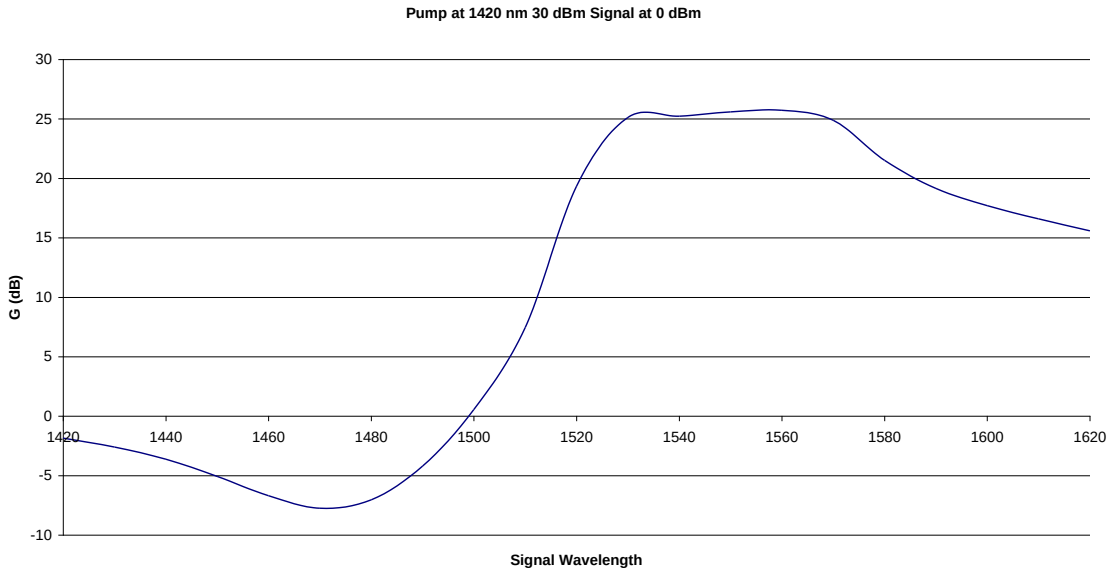

Fig. 18 Swept Signal Gain from a 1420 Pump

Figure 17 shows that signal gain occurs when pumped anywhere from 1420 to 1530 nm. Figure 18 shows signal gain due to pumping at 1420 nm.

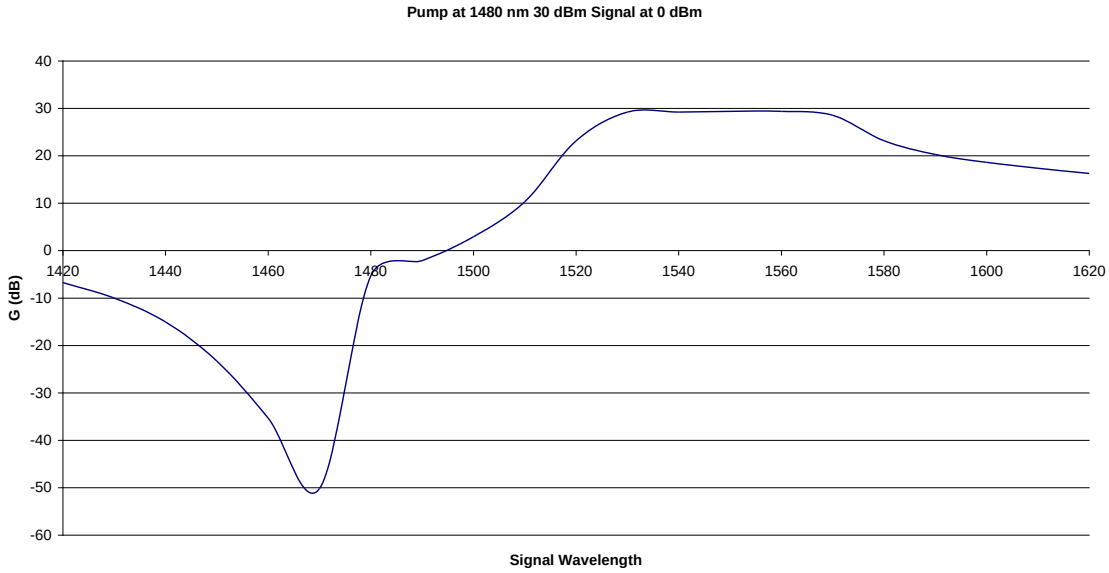

Fig. 19 Simulated Signal Gain for Pump at 1480 nm at Swept Wavelengths

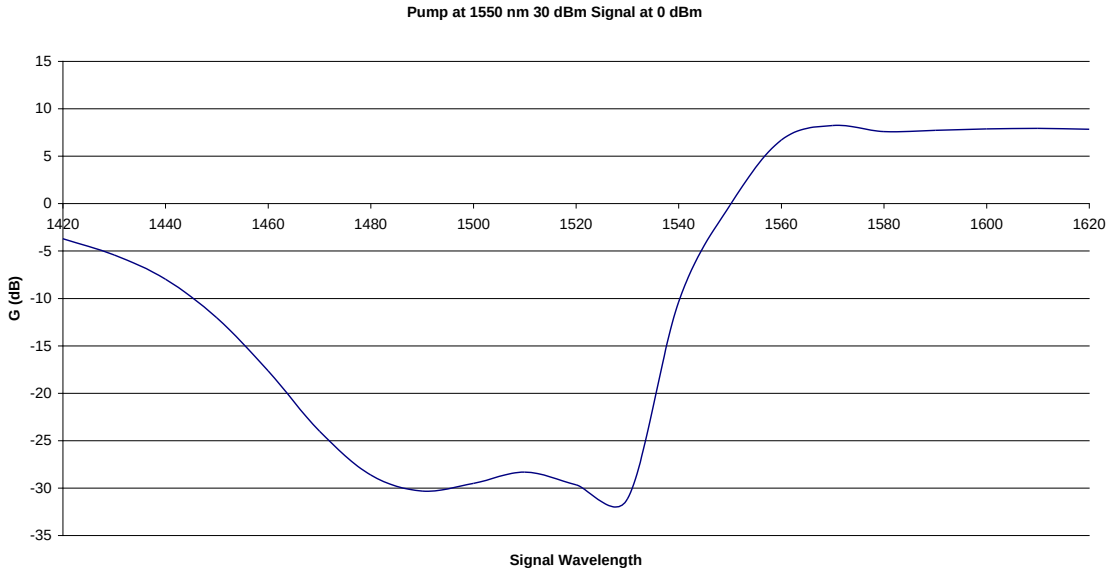

Fig. 20 Simulated Signal Gain for Pump at 1550 nm at Swept Wavelengths

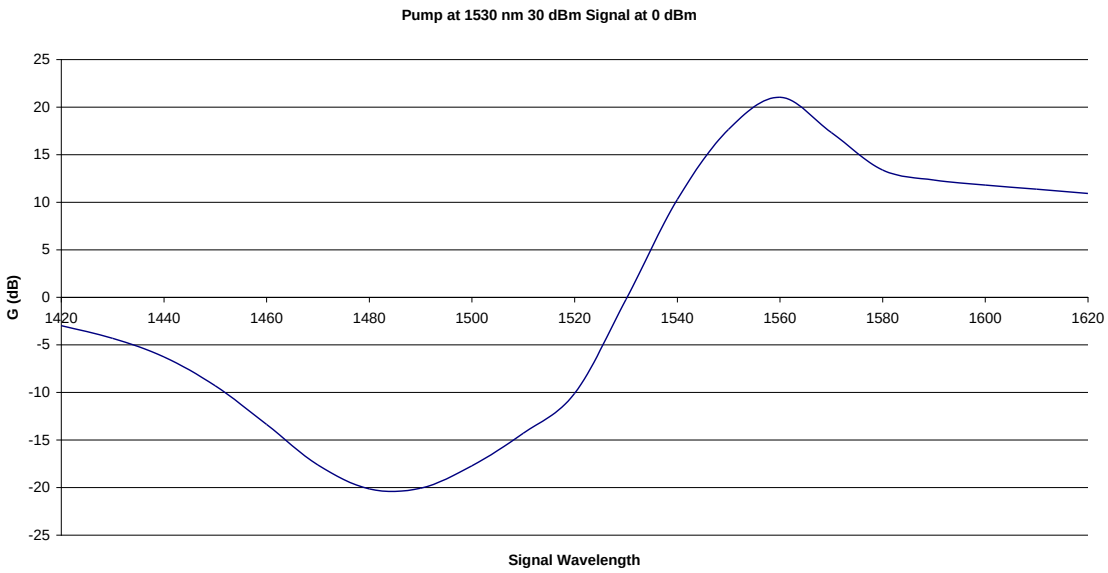

Fig. 21 Simulated Signal Gain for Pump at 1530 nm at Swept Wavelengths

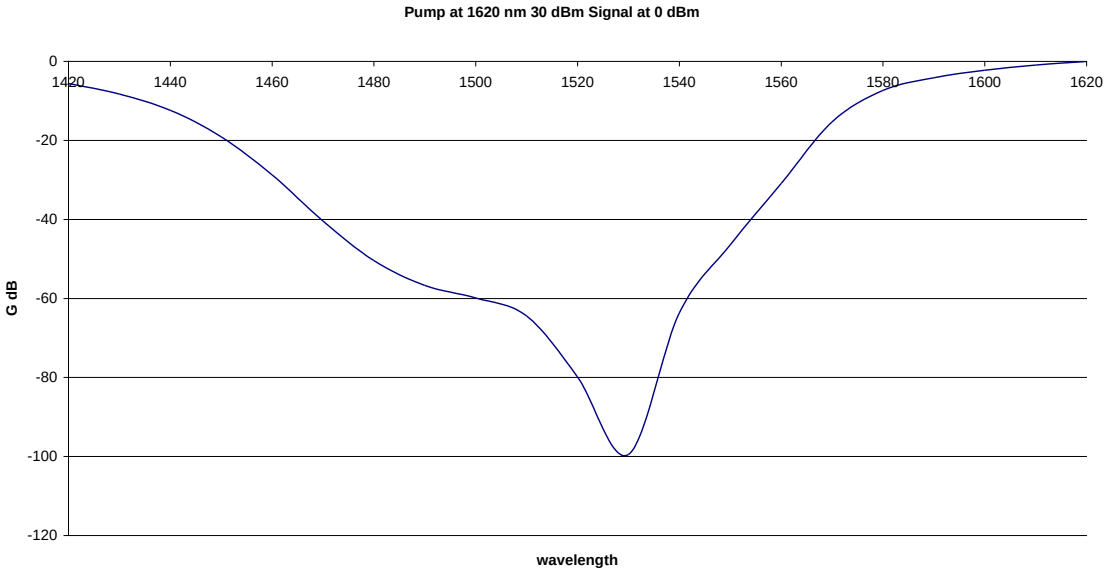

Fig. 22 Simulated Signal Gain for Pump at 1620 nm at Swept Wavelengths

Figure 19 shows high peak and wide bandwidth gain from pumping at 1480 nm. Figure 20 shows that it is possible to pump at a high wavelength, but minimal gain is induced. Figure 21 shows that 1530 nm is the highest pump wavelength that will induce gain. Figure 22 is pumped at 1620 nm and shows that gain cannot be induced at a lower wavelength.

Noise

The Noise Figure is governed by equation seen in Figure 23:

$$Noise\ Figure \overset{\Delta}{=} \frac{N_{EDFA}}{hvGB_W} + \frac{1}{G} = \frac{N_{out} - N_{in}G}{hvGB_W} + \frac{1}{G}$$

Fig. 23 Noise Figure Equation

This equation, which describes Noise Figure response, was obtained from EDFA for SCM Transmission Systems. Figure 24 demonstrates that noise figure is essentially inversely proportional to gain when gain (or loss) becomes large [13].

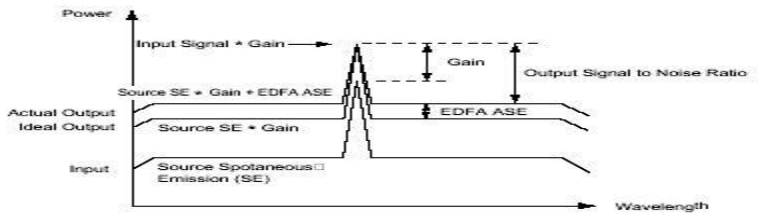

Fig. 24 Noise Figure Demonstration

For example, included below are some examples of how the noise figure grows as the signal is increased.

Figures 25, 26 and 27 are optical spectrum charts with the pump at 1480 nm 20 dBm and the signal at 1550 nm and -10 dBm. They are before and after, which demonstrate how the noise figure raises with gain through the EDFA.

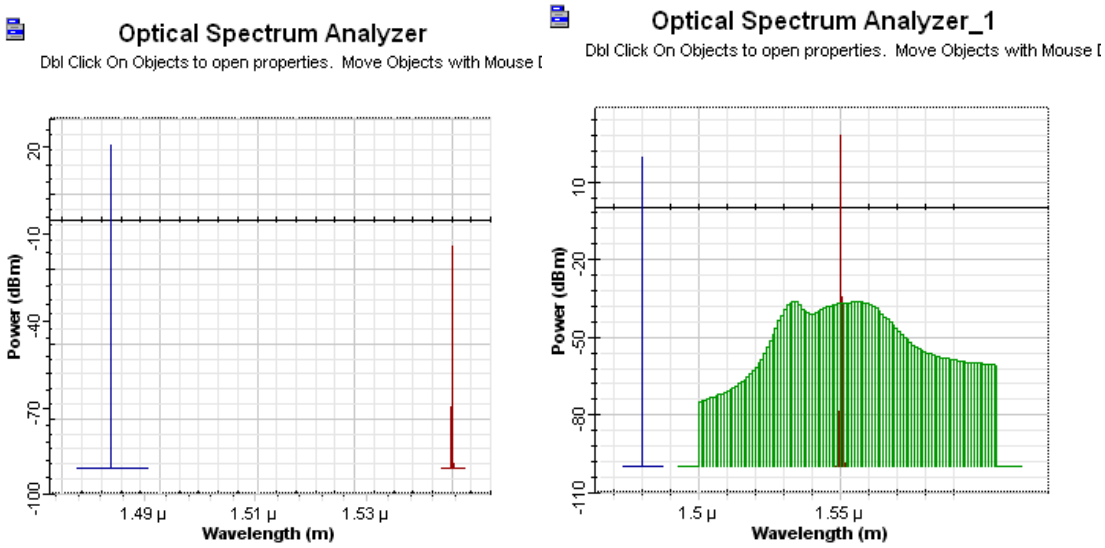

Fig. 25 Simulated Full Spectrum Before and After

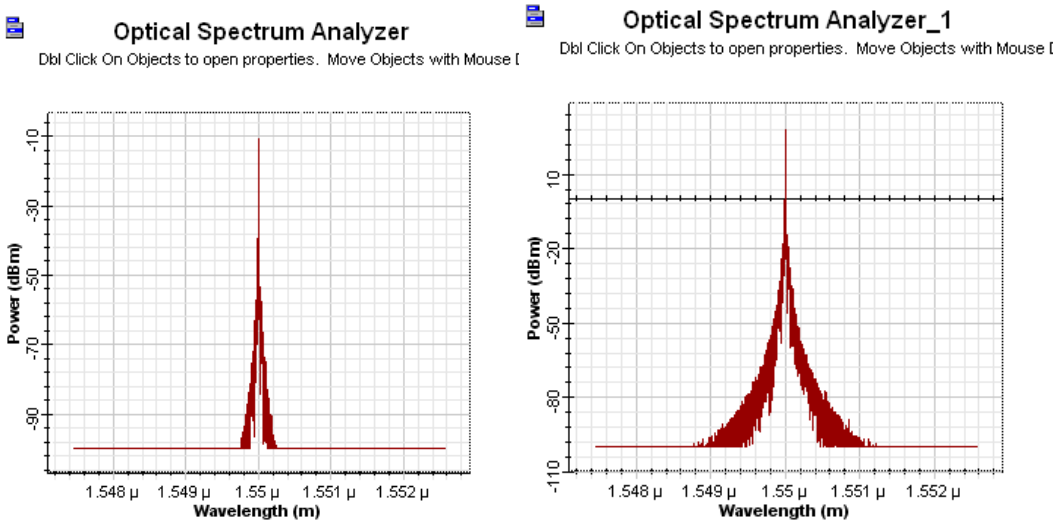

Fig. 26 Simulated Signal Before and After

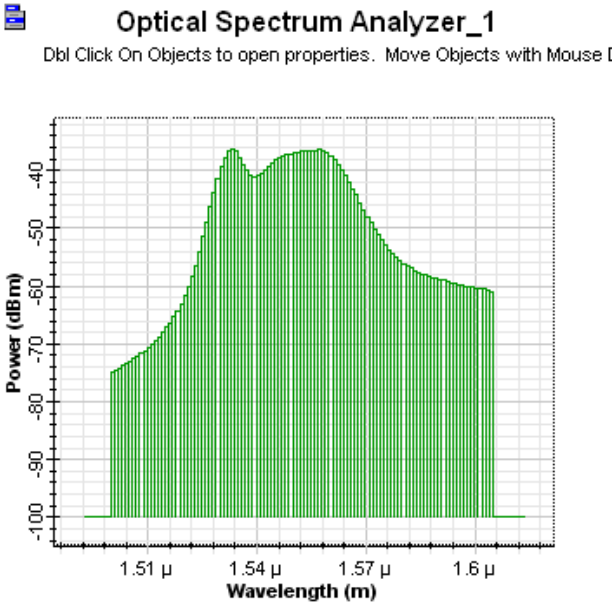

Fig. 27 Simulated Induced noise

With a loss or negative gain, the first term of the equation becomes insignificant, leaving the equation to be dominated by the second term, effectively an inverse of the gain. Figure 28 demonstrates this.

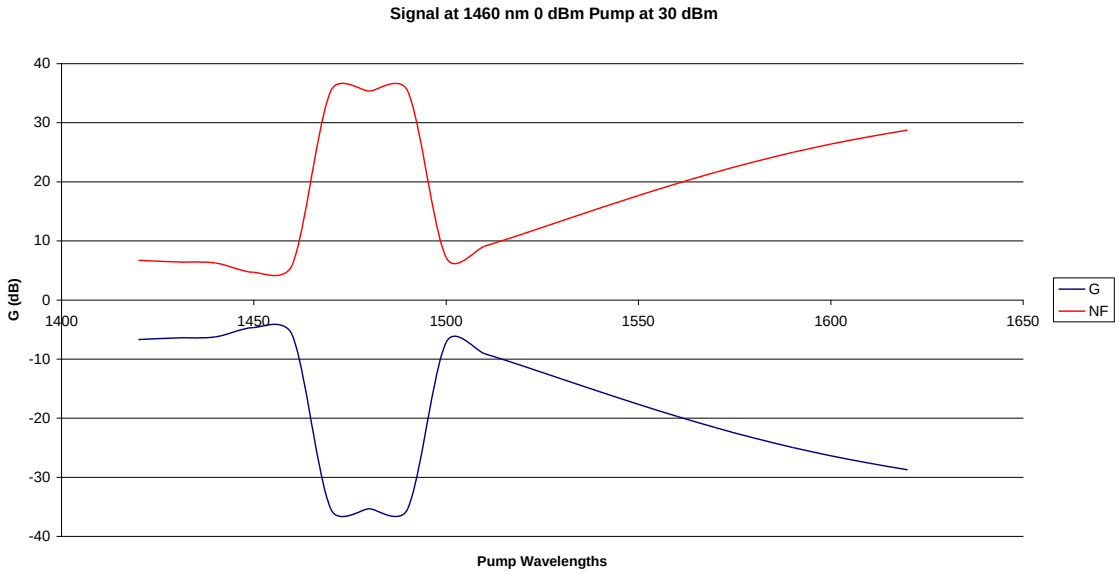

Fig. 28 Simulated Noise Figure for Signal Loss at Swept Pump Wavelengths

However, when the gain is non-negative, the noise figure is suppressed. It is possible to identify regions where the first term is significant by plotting the sum of the gain and noise figure. Figure 29 shows three regions: negative gain, rising gain and high gain.

In the negative gain the noise figure is the exact opposite. This demonstrates that the noise figure reflects negative gain. In the rising gain region, the noise figure actually

increases some, possibly due to simulated emissions from the erbium. In the high gain region, the noise figure is suppressed and stuck to within the 3-5 dB.

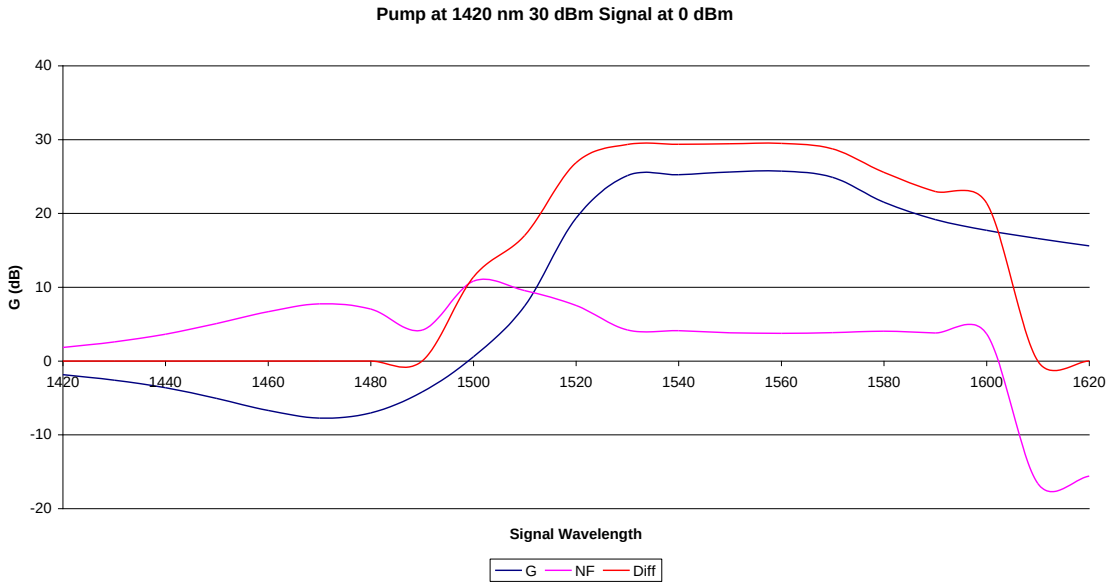

Fig. 29 Simulated Noise Figure for Signal Losses when Pumped at 1420 with Swept Signal Wavelengths

Figure 30 below demonstrates how the noise figure rises as gain decreases. The red line is the sum of Noise Figure and Gain. It demonstrates high noise level with significant loss, but low noise with gain.

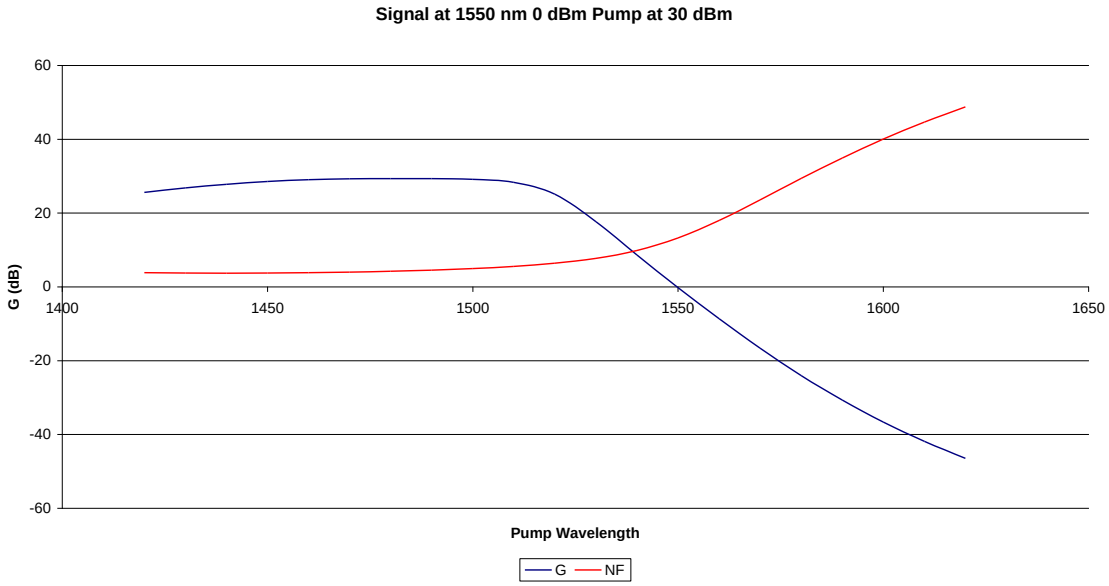

Fig. 30 Simulated Noise Figure for Signal Gain at Swept Pump Wavelengths

By plotting the gain, noise figure and output power as a function of the signal power level, it demonstrates that power level reaches a saturation level and therefore the optimal signal power level is in the knee where the gain begins to roll off. This region provides the output power near saturation and the minimum noise figure.

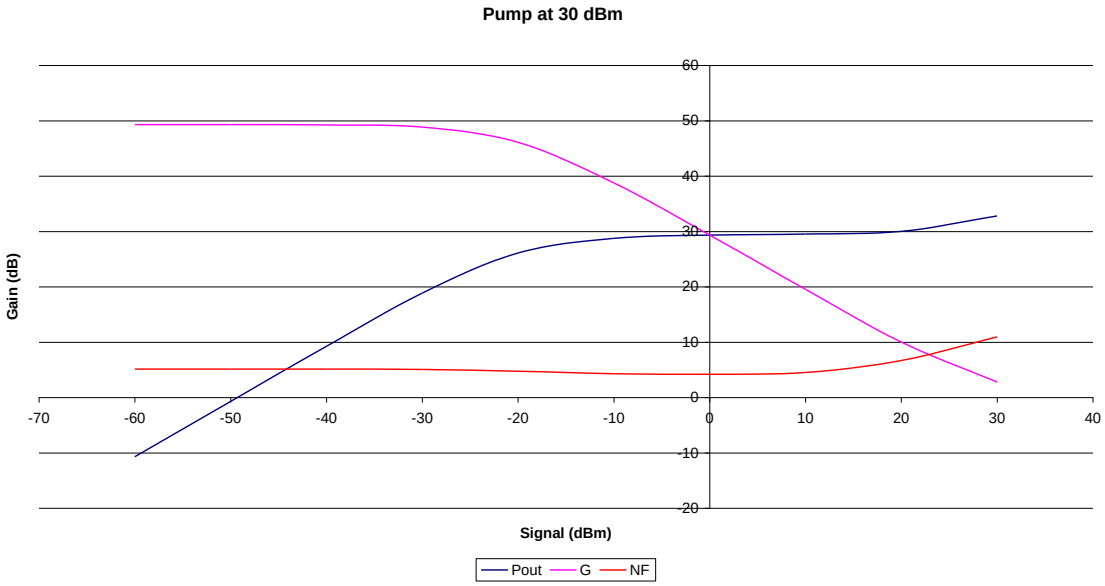

Fig. 31 Simulated Signal Gain at Various Power Levels for Pump at 30 dBm

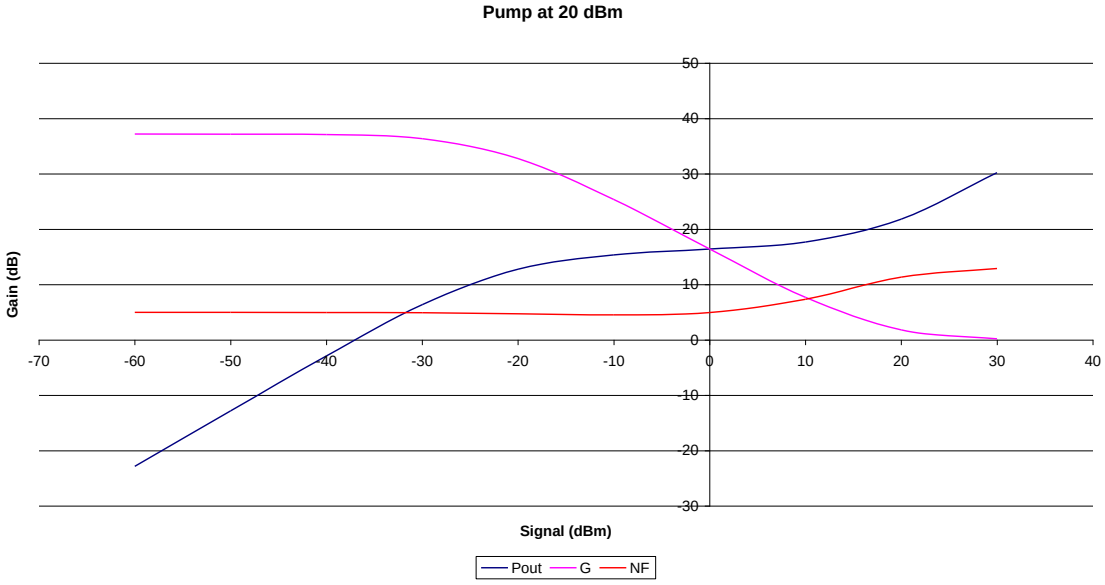

Fig. 32 Simulated Signal Gain at Various Power Levels for Pump at 20 dBm

Figure 31 illustrates that with a high pump power, the signal out power reaches a saturation level until the signal in power is approximately the same as the pump power. Figure 32 illustrates that as the signal power level approaches 30 dBm, the noise figure and output power level begin growing. This is due to the very high power level of the signal and that at this level the noise is being generated by both the pump and signal emissions.

From this analysis, it is possible to conclude that the optimal pump wavelength is 1480 nm and the best signal wavelength is at 1560-1570 nm. In order to obtain sufficient gain, the pump power must be near to 17 dBm [14]. Similarly significant loss occurs at the lower wavelength when pumped at two wavelengths. Noise is high with loss but is suppressed by high gain levels. Additionally, all these gains and losses have been normalized on a per-meter scale. The EDFFPI has only 1 cm of EDFA, so the decibel is only one hundredth of the scale. Without any pumping, 1480 nm has absorption of 45 dB/m. However, with proper pumping, 1550 nm can have a gain up to 30 dB/m. For 1 cm, these gains or losses are -0.45 dB, and 0.3 dB respectively. Nominally these are 0.95, and 1.04. The noise figure should be negligible except in circumstances of high loss, where it is the opposite of the loss.

CHAPTER III

EQUIPMENT MEASUREMENTS

To take accurate measurements and to correctly interpret results, it is important to accurately characterize the equipment which is used. Figure 33 shows the setup used to take equipment measurements.

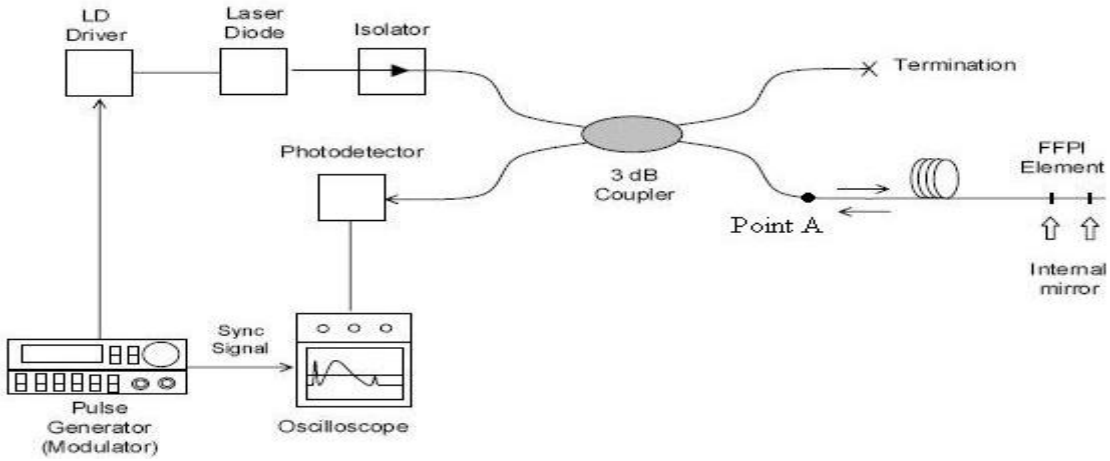

Fig. 33 Equipment Setup

System loss is calculated by measuring the reflections off of a square cleave of fiber [15]. Using a refractive index of 1.5 and 1 for air, the reflectance is 0.04, which corresponds to a -13.98 dB loss. The input was measured at -5.04 dBm but the reflected power was -26.78 dBm. This leads to a 7.76 dB system loss.

Reflection measurements are taken of an uncleaved un-refractive index matching gel fiber, an uncleaved gelled fiber, a cleaved ungelled fiber, a cleaved gelled fiber, a TiO_2 coated fiber, and a gold coated FFPI. Of particular note are the last two. A

reflection maximum voltage of 1.1 V (1.9 V swing) is measured for the TiO_2. Below are the reflection graphs for TiO_2 and a cleaved fiber. As can be seen from Figures 34 and 35, the reflection graph for a clean cleaved fiber shows a response of V= -1.2V, which responds to P= -26.78 dBm. The reflection graph for the TiO_2 coated fiber shows a response of V=1.0V, which responds to P= -19.95 dBm. Using the calculated system loss, this correlates to a power reflection value of R =0.1871 for TiO_2.

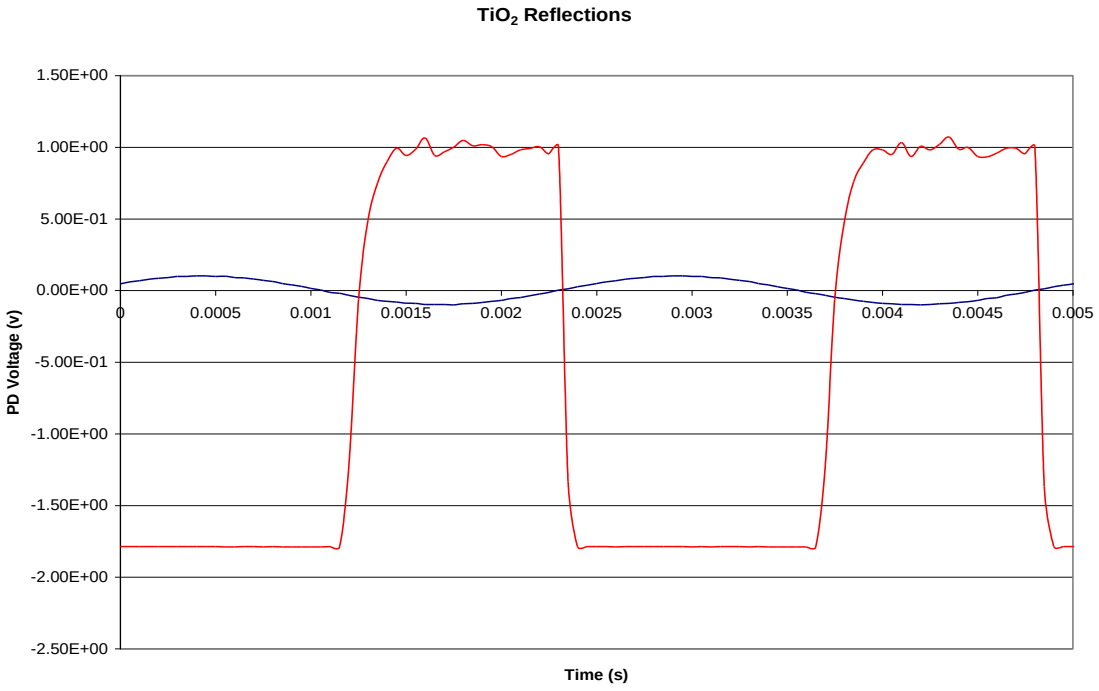

Fig. 34 Measured Reflections of TiO_2 Deposited Fibers

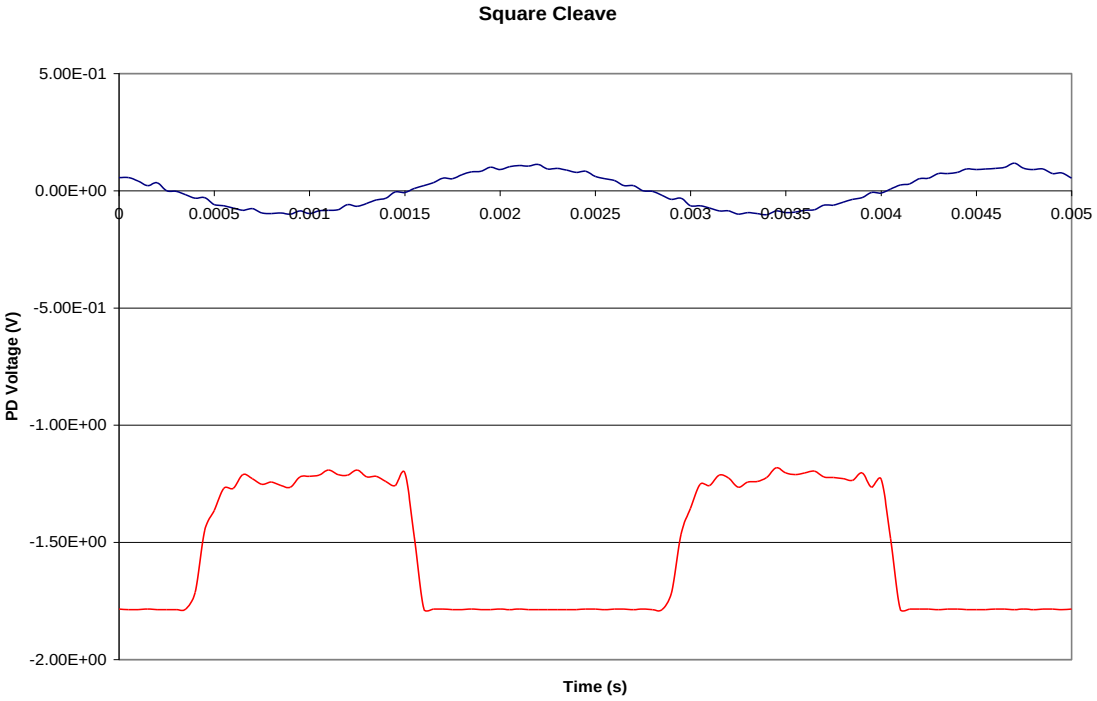

Fig. 35 Measured Reflections of Square Glass Cleave

Response Measurements of Photodetector and Laser

From sampling data points of power measurements taken from point A of Figure 33, a P-V_{in} graph characterizing the laser is derived. Additionally, data points from output current versus input voltage are sampled.

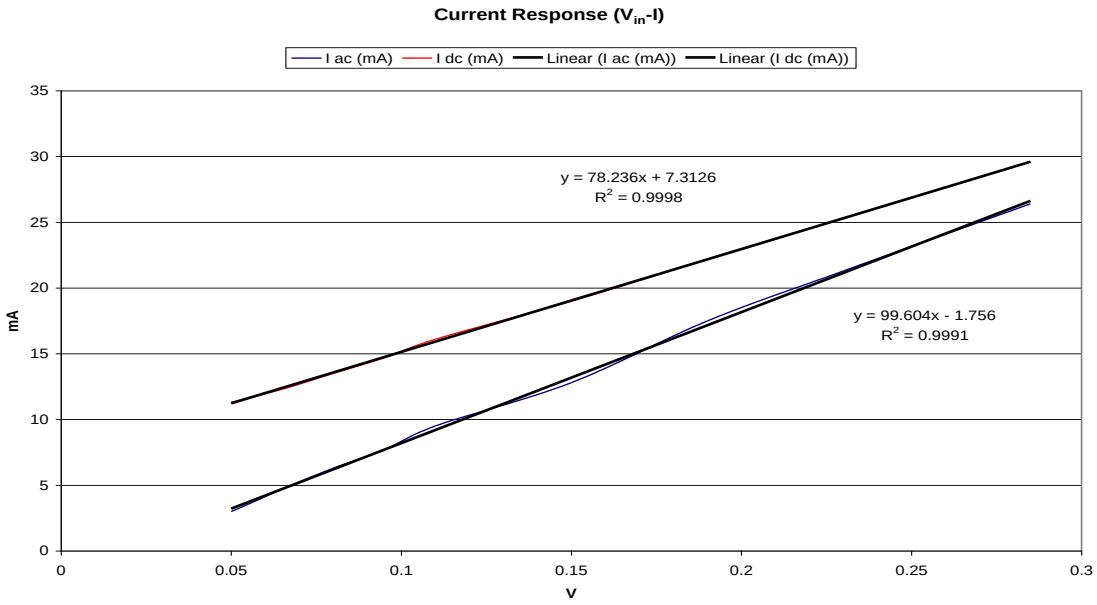

Fig. 36 Measured Monitor Voltage versus Current Output

The equations describing Figure 36, for the modulating current, is $I_{ac} = 99.6\,V - 1.756$ and, for the bias current, is $I_{dc} = 78.24\,V + 7.31$. Since the bias current drives the laser, then the V from the previous P-V_{in} equation can be substituted with an I_{dc}. Additionally, switching the measured points from dBm to mW can be achieved by using the equation $P_{mW} = 10^{\frac{P_{dBm}}{10}}$. With these two substitutions, the Figure 36 turns into a traditional P-I graph (Figure 34) with a threshold current of 11.3 mA:

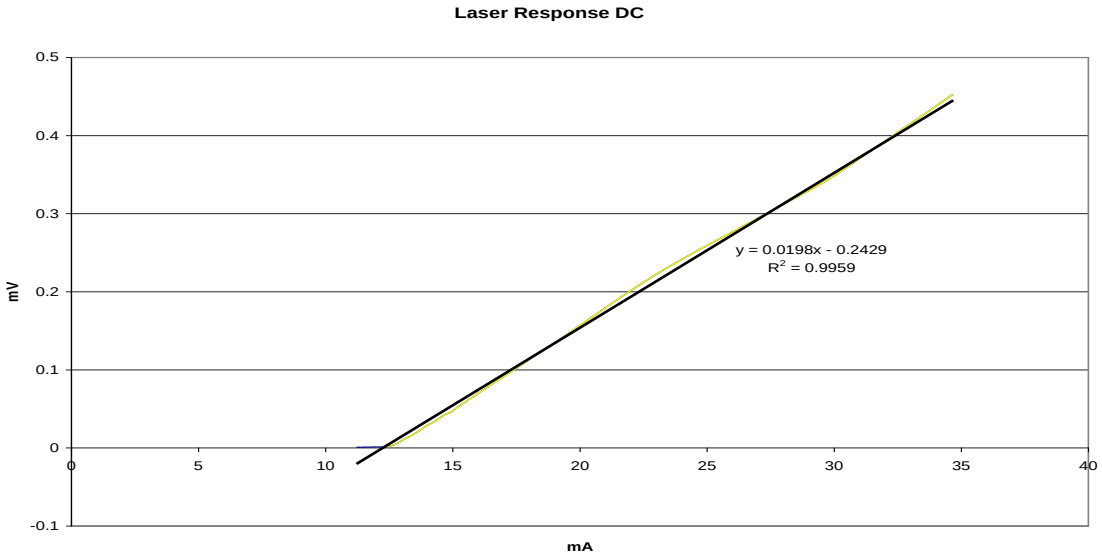

Fig. 37 Measured Laser Response to DC Current

Figure 37 shows that the linear region of the laser is governed by the equation $P = 0.0198 * (I - 11.3mA) = 0.0198 * (V - 65mV)$. Additionally, from data points sampled at point A, the photodetector is characterized by plotting the Power verse the output Voltage level. In mW it is:

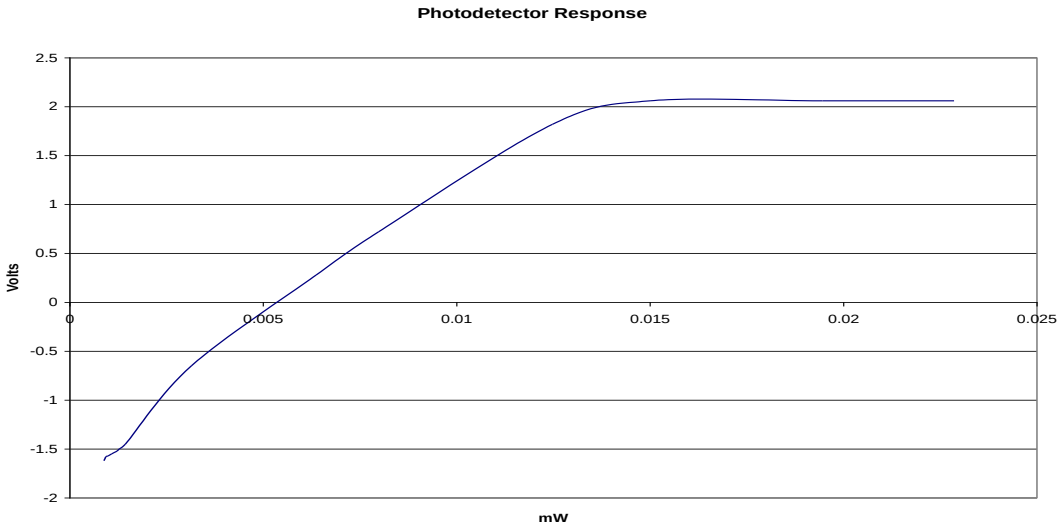

Fig. 38 Measured Photodector Response to Laser Stimulation in mW

Figure 38 shows three response regions: pre-threshold, linear and saturation. An additional loss of 5.8 dB is induced to shift the photodetector away from the threshold knee of the P-I equation, allowing the gathering of more accurate sample points:

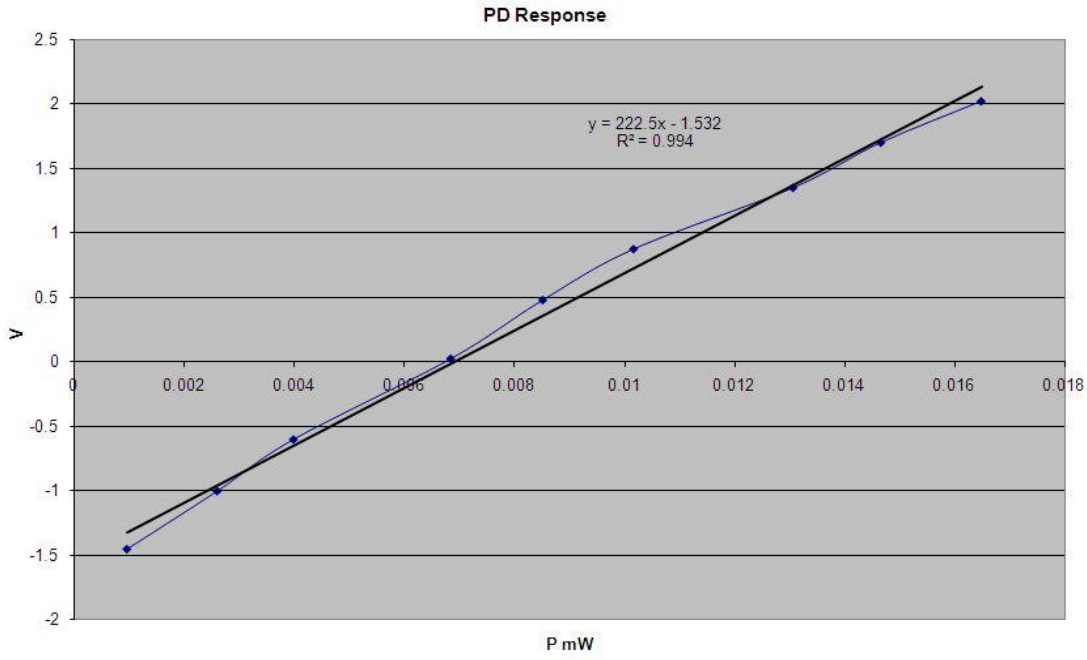

Fig. 39 Measured Photodetector Response with Induced Loss

The photodetector response in Figure 39 derives the equations $V_{PD} = 222.6 * P_{mW} - 1.53$ or $P_{mW} = .0443 * V_{PD} + 0.0679$ for the interval $-1.5 < V_{PD} < 2.06$ or $1.45 < P_{\mu W} < 159.16$. Since the correlation is stronger between mW and V rather than dBm and V, the equation with those units is used.

By observing the output of the laser driver, the response is the same regardless of the waveform or bias level. In order to characterize the current output of the driver and corresponding laser response, different Voltage values are sampled and plotted against the rise of the current and laser power responses. Figure 40 shows the laser and current driver response to display voltage levels.

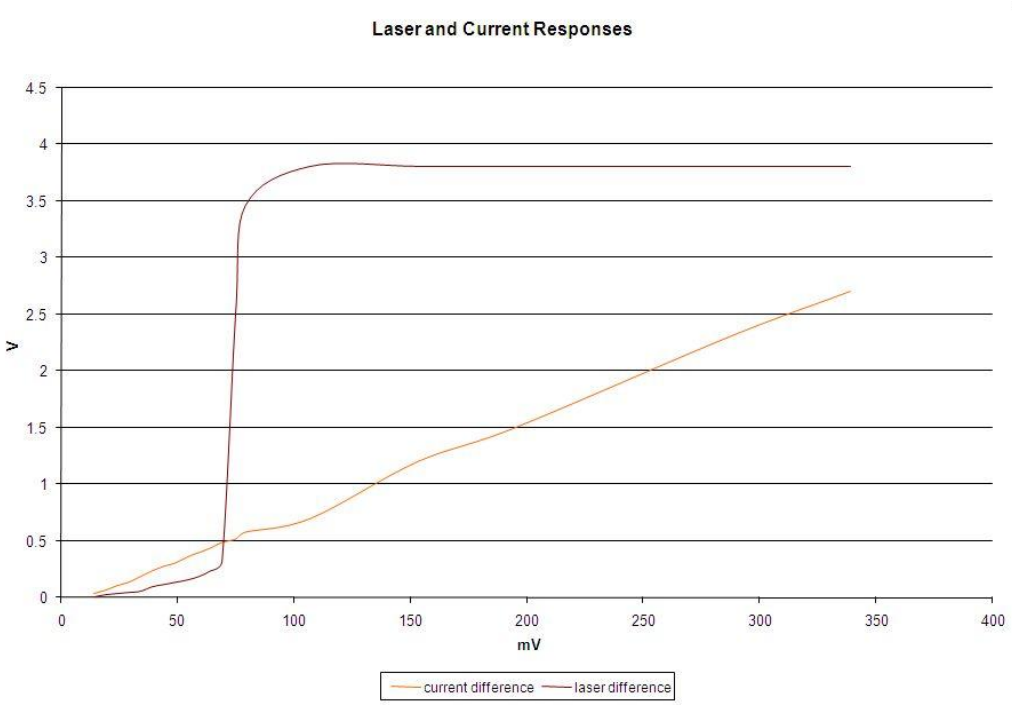

Fig. 40 Measured Laser and Current Responses to Monitor Voltage

Regardless of the input waveform's type or bias level the laser current driver generates a square wave. The output waveform is shown to be a square wave with a high of -1.1 V and a lower voltage level that varies linearly with the display voltage level. Therefore, with the existing setup, the only parameters which can influence the laser driver are frequency, duty cycle, and display voltage level. Because of this, the frequency and duty cycle parameters are disregarded, because they have been kept constant at 1 kHz and 50% respectively, and focused on the impact of a changing display voltage level. Some power level variances are noted depending on the type of wave generated, but since the current driver only outputs square waves, the waveform generator is held on sine waveform to be consistent with previous measurements.

The laser has a threshold at approximately 72 mV display volts. It also has a knee occurring around 600 mV. At 750 mV it goes bimodal, and actually loses peak power. Figure 41 shows the laser response to monitor voltage. It provides the equation:

$$P_{mW} = 1.598 * V_d - 0.1151 \qquad \text{for } 70 < P_{mW} < 600$$

Since the laser driver output (anode and cathode) voltage level (V_a) occurs as a function of the display voltage, it follows $V_a = -0.0086 * V_d - 1.1087$. Combining this equation and laser response, the laser response to the cathode and anode voltage levels are derived by equating the display voltage:

$$P_{mW} = 1.5987 * V_d - 0.1151 = 1.5987E-3 * V_d(in\ mW) - 0.1151$$

$$V_a = -0.0086 * V_d - 1.1087$$

$$V_d = \frac{V_a + 1.1087}{-0.0886}$$

$$P_{mW} = 1.5987E-3 * \frac{V_a + 1.1087}{-0.0886} - 0.1151$$

$$P_{mW} = -0.1859 * V_a - 0.3212$$

Setting the power equal to 0 mW, the anode to cathode voltage is -1.72 V, which leads to a display voltage of around 71.96 mV, which is approximately the same as the observed lasing voltage.

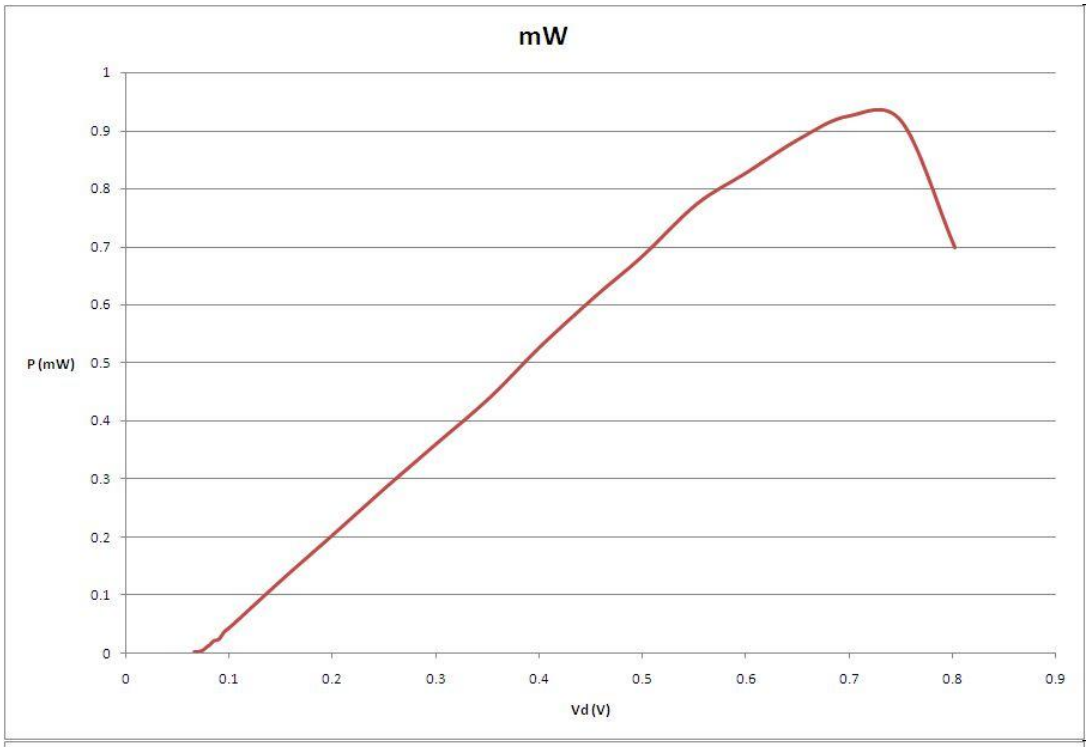

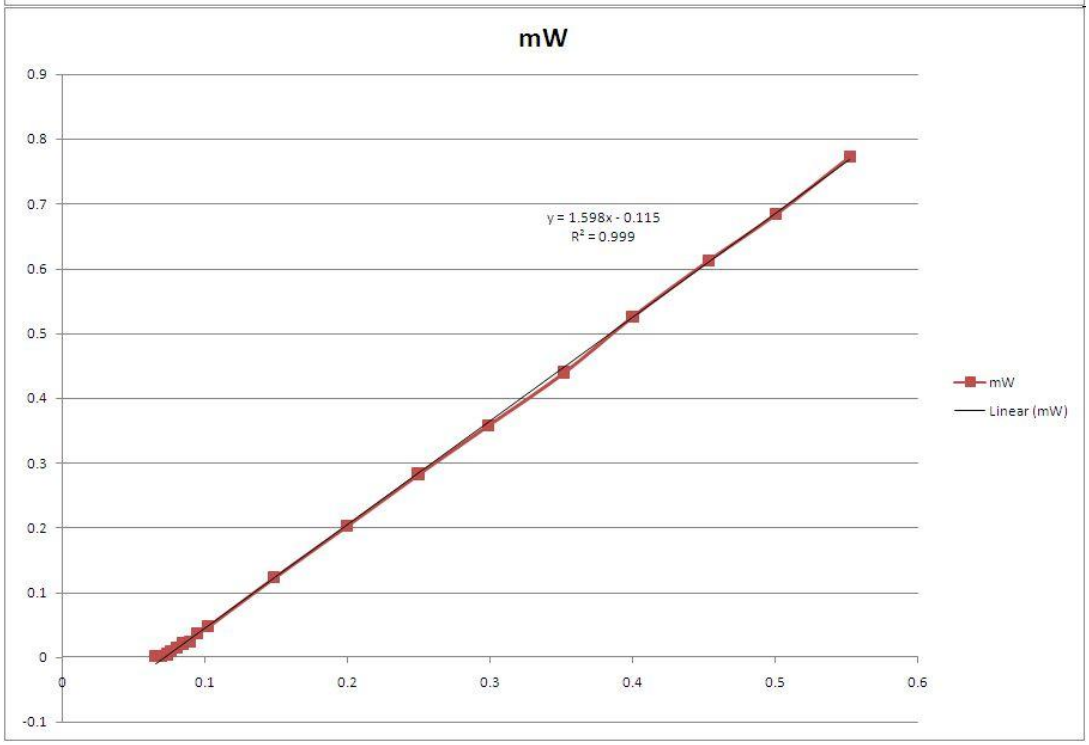

Fig. 41 Measured Laser Response versus Monitor Voltage with and without Trendline

CHAPTER IV

FUSING AND FABRICATION

Fusing optical fibers is a complicated process. It takes into account factors like surface cleave angle, vertical and horizontal alignment, fuse power and duration and feed. These combine to provide an optimal combination of proof (strain) strength and minimized transmission losses. Because of this, most fusion splicer manufacturers automate the process as much as possible to provide a consistent output. However when dealing with special fibers, like the TiO_2 coated fibers, the process extends beyond the range of the automated process [16].

A major concern is retaining the reflective capability of the fibers (which decrease with large fusion currents) while enhancing the proof strength. In a typical fuse, overpowering the fuse current will result in a much larger proof strength but will only lose approximately an additional 0.05 dB (a normally powered current results in about 0.01 dB loss, so an overpowered loss multiplies the effect five times, but an additional 0.04 dB is negligible compared to the system losses). TiO_2 fibers, on the other hand, can lose reflectivity from -19 dB to -26 dB, which is significant not only due to the comparative loss, but because the TiO_2 fiber is usually the only source of reflection. As such it was vital to the project to understand how to minimize reflective losses.

By identifying variables like fuse power and duration which may cause reflective losses and isolating them while holding other variables constant, it is possible to sweep them through a range to see how they react. However, the fibers respond differently to the same stimuli, because not all fibers are deposited the same. The reflectivity of a fiber

(after the prefuse current removes some reflective, but unstable TiO_2) is measured to use that as the baseline measurement. Figure 42 demonstrates Fuse Reflection decay as Pulse duration increases. The Laser power is -4.7 dBm and system loss of 7.76 dBm.

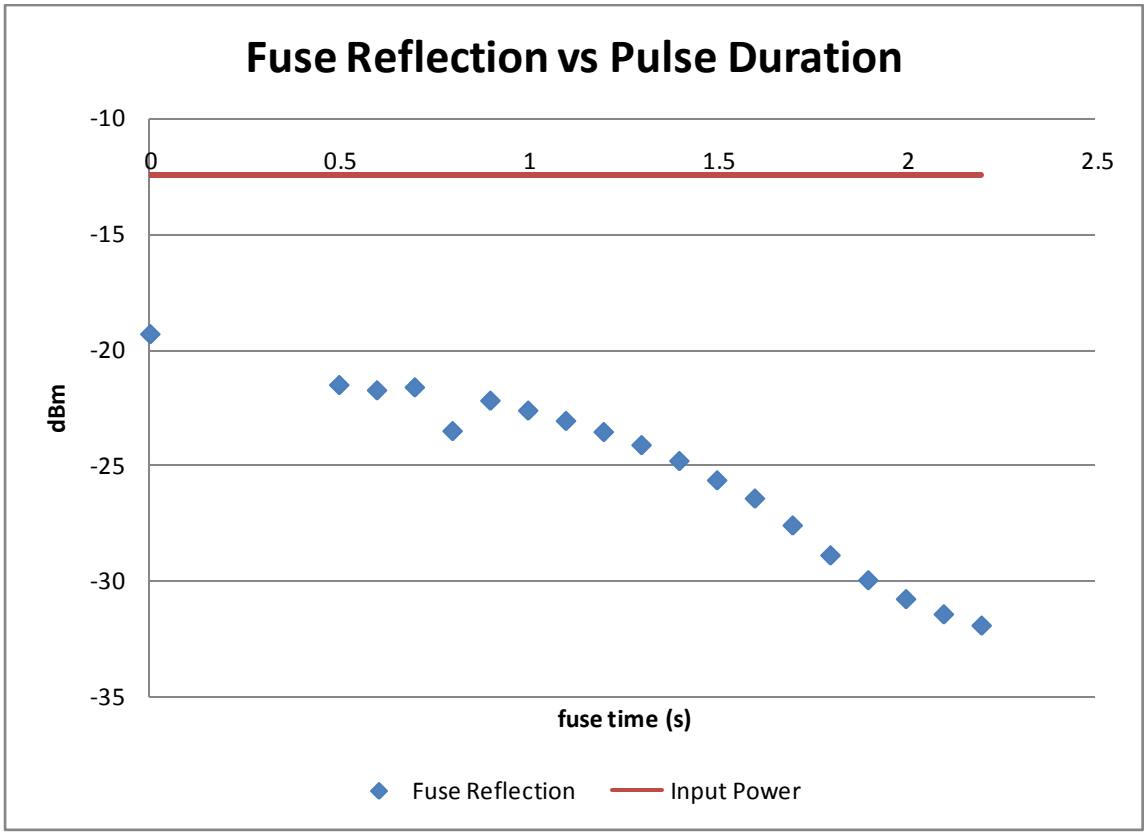

Fig. 42 Measured Reflection Decay with Extend Pulse Durations.

After recording irregularities in the data, it becomes apparent that it is important to have the feed set at about 15 microns for the first fuse, but needs to be turned off for successive fuses; otherwise the fibers would shift and ruin the fusing process.

The maximum pulse duration which will not ruin the reflection is around 1.0 second and the maximum current is around 5 mA. Therefore, fusing at these parameters and repeating the process 10 times optimizes the reflection and proof strength.

Fabrication Process of FFPI with Erbium Fiber

With a better grasp of how to fuse TiO_2 fibers without breaking them or melting the mirrors, fabricating an actual FFPI is the next step. Although a compromise between TiO_2 integrity and proof strength is found, the fiber will still be more fragile at the fuse than elsewhere. Because of this, it is not possible to cleave the fiber very close to the fuse without it breaking. In order to shield the fuse from lateral forces, it must be at least 10 mm. Recall that the free spectral range is a function of the cavity length ($\frac{c}{2nL}$). A higher FSR would lead to a more sensitive FFPI.

Erbium doped fiber is harder to splice and requires more current than most single mode fibers. Considering the delicate reflectance of Ti coated fibers, it is practically impossible to fuse the two together. To overcome this, it is necessary to fuse Ti fibers normally and then cleave them as close to the splice as possible (typically around 5 mm). This cleave is then fused to a length of Erbium doped fiber, which is then cleaved and fused to another cleaved Ti fiber. Since gain from Erbium fibers varies linearly with the length, yet excessive length would compromise the Free Spectral Range, it is decided to use 10 mm of Erbium fiber with two 5 mm buffer zones on each side for a total length of 20 mm, which corresponds to a FSR of 5 GHz. Also, note that a gain calculated to be 20 dB/m becomes a real life gain of 0.2 dB with an Erbium length of 1 cm. Figure 43 displays the layout of an Erbium Doped FFPI.

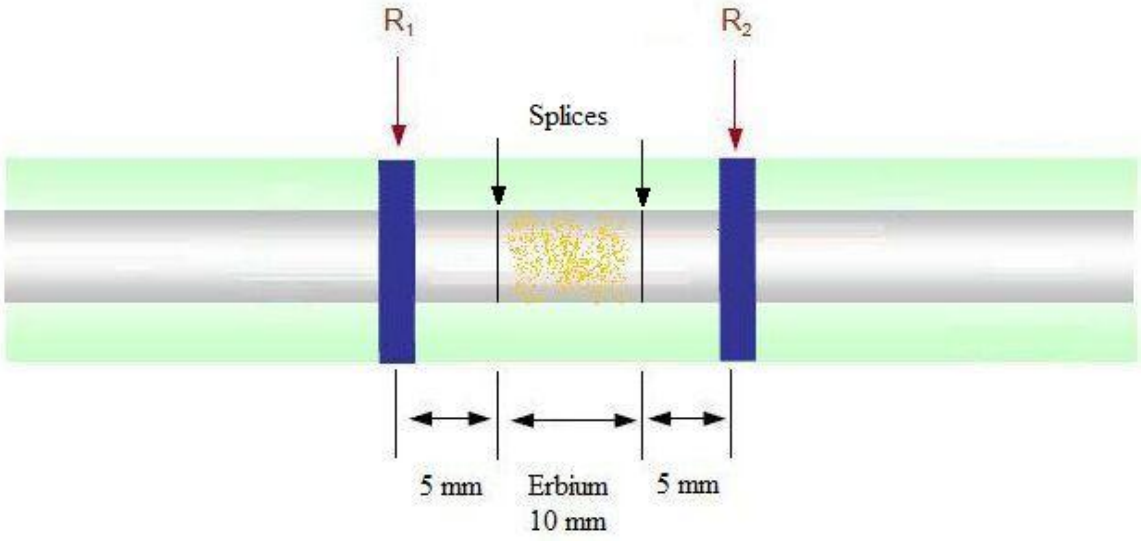

Fig. 43 Erbium Doped FFPI

Effects of Chirp

Direct power modulation increases the linewidth of a laser and causes frequency chirp ($\Delta f = \frac{c}{\Delta\lambda}$) [17]. Figure 44 shows a FFPI response for a pulse duration of 0.1 second.

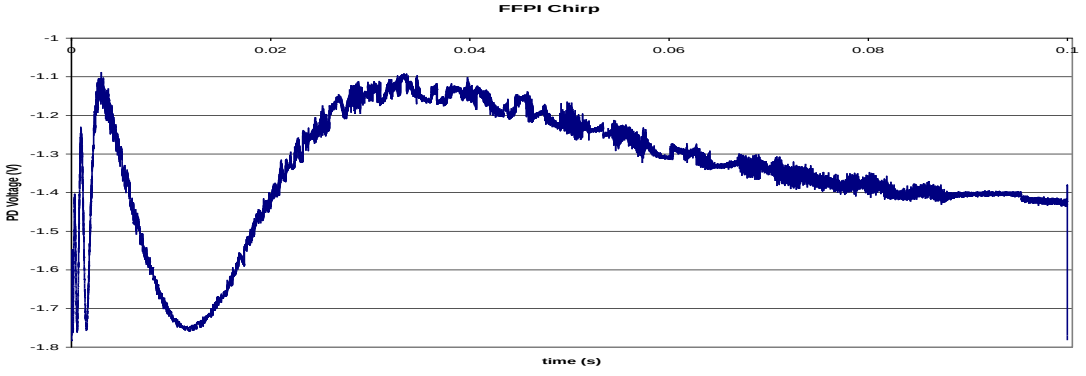

Fig. 44 Measured Chirped Pulse

Figure 45 shows the chirp plotted against a logarithmic time scale, which more acurately displays the number of fringes.

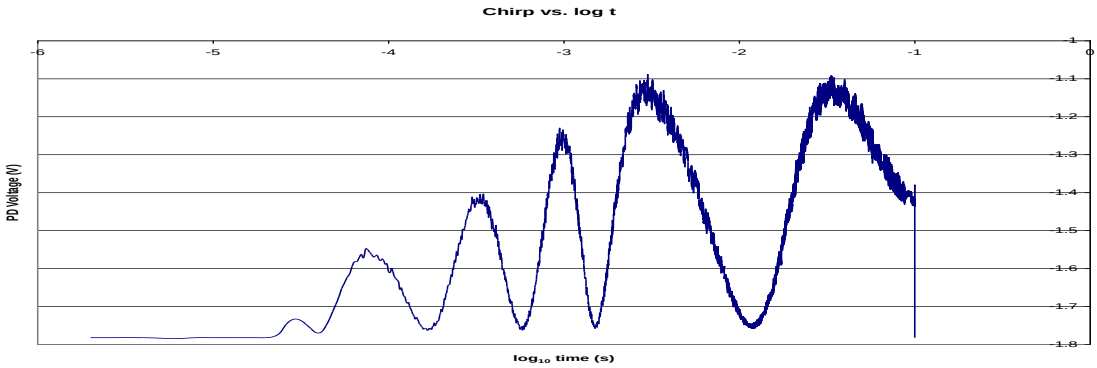

Fig. 45 Measured Chirped Pulse on a log t Scale

This was modeled after exponential chirp (i.e. $\sin(f * [k^t - 1])$) in Figure 46.

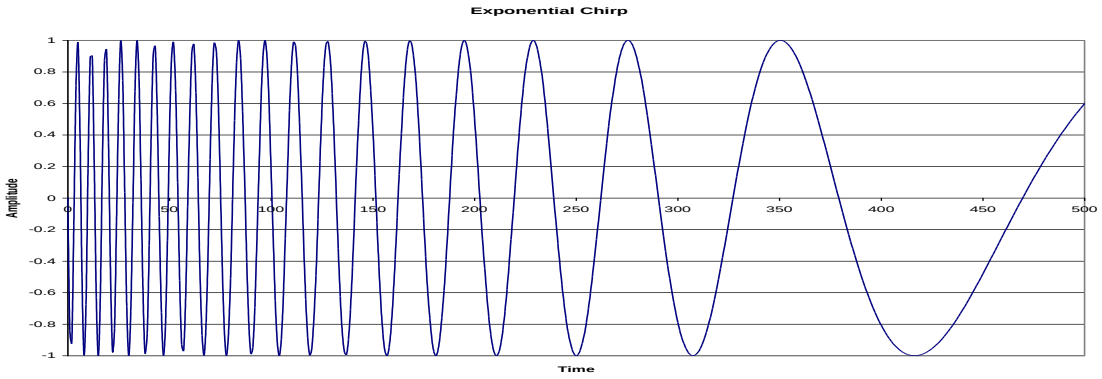

Fig. 46 Simulated Exponential Chirp

The reflection response is not a simple sinusoid, nor is the frequency the only determining factor. However, for small r values (less than 0.5), the reflection response can be simplified. Using the approximate reflectance value of 0.2, it is possible to simplify the response to $\frac{\cos\theta-1}{\cos\theta-2.6}$, which is essentially the same as a scaled and shifted sinusoid, $0.555 * (\frac{1}{2}-\frac{1}{2}cos\,\theta)$. Additionally, the object of the cosine $\theta = \frac{2\pi f}{FSR}$, which with a constant unmodified cavity length can be simplified to θ=A*f where A is a constant and f is the chirped frequency. With these subsitituions, Figure 47 demonstrates the response equation.

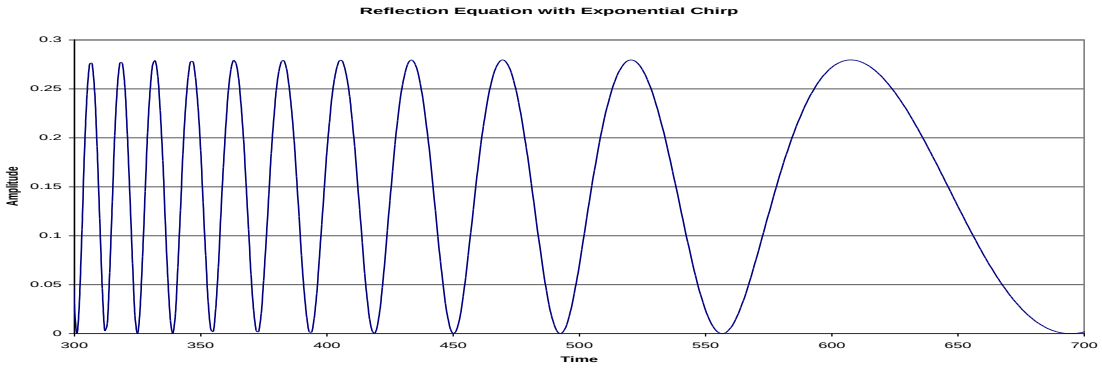

Fig. 47 Simulated Exponential Chirp in Reflection Equation

Inspection shows these are nearly equal, therefore explaining the chirping phenomenon [18]. In a laser whose linewidth has stabilized the frequency is

approximated as constant over short periods of time. For the prefabricated FFPI whose cavity length was measured to be 12.3 mm, the FSR ($\frac{c}{2nL}$) is 8.125 GHz. Likewise, for the EDFFPI with a cavity length of approximately 2 cm, the FSR is 5 GHz. A laser with a frequency drift of 3 MHz/min would require 1666.67 minutes to go through a full 2π revolution. Since measurements are taken over shorter time period than 27.8 or 45.1 hours, the frequency is relatively constant.

Because of this, the phase component is simplified to $\Delta\theta = 2\pi f * \frac{2n(L+\Delta L)}{c}$ where all factors besides ΔL are constant. By substituting this into the equation, it is possible to derive that

$$\theta = \frac{2\pi}{\lambda} * 2n(L + \Delta L)$$

$$\theta = \frac{2\pi}{1550nm} * 2 * 1.5 * (2cm + \Delta L)$$

$$\theta = 2\pi * 38706.67 + 1935.48 * \Delta L/mm$$

$$\Delta\theta = 2\pi * 1935.48 * \frac{\Delta L}{mm}$$

Thus, every 1/1935.48 mm or 516.67 nm change in cavity length should lead to a fringe revolution [19].

Power Envelope

In order to interpret the reflection feedback, it is necessary to know the power level of the laser, both to measure the reflection percentage and also to know the amount of chirp associated with varying power levels.

Figure 48 shows the power envelope at 288 mV and the FFPI response within the envelope. A 19.1 dB loss is induced to capture it fully on the photodetector.

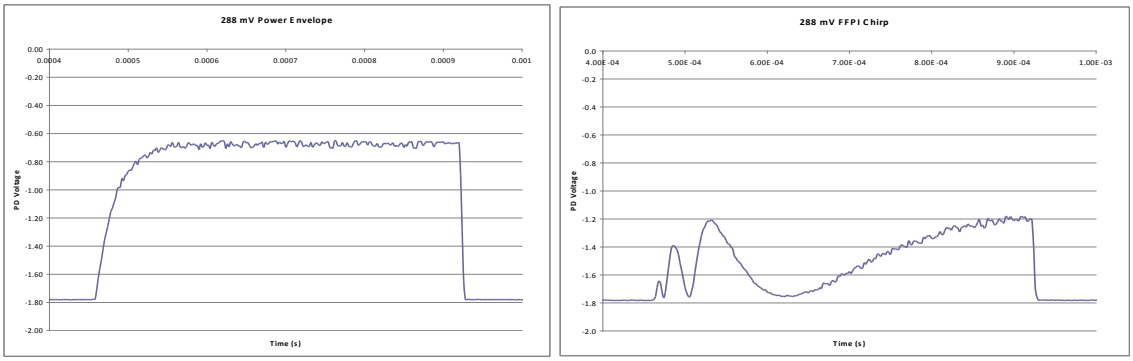

Fig. 48 Measured Power Envelope and Chirp with 288 mV Monitoring Voltage

Figure 49 is the same with a 400 mV power envelope. Notice how the initial frequency of the chirp increases with power level, but they decay at roughly the same rate:

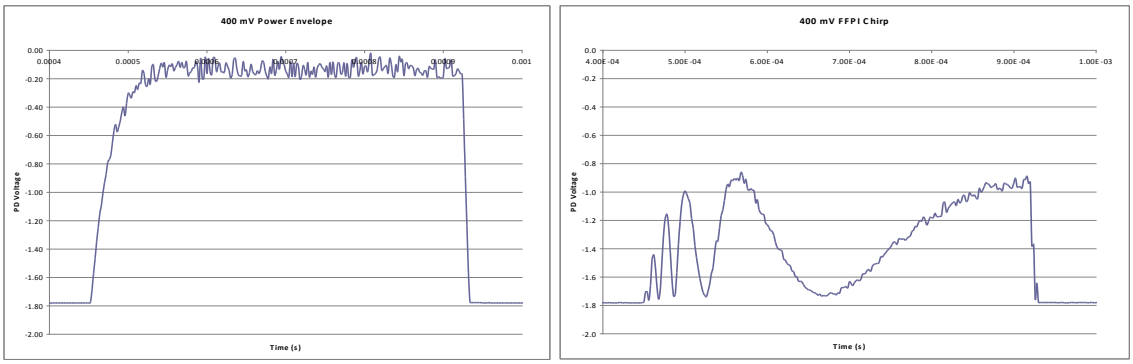

Fig. 49 Measured Power Envelope and Chirp with 400 mV Monitoring Voltage

CHAPTER V

MEASUREMENTS AND INTERPRETATIONS

In order to understand and interpret responses from the EDFFPI and Reference FFPI, it is essential to understand the reflection as well other characteristics of the FFPIs.

Reflection Levels

To measure the reflection levels for the EDFFPI and the reference FFPI, it is necessary to compare it to gold, which has approximately 100% reflectance. Figure 50 measures the power level as 236.16 units. The Luna Manual specifies linear arbitrary units for the x-axis. The y-axis is in nanoseconds.

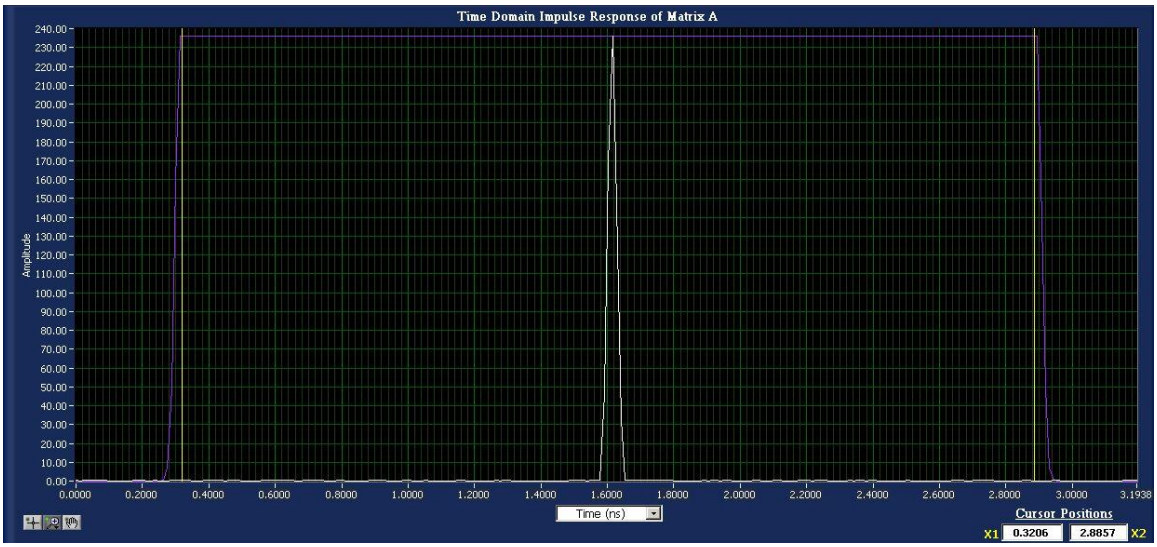

Fig. 50 Gold Standard

By comparison, Figure 51 shows the reference FFPI has levels of 47.1 for the first mirror and 23.75 for the second mirror. Reflectance for the first mirror is measured as $\frac{47.1}{236.16} = 0.1994$. The transmitted power is $236.16 * (1 - 0.1994) = 189.07$. The Reflectance of the second mirror is $\frac{23.75}{189.07} = 0.1256$.

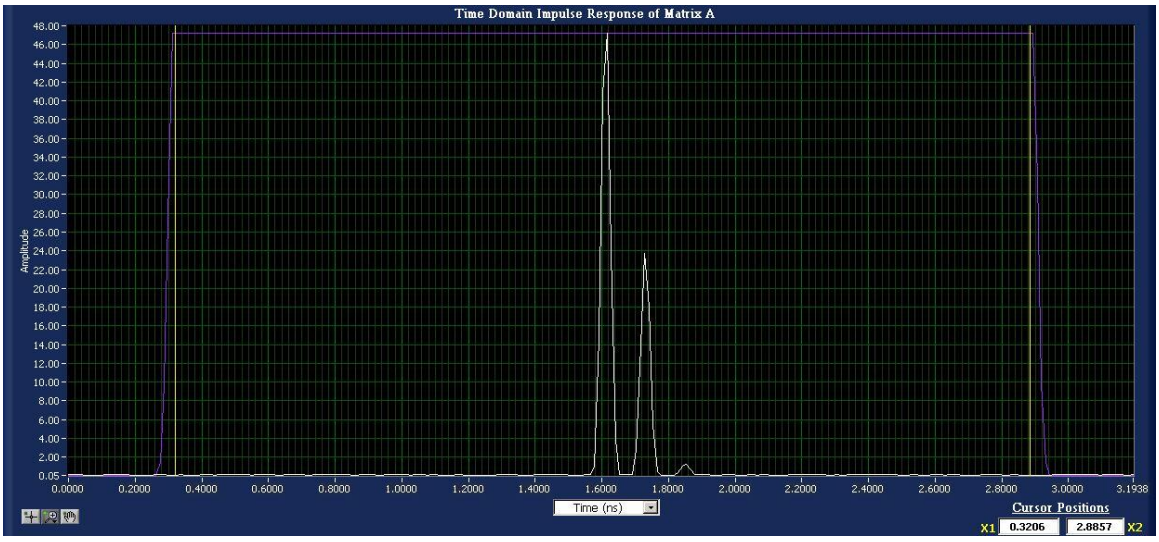

Fig. 51 Measured Reference FFPI Reflection

The EDFFPI was measured similarly, but it is separated into three regions: 1550 nm, 1530 nm and 1480 nm in order to account for Erbium absorption. Using the same method at 1550, Figure 52 demonstrates that averaging measurements gives 0.2399 for the first mirror and 0.1788 for the second mirror. Figure 53 shows that at 1530, it is 0.2479 for the first mirror and 0.1922 for the second mirror.

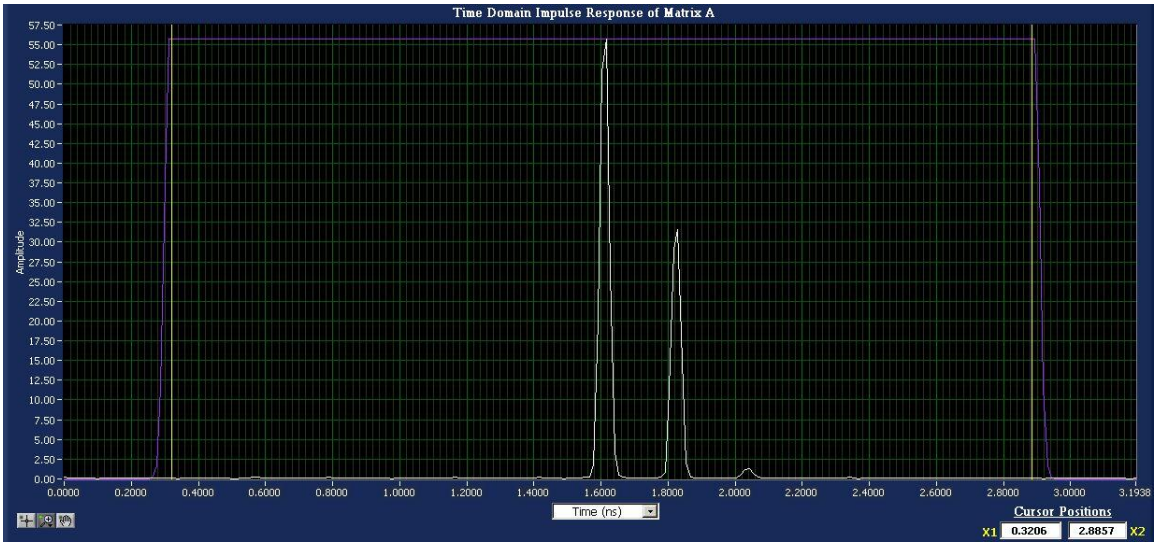

Fig. 52 Measured EDFFPI Reflection at 1550 nm

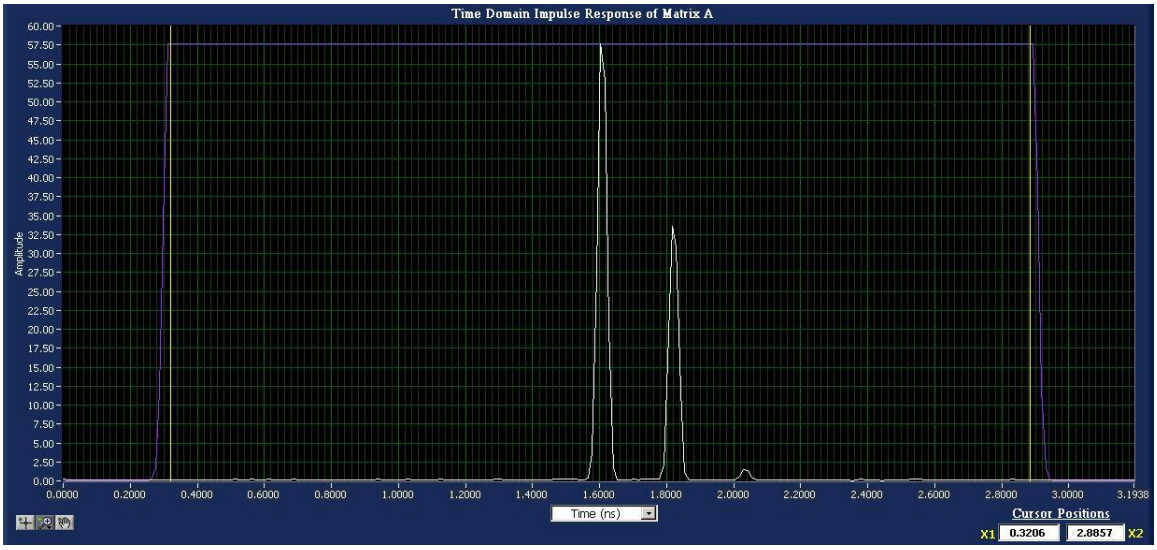

Fig. 53 Measured EDFFPI Reflection at 1530 nm

When calibrating for the 1480 nm range, the gold reflection measures much higher than before around 430, as seen in Figure 54. Repeated recalibrations did not

change so it was accepted since the units were arbitrary. Figure 55 shows that at 1480, the first mirror was 0.2806 and the second mirror was at 0.2046.

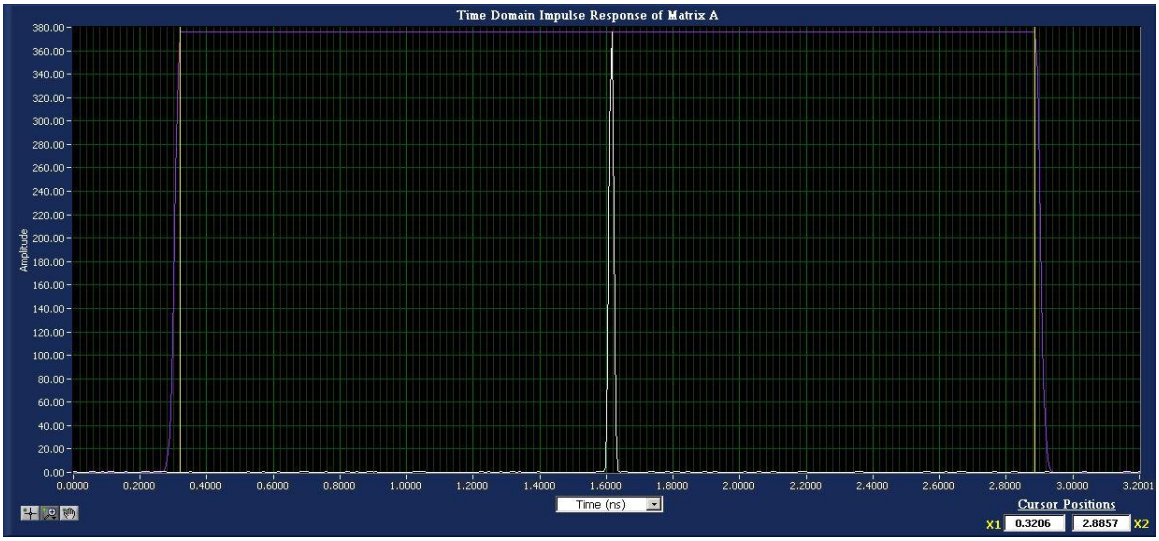

Fig. 54 Measured Gold Reflection at 1480 nm

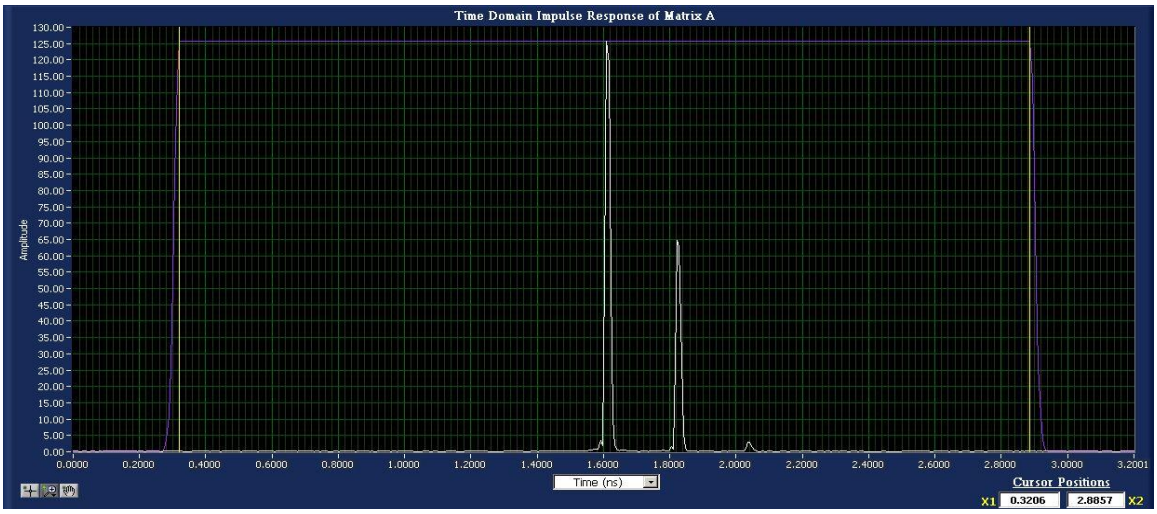

Fig. 55 Measured EDFFPI Reflection at 1480 nm

	R_1	R_2
Reference FFPI	0.20	0.13
EDFFPI at 1550	0.24	0.18
EDFFPI at 1530	0.25	0.19
EDFFPI at 1480	0.28	0.20

Fig. 56 Table of Reflection Measurements

The reflections increase at lower wavelengths. The first mirror increases from 0.2399 to 0.2479 to 0.2806, and the second mirror goes from 0.1788 to 0.1922 to 0.2046 as they goes from 1550 nm to 1530 nm to 1480 nm. This is displayed in Figure 56. However, notice that although the reflections increase, the ratio of reflectances between the mirrors, which will indicate the effects of the erbium, goes from 0.7452 (1550 nm) to 0.7750 (1530 nm) to 0.7291 (1480 nm). Since the lower wavelengths seem to increase lesser reflection levels by a higher percentage, the last ratio should be the greatest of the three yet it decreases, indicating that the Erbium is absorbing the light. Unfortunately, without knowing exactly how lower wavelengths increase reflectance, it is not possible to calculate the exact amount of absorption.

Recall from the Gain chapter that nominal gains and losses are -0.45 dB (1480 nm) and 0.3 dB (1550 with pump). Nominally these are 0.95 and 1.04 respectively. Using these values along with the reflections measured on the Luna, it is possible to calculate the effective reflection as a function of phase using the derived equation.

$$\frac{I_r}{I_o} = \frac{{r_1}^2 + {r_2}^2 g^4 - 2\, r_1 r_2 g^2 \cos\theta}{1 - 2 r_1 r_2 g^2 \cos\theta \; + \; {r_1}^2 {r_2}^2 g^4}$$

Figure 57 displays the calculated reflectance and the dB equivalent of the EDFFPI at 1550 nm. Reflectance varies from -2.43 dB to -21.47 dB.

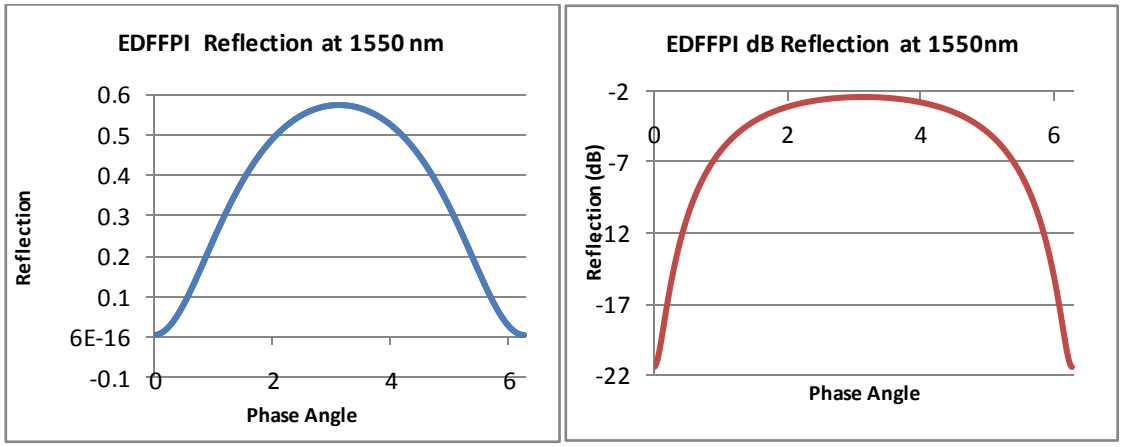

Fig. 57 Calculated EDFFPI Reflections Nominal and dB at 1550 nm

Figure 58 has calculated reflectance and dB equivalent of the EDFFPI at 1480 nm. Reflectance varies from -2.49 dB to -13.86 dB.

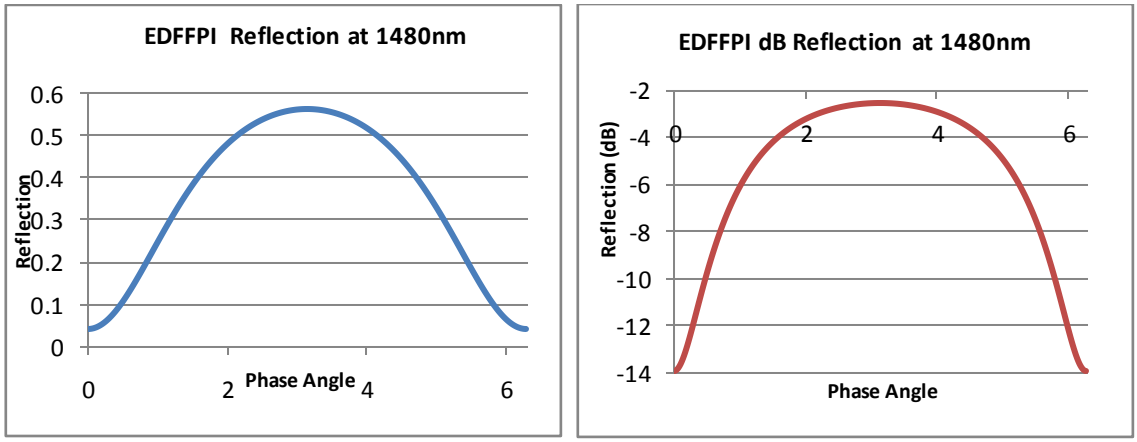

Fig. 58 Calculated EDFFPI Reflections Nominal and dB at 1480 nm

Figure 59 shows the calculated reflectance and the dB equivalent of the reference FFPI. The reflectance can vary anywhere from -3.26 dB to -18.47 dB.

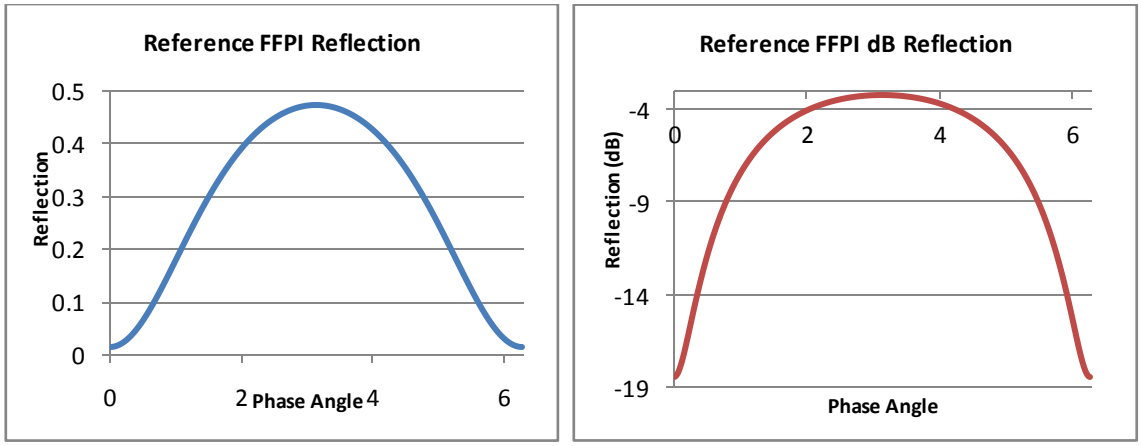

Fig. 59 Calculated Reference FFPI Reflections Nominal and dB

Spectral Analysis

Spectral analysis of the EDFFPI and reference FFPI can help understand the responses. At the input to the FFPI the pump laser at 1480 nm had a power level of -1.50 dBm, or 0.707 mW, and the signal laser at 1550 nm had a power level of -2.65 dBm, or 0.543 mW. The combined power level is 1.25 mW which is 1.0 dBm. These power levels were chosen to satisfy both erbium gain criteria and in order to remain within the bounds of the photodetector.

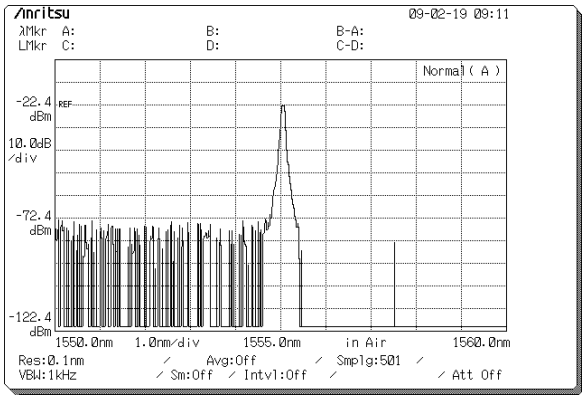

Fig. 60 Spectral Analysis of Reference FFPI Reflection with Only Signal Power

Figure 60 is a spectral analysis of the reference FFPI with only signal power. Despite having -2.7 dBm input into the FFPI and a coupler loss of 4 dB, it still reads out having a peak power of -22.4 dBm, which indicates a loss of 15.7 in the reference FFPI, which is within the calculated range.

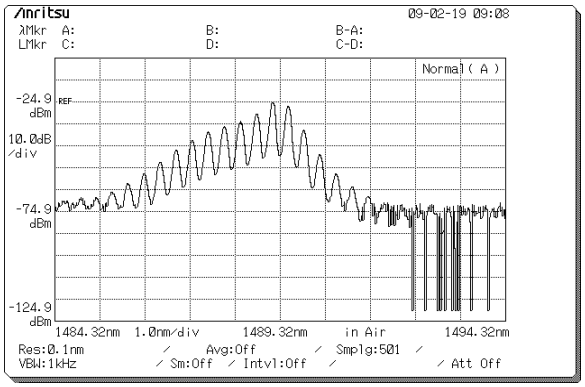

Fig. 61 Spectral Analysis of Reference FFPI Reflection with Only Pump Power

Figure 61 is a spectral analysis of the reference FFPI with only pump power. The pump had an input power level of -1.5 dBm, higher than that of the signal but since it is a broad spectrum laser, the power is more widely distributed. Approximating the same 15.8 dB FFPI loss as despite a slightly different phase for a different wavelength, this leads to a loss of 3.6 for the widespread power distribution.

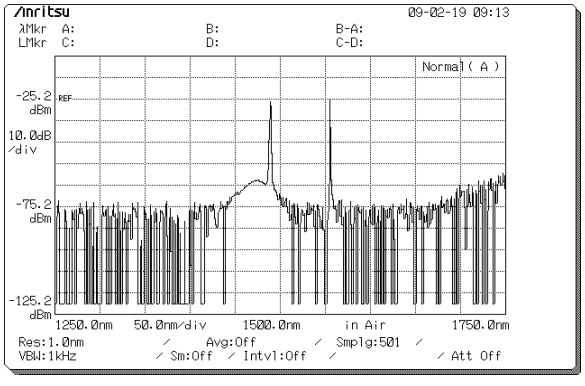

Fig. 62 Spectral Analysis of Reference FFPI Reflection with Pump and Signal Power

Figure 62 is a spectral analysis of the reference FFPI with both signal and pump power. As can be observed, the signal has a slightly higher power level which is consistent with what was observed above.

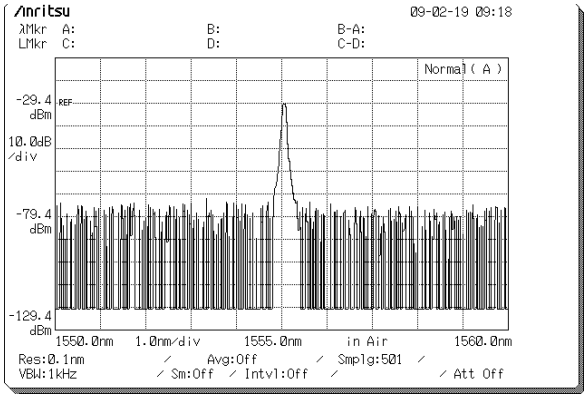

Fig. 63 Spectral Analysis of EDFFPI Reflection with Only Signal Power

Figure 63 is a spectral analysis of the EDFFPI with only signal power. This has a loss of around 22.7 dB which is at the low end of the acceptable range.

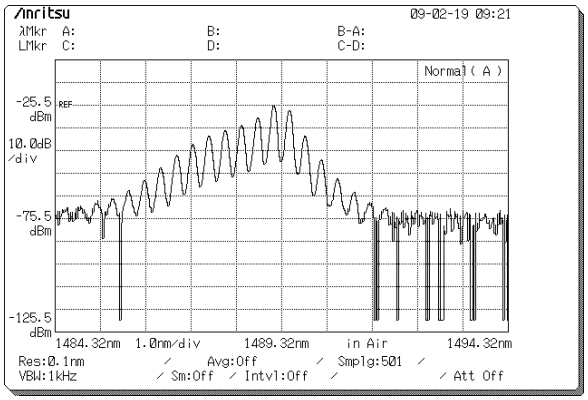

Fig. 64 Spectral Analysis of EDFFPI Reflection with Only Pump Power

Figure 64 is a spectral analysis of the EDFFPI with only pump power. Using the 3.6 dB spectrum loss, this calculates to have a 16.4 dB which is also at the low end of the acceptable range.

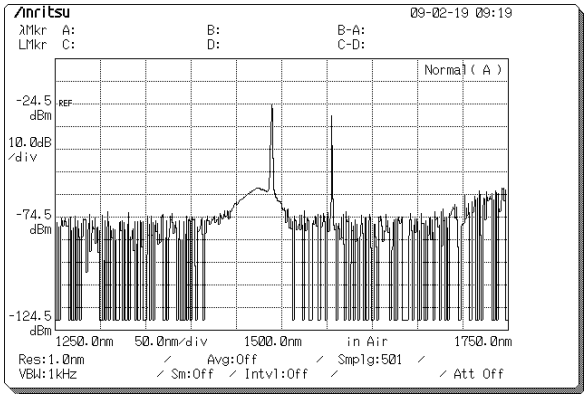

Fig. 65 Spectral Analysis of EDFFPI Reflection with Pump and Signal Power

Figure 65 is a spectral analysis of the EDFFPI with both signal and pump power. These are consistent with the two previous charts. The pump power level is higher despite operating in an Erbium filter, due to the observed higher reflectance at lower wavelengths.

Erbium Measurements

In order to confirm the Erbium Doped Fiber Simulations, simulation tests are run on a length of 10 mm EDF, the same as the EDFFPI. Figure 66 shows the test setup.

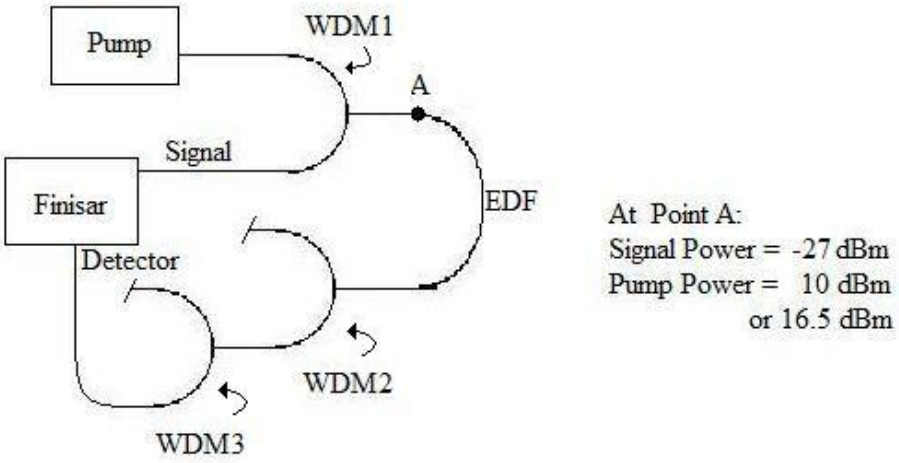

Fig. 66 Erbium Test Setup

With no pump power, -9.4 dB Insertion loss is measured at 1530 nm. At 10 dBm, Insertion loss is -9.2 dB, a gain of 0.2 dB. At 16.5 dBm, -8.6 dB loss is measured, a gain of 0.8 dB. The same measurements are taken at 1550 nm. With no pump power, -11.2

dB loss is measured. At 10 dBm, -10.75 Insertion Loss is measured, indicating 0.45 dB gain. At 16.5 dBm, -10 dB Insertion Loss is measured, indicating 1.2 dB gain. This verifies the simulation that pump power around 17 dB is needed to induce gain even with a length of 1 cm. Results are displayed in Figure 67.

Pump dBm	1530 IL	Gain	1550 IL	Gain
none	-9.4	N/A	-11.2	N/A
10	-9.2	0.2	-10.75	0.45
16.5	-8.6	0.8	-10	1.2

Fig. 67 Table of Erbium Test Results

Finisar Sweeping Laser Measurements

Additionally, both the EDFFFPI and Reference FFPI are connected to the Finisar laser which sweeps from 1520 to 1570 nm. Figure 68 shows the measurement setup.

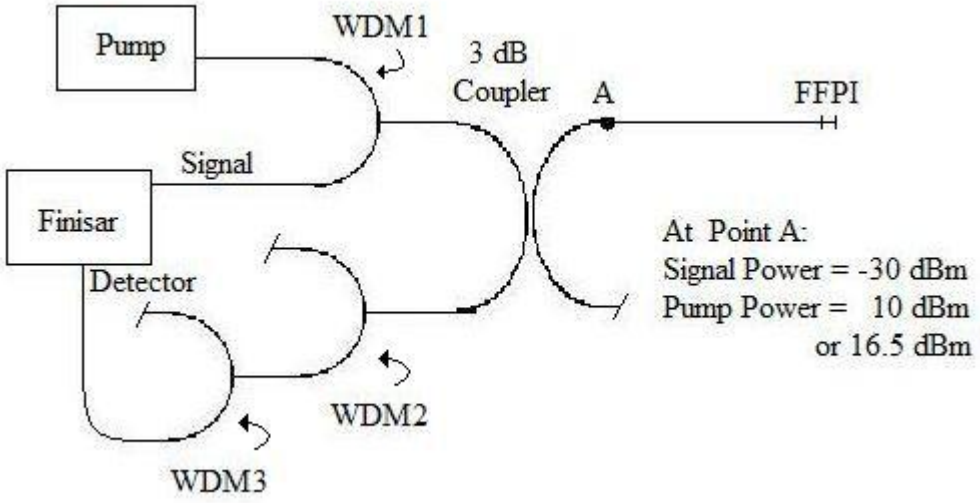

Fig. 68 Finisar Setup

Initially the FFPIs are connected only through a simple coupler, which has approximately a 6 dB roundtrip loss. Notice that in figure 69 and 70, although the reference FFPI is consistent throughout the entire spectral range, the EDFFPI is very frequency dependent due to the Erbium cavity.

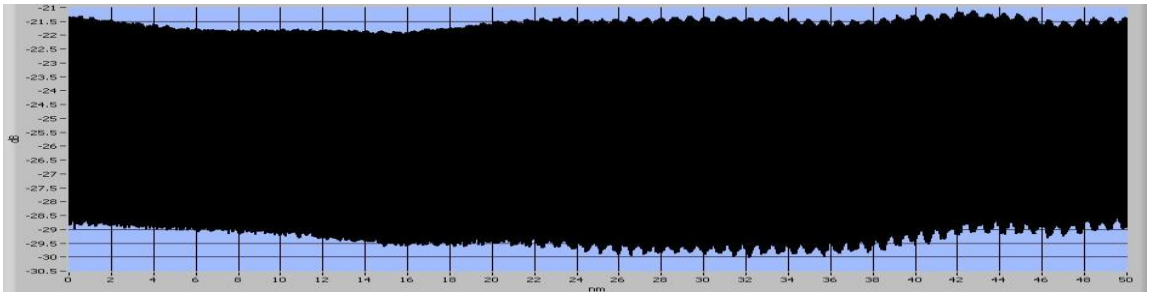

Fig. 69 Measured Reference FFPI Baseline 1520-1570 nm

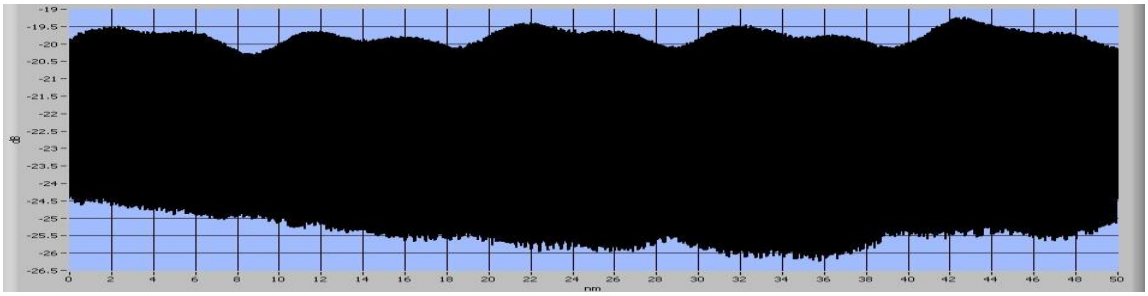

Fig. 70 Measured EDFFPI Baseline 1520-1570 nm

Notice that these graphs range from 0 to 50 nm, rather than 1520 to 1570 nm, due to a plotting error. Therefore the x-axis should be interpreted as "nm above 1520" rather than "nm". Thus, a graph centered at 10 nm is really centered at 1530 nm and graph centered at 30 nm is really centered at 1550 nm. Note the y-axis is plotted in terms of dB. This is calibrated to the output power of the Finisar, -23.5 dBm.

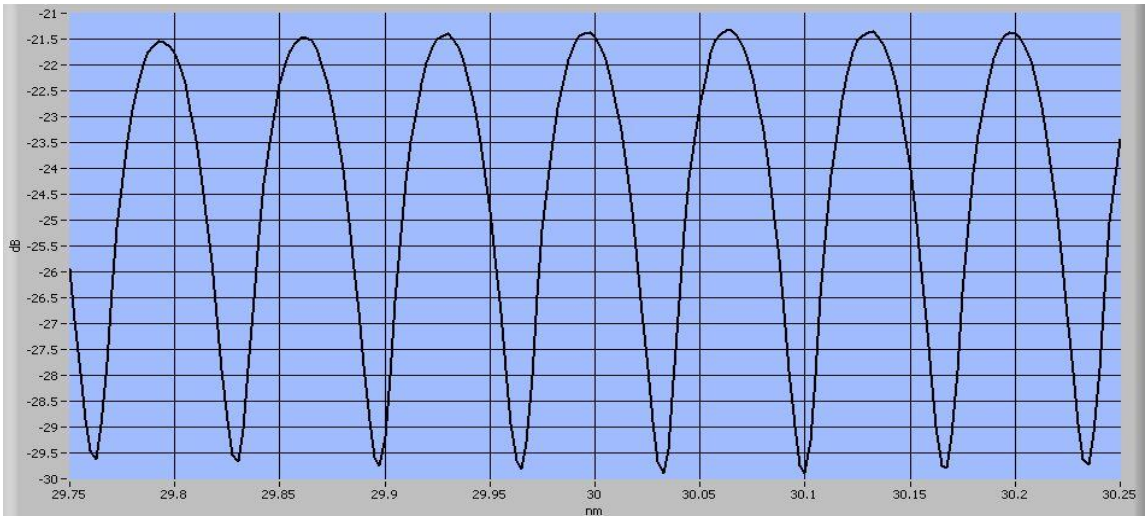

Fig. 71 Measured Reference FFPI Baseline Centered at 1550 nm

These baseline measurements can be used to calculate the FSR and therefore verify the cavity length. According to Figure 71, the $\Delta\lambda$ of the Reference FFPI is approximately 0.065 nm, which should put the FSR at 8.125 GHz.

Centered at 1550 nm: $FSR = \frac{\Delta f}{\Delta \lambda} * \Delta\lambda = 125 \frac{GHz}{nm} * 0.065nm = 8.125\ GHz$

$FSR = \frac{c}{2nL}$ $\quad$ $8.125\ E\ 9 = \frac{3E8}{2*1.5*L}$ $\quad$ L=12.3mm

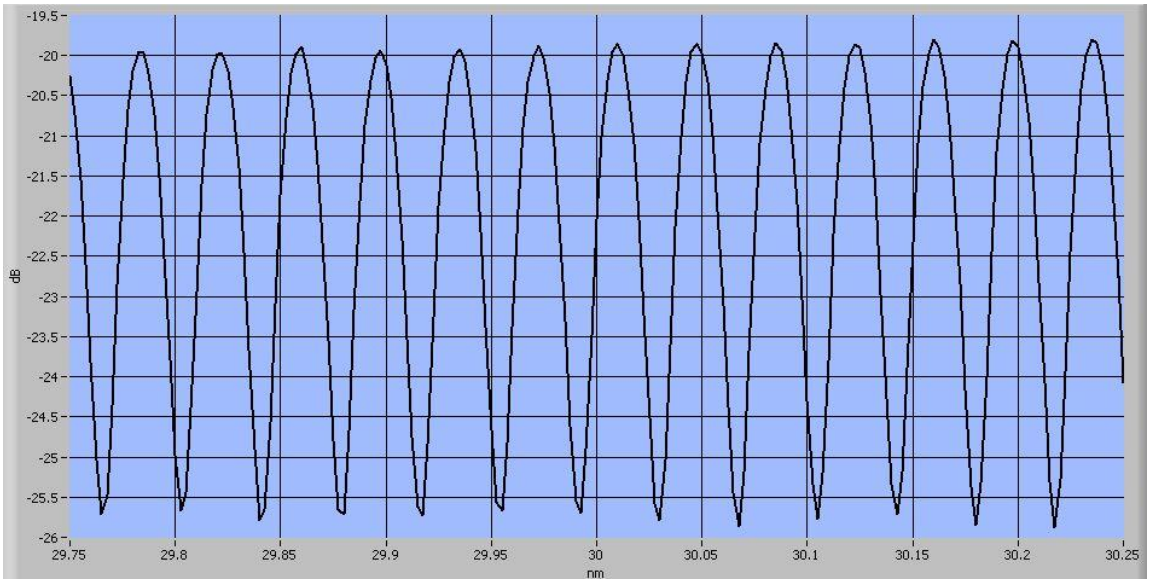

Fig. 72 Measured EDFFPI Baseline Centered at 1550 nm

Figure 72 shows an EDFFPI $\Delta\lambda$ of about 0.04 nm; therefore the FSR is 5 GHz.

Centered at 1550 nm: $FSR = 125 \frac{GHz}{nm} * 0.04\ nm = 5\ GHz$

$5E9 = \frac{3E8}{2*1.5*L}$ $\quad$ L= 20 mm

Next, the FFPIs were connected to the Finisar through a Wavelength Division Multiplexer and a Wavelength Division Demultiplexer so that a 1480 pump laser could be sent into the FFPIs and filtered out before returning to the Finisar. However, the WDMs induced further loss and they are not ideal filters. In order to characterize the loss obtained from the WDMs, Finisar measurements were taken of the system with the gold coated fiber, an ideal reflector, replacing the FFPI.

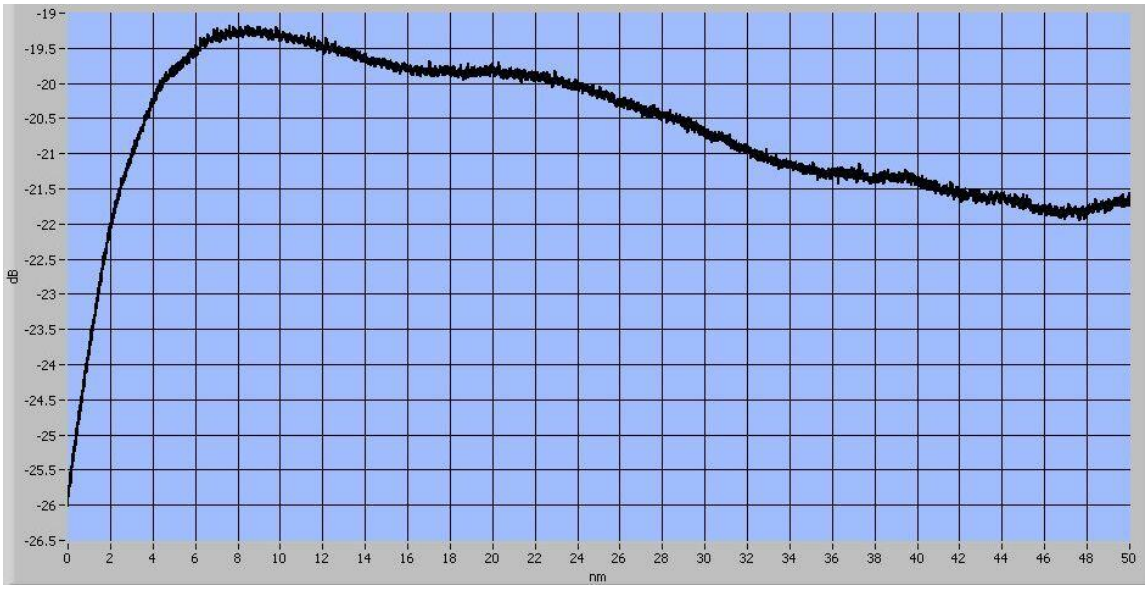

Fig. 73 Measured System Loss with a Gold Coated Fiber

Notice that instead of having a linear response, significant wavelength dependence exists. In order to remove the wavelength dependence, the measured FFPI reflections are all compared against Figure 73. Unfortunately, while this corrects the

reflections, they do not appear as smooth since the measurements were taken at different times. Similar measurements and calculation are made for pump power, but slight differences exist since they take slightly different paths. Also of note is that the measurement is taken again with the path running twice through a 3 dB coupler. Comparing the results shows a 6 dB loss, confirming the linearity of the photodetector.

Initially the signal power is -31.3 dBm at the input to the FFPIs, and the pump power is at 10.0 dBm. However, recalling from the gain chapter, maximum emission occurs near 1530 nm and pump power needs to be around or above 17 dBm for significant gain regardless of signal power. Similar measurements are taken centered at 1530 nm with a pump power at 16.5 dBm, as high as the laser goes.

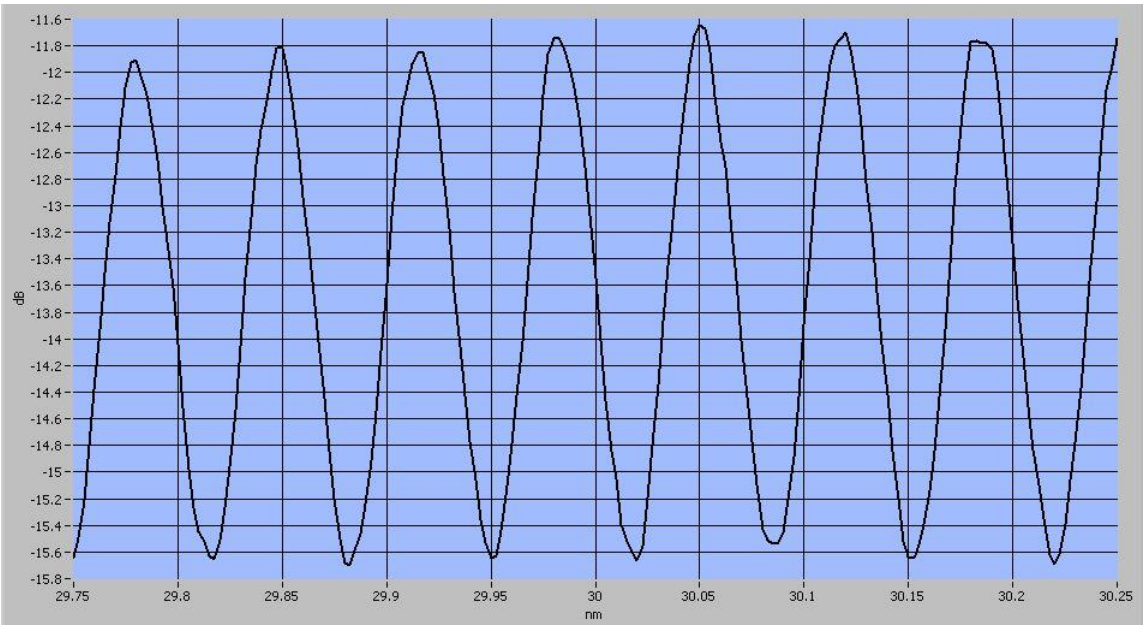

Fig. 74 Measured Reference FFPI Signal Only at 1550 nm

The baseline reference FFPI reflection, Figure 71, has an Insertion Loss Ratio of 8 dB but with the WDMs, Figure 74, the Ratio is reduced to 3.7 dB so the WDMs significantly reduce the Insertion Loss Ratio.

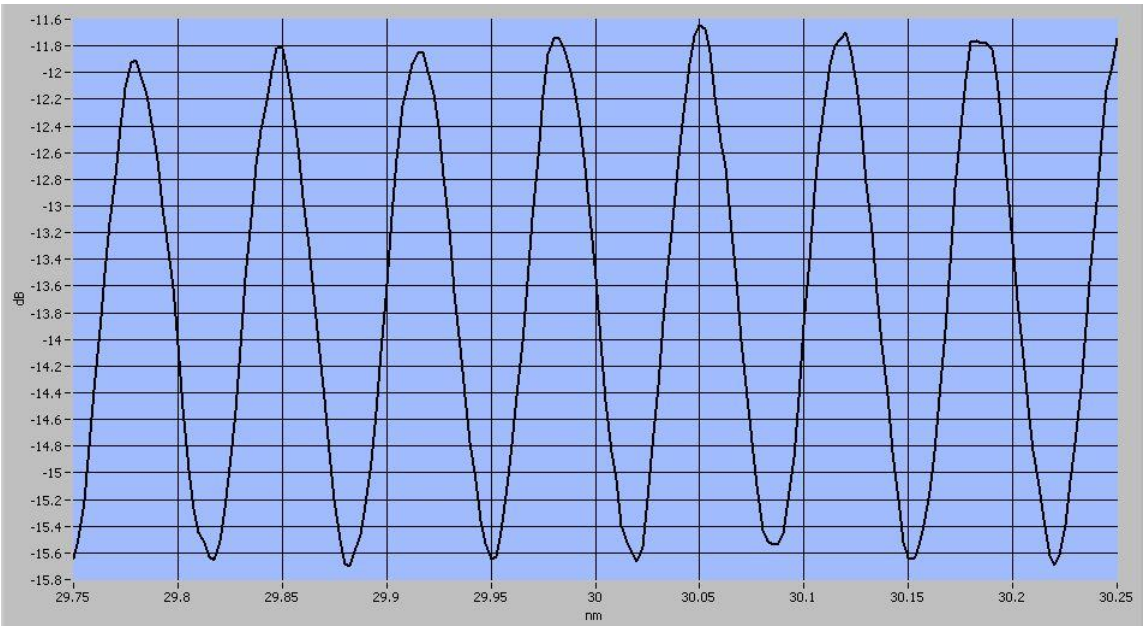

Fig. 75 Measured Reference FFPI 10 dBm Pump and Signal Centered at 1550 nm

With the 10 dBm pump added, the reference FFPI Insertion Loss, Figure 74, ranges from -11.8 to -15.6 dB, a ratio of 3.8 dB, compared with signal only Insertion Losses. Figure 75, of -12.1 to -15.8 dB, a ratio of 3.7 dB.

The pump power was detected at -51.3 dB, but when corrected it corresponds to -28.2 dB. To factor out the pump power, the two power levels need to be subtracted

nominally using the formula: Corrected Insertion Loss = $10\log_{10}\left(10^{IL/10} - 10^{Pump/10}\right)$, where IL is the minimum or maximum insertion loss and Pump is the correct pump power.

Using the corrected Insertion Losses, -11.9 and -15.8 dB, the Insertion Loss ratio becomes 3.9, which is an increase of 0.2 dB.

Note that the measurements of signal only have no pump power, and therefore cannot be corrected with respect to pump power.

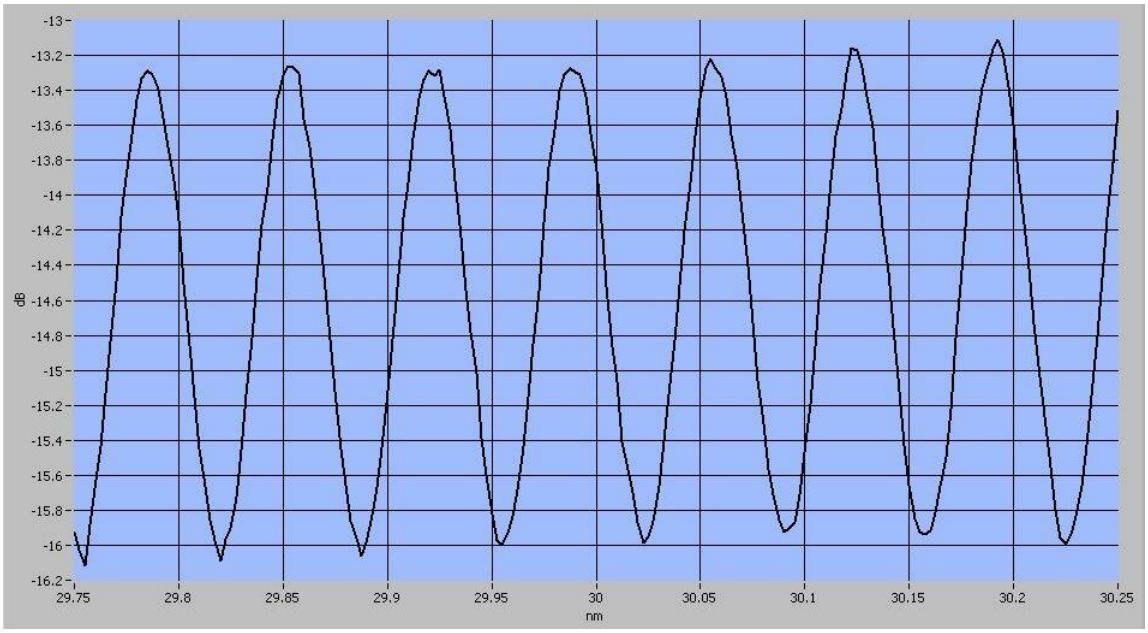

Fig. 76 Measured Reference FFPI 16.5 dBm Pump and Signal Centered at 1550 nm

With the 16.5 dBm pump added, the reference FFPI Insertion Loss, Figure 76, ranges from -13.2 to -16.0 dB, a ratio of 2.8 dB. The pump power for Reference FFPI at 16.5 dBm was measured at -44.5 dB, but it corrects to -21.3 dB. Corrected for this, Insertion Loss ranges from -13.9 to -17.5 dB, a ratio of 3.6. Compared with signal only Insertion Loss Ratio of 3.7 dB, from Figure 74, this is a decrease of 0.1 dB.

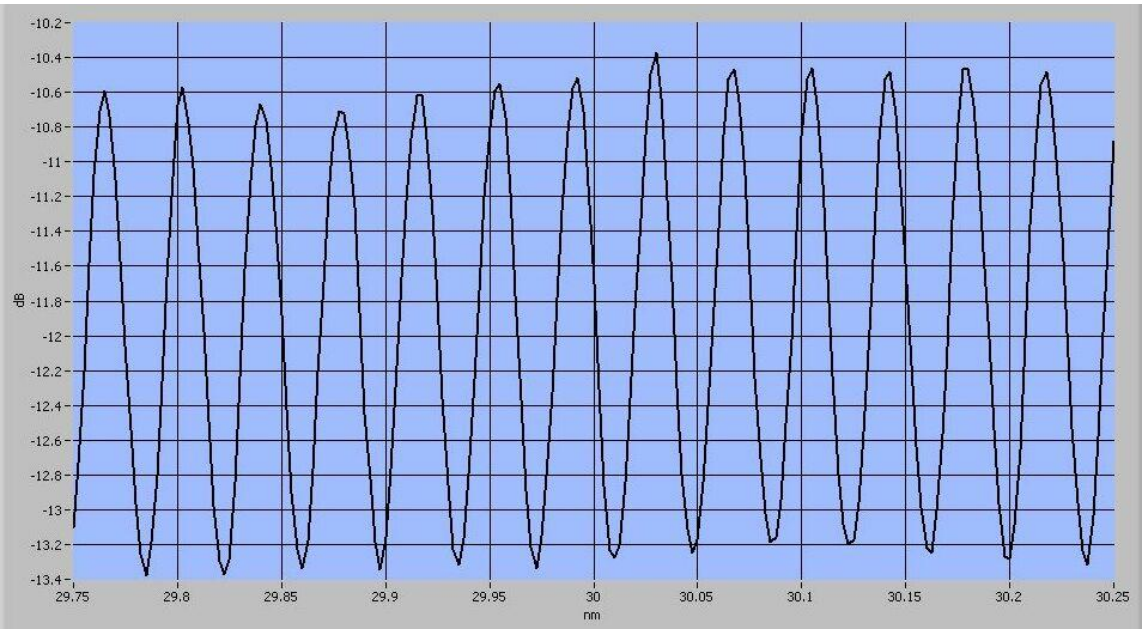

Fig. 77 Measured EDFFPI Signal Only at 1550 nm

The Insertion Loss Ratio is reduced by WDMs since the baseline measurement, Figure 72, has a ratio of 5.5 dB for but in Figure 77 Insertion Loss varies from -10.5 to -13.3 dB, 2.8 dB. Regardless, the EDFFPI reactions with the pump will be compared against the measurements without a pump, not the baseline measurements.

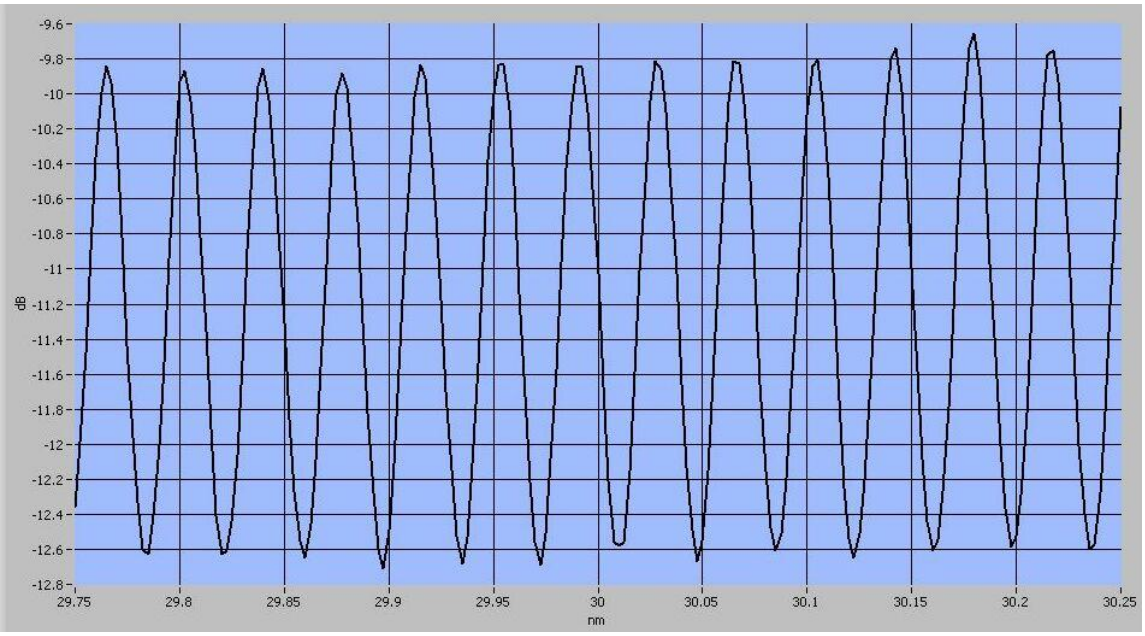

Fig. 78 Measured EDFFPI 10 dBm Pump and Signal Centered at 1550 nm

With the 10 dBm pump added, the EDFFPI Insertion Loss, Figure 78, ranges from -9.8 to -12.6 dB, a ratio of 2.8 dB. The pump power for EDFFPI at 10 dBm is measured at -41.7 dB, but it corrects to -19.2 dB. Corrected, Insertion Loss ranges from -10.3 to -13.7 dB, a ratio of 3.4. Compared with signal only Insertion Loss Ratio, from Figure 77, of 2.8 dB, this is an increase of 0.6 dB.

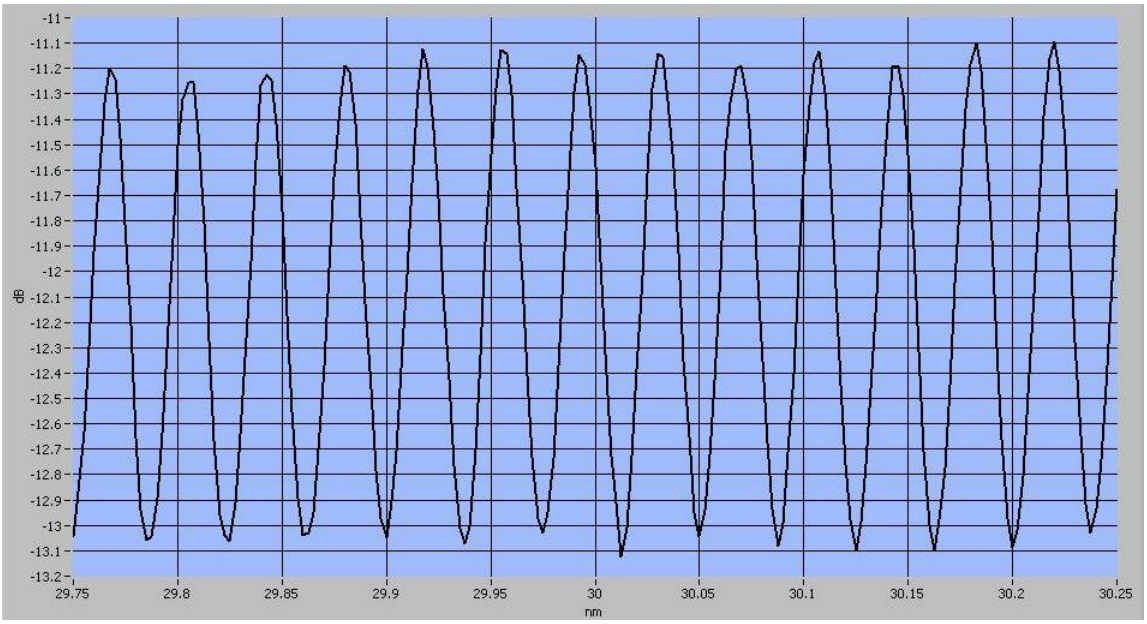

Fig. 79 Measured EDFFPI 16.5 dBm Pump and Signal Centered at 1550 nm

With the 16.5 dBm pump added, the EDFFPI Insertion Loss, Figure 79, ranges from -11.1 to -13 dB, a ratio of 1.9 dB. The pump power for EDFFPI at 16.5 dBm is measured at -38.6 dB, but it corrects to -15.3 dB. Corrected, Insertion Loss ranges from -13.2 to -16.9 dB, a ratio of 3.7. Compared with signal only Insertion Loss Ratio, from Figure 77, of 2.8 dB, this is an increase of 0.9 dB.

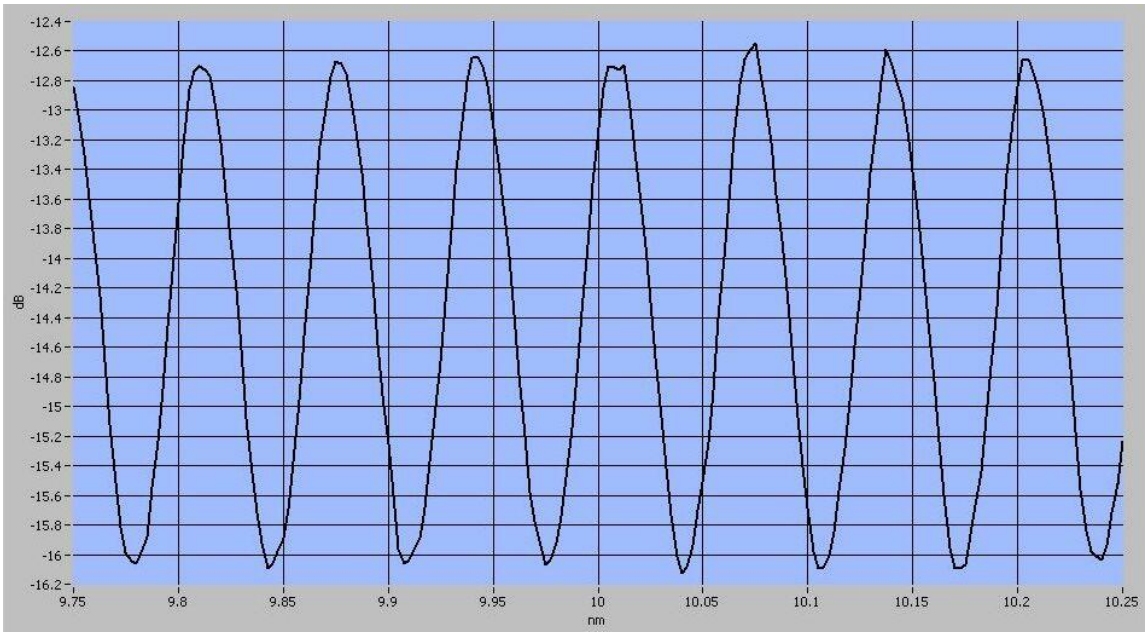

Fig. 80 Measured Reference FFPI Signal Only at 1530 nm

Figure 80 shows that at 1530 the Insertion Loss goes from -12.7 to -16.1 dB, a ratio of 3.4 dB.

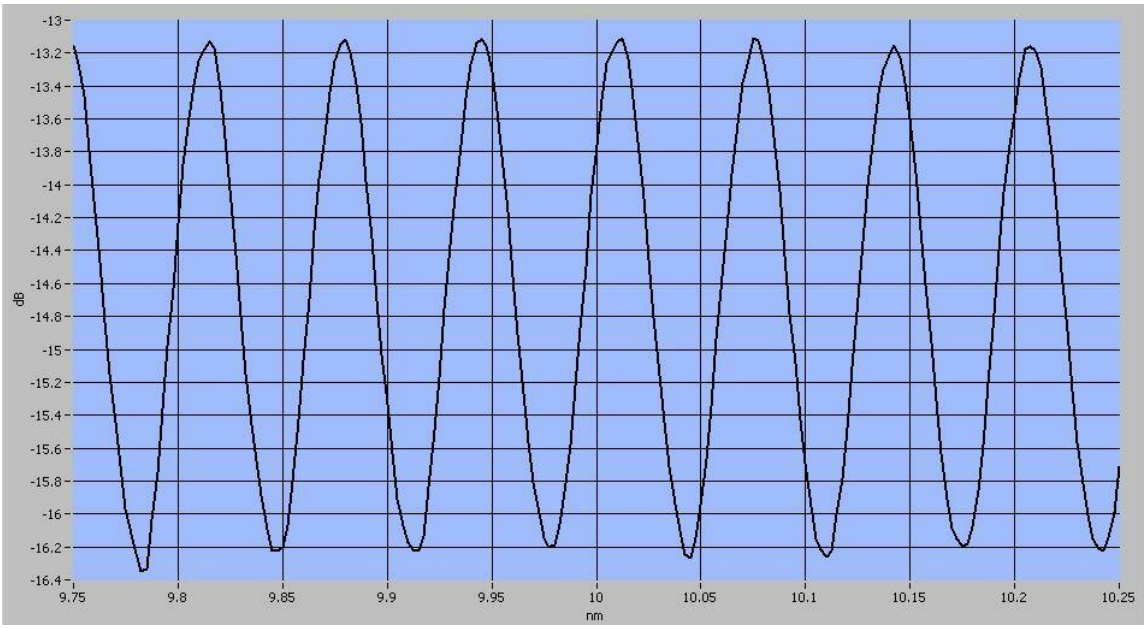

Fig. 81 Measured Reference FFPI 10 dBm Pump and Signal Centered at 1530 nm

With 10 dBm pump added, the reference FFPI Insertion Loss, Figure 81, ranges from -13 to -16.2 dB, a ratio of 3.2 dB, but when corrected, Insertion Loss ranges from -13.1 to -16.5 dB, a ratio of 3.4. Compared with signal only Insertion Loss Ratio, from Figure 80, of 3.4 dB, this stays the same.

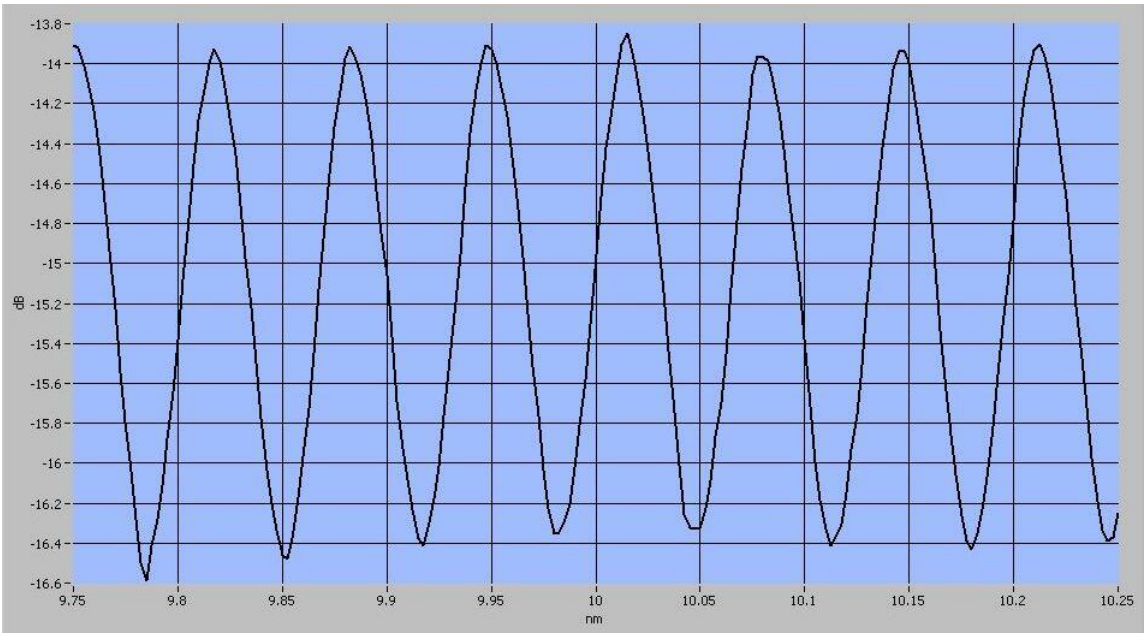

Fig. 82 Measured Reference FFPI 16.5 dBm Pump and Signal Centered at 1530 nm

With the 16.5 dBm pump added, the reference FFPI Insertion Loss, Figure 82, ranges from -13.9 to -16.4 dB, a ratio of 2.5 dB, but when corrected, Insertion Loss ranges from -14.7 to -18.1 dB, a ratio of 3.4. Compared with signal only Insertion Loss Ratio, from Figure 80, of 3.4 dB, this stays the same.

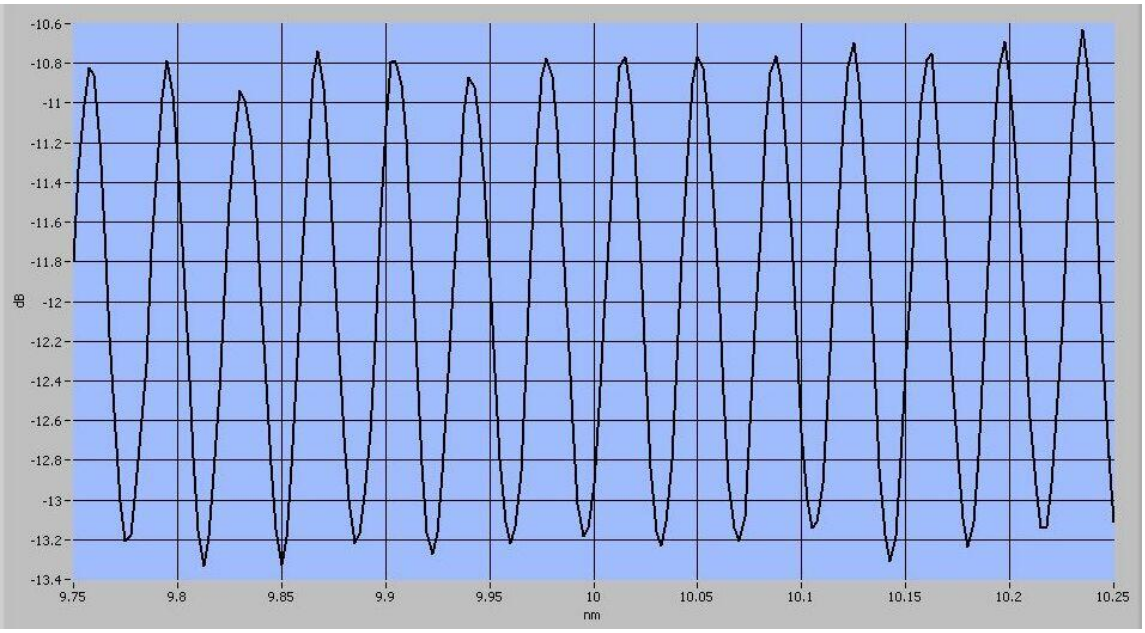

Fig. 83 Measured EDFFPI Signal Only at 1530 nm

Figure 83 shows that at 1530 the Insertion Loss varies from -10.8 to -13.2 dB, a ratio of 2.4 dB.

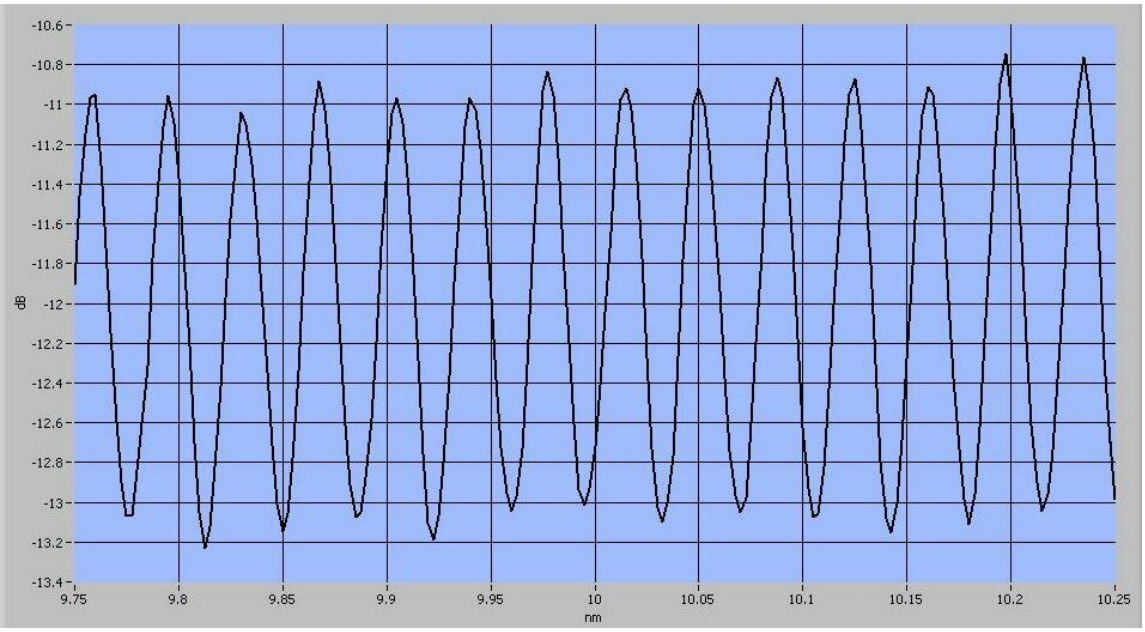

Fig. 84 Measured EDFFPI 10 dBm Pump and Signal Centered at 1530 nm

With the 10 dBm pump added, the EDFFPI Insertion Loss, Figure 84, ranges from -10.8 to -13.0 dB, a ratio of 2.2 dB, but when corrected, Insertion Loss ranges from -11.5 to -14.2 dB, a ratio of 2.7. Compared with signal only Insertion Loss Ratio, from Figure 83, of 2.4 dB, this is an increase of 0.3 dB.

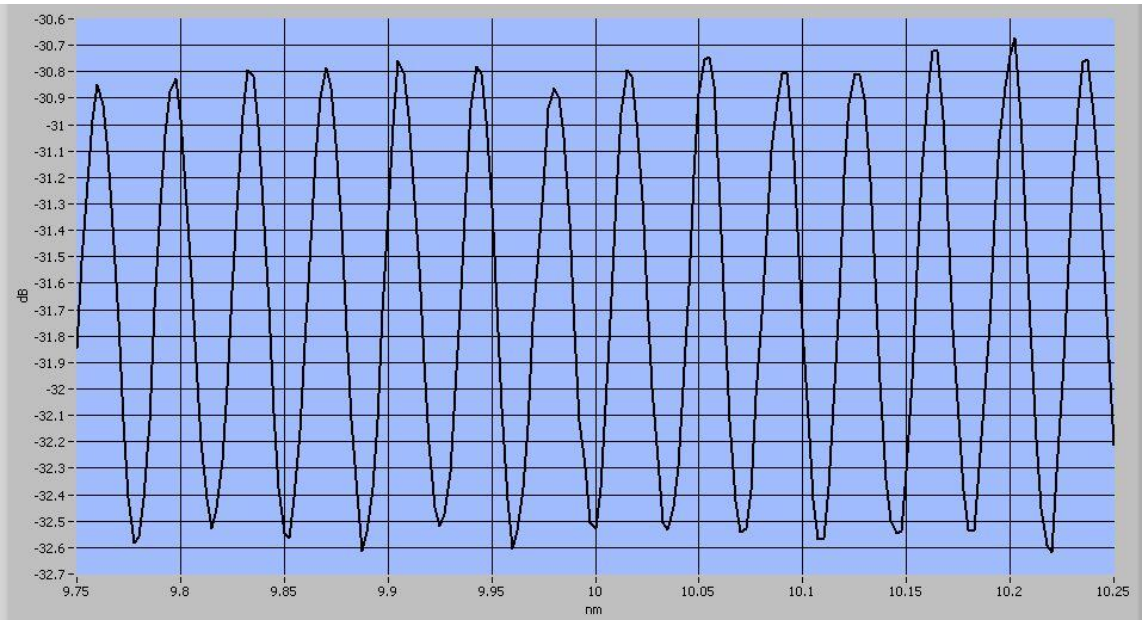

Fig. 85 Measured EDFFPI 16.5 dBm Pump and Signal Centered at 1530 nm

With the 16.5 dBm pump added, the EDFFPI Insertion Loss, Figure 85, ranges from -11.4 to -13.2 dB, a ratio of 1.8 dB, but when corrected, Insertion Loss ranges from -13.7 to -17.4 dB, a ratio of 3.7. Compared with signal only Insertion Loss Ratio, from Figure 83, of 2.4 dB, this is a decrease of 1.3 dB.

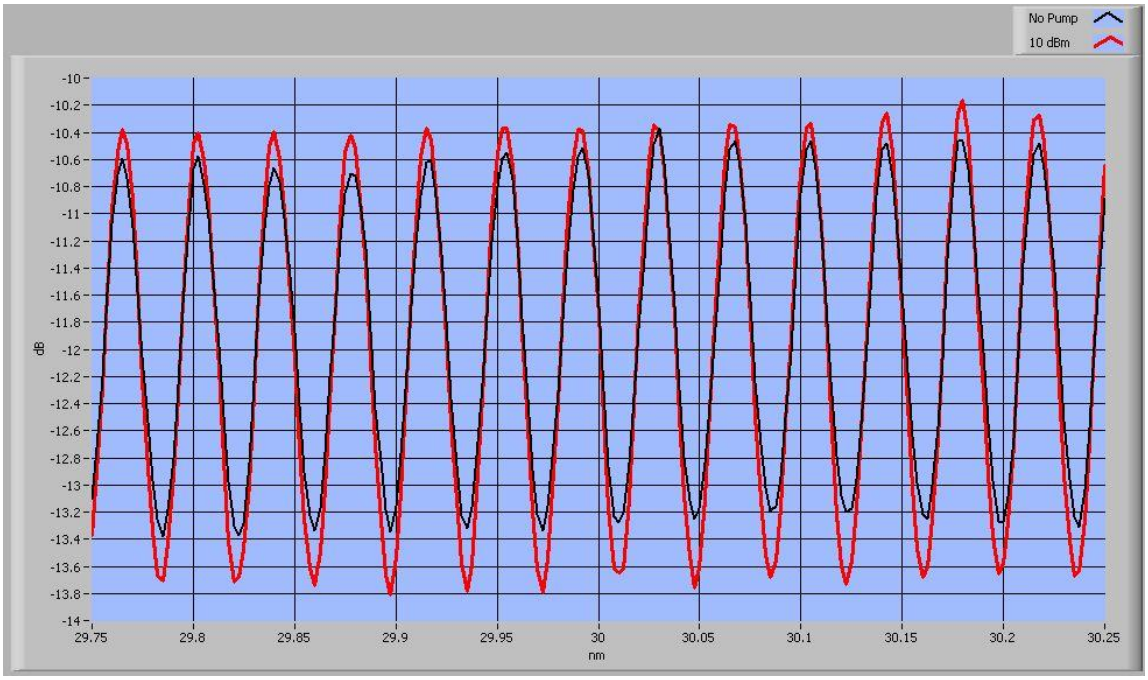

Fig. 86 Comparison of EDFFPI No Pump Power vs 10 dBm at 1550 nm

Figure 86 shows how pump power noise floor distorts the waveform and compares the EDFFPI signal only waveform with the 10 dBm pump power waveform.

Table 1 Table Of Results

		Reference FFPI			EDFFPI		
λ	Pump Power	IL Min (dB)	IL Ratio (dB)	Ratio Improvement	IL Min (dB)	IL Ratio (dB)	Ratio Improvement
1550 nm	None	-12.1	3.7		-10.5	2.8	
	10 dBm	-11.9	3.9	**0.2**	-10.3	3.4	**0.6**
	16.5 dBm	-13.9	3.6	**-0.1**	-13.2	3.7	**0.9**
1530 nm	None	-12.7	3.4		-10.8	2.4	
	10 dBm	-13.1	3.4	**0**	-11.5	2.7	**0.3**
	16.5 dBm	-14.8	3.4	**0**	-13.7	3.7	**1.3**

Table 1 offers two distinct conclusions to be drawn from the Finisar measurements. First, there is no correlation between average signal power level and pump power. Signal power level depends more on the reflectivity of the mirrors in the FFPI. The more reflective EDFFPI has a power level centered near -12 dB. The reference FFPI which is less reflective centered near -14 dB. However, a pump power increase does not correlate to a shift in either direction. Second, the Insertion Loss Ratio stays relatively unchanged for the reference FFPI. However, the Insertion Loss Ratio of the EDFFFPI increases as pump level does.

CHAPTER VI

CONCLUSION AND APPLICATIONS

In efforts to improve the signal to noise ratio and reflected power of a FFPI, Erbium doped fiber is inserted in the cavity of the sensor. It is hoped that the gain from the Erbium will develop a better sensor. Calculations confirm that the Insertion Loss Ratio can increase up to 1.3 dB with pumping, however difficulties separating pump and signal wavelength skew the measured results. High levels of pump power are chosen due to results from computer simulations, but future efforts may provide better results with a higher signal power and lower pump power levels. This combination could prevent the pump power floor from seriously altering the signal and also reduce the need for additional WDMs, which by themselves altered the signal strength and Insertion Loss Ratio.

When an optimal combination of pump power, signal power and filter use is discovered, the EDFFPI has potential to become a very important sensor. Often multiple FFPIs are driven by a single laser signal source. Thus, increasing the reflection can provide a significant advantage. Also, it can provide filtering abilities like modulating waveforms without directly applying heat or strain to the sensor.

REFERENCES

[1] G. P. Agrawal, *Fiber-Optic Communication Systems*. New York: Wiley-Interscience, 2002.

[2] J.C. Palais, *Fiber Optic Communications*. Upper Saddle River, NJ: Prentice Hall, 2004.

[3] E. Hecht, *Optics*. New York: Addison-Wesley Longman, Limited, 2001.

[4] F. L. Pedrotti, Leno M. Pedrotti, and Leno Pedrotti. *Introduction to Optics*. Upper Saddle River: Prentice Hall, 2006.

[5] J.S Lee, "Fiber optic hydrophone sensor arrays using low reflectance internal mirrors," M.S. thesis, Texas A&M University, College Station, 1998.

[6] T. Bae, "Fiber Optic Sensing Technology For Measuring In-Cylinder Pressure in Automotive Engines" Ph.D. dissertation, Texas A&M University, College Station, 2006.

[7] X. Fang and Richard O. Claus, "Polarization-independent all-fiber wavelength-division multiplexer based on a Sagnac interferometer," *Opt. Lett*. 20, 2146-2148 (1995)

[8] A.A.M. Saleh, Jopson, R.M.; Evankow, J.D.; Aspell, J., "Modeling of gain in erbium-doped fiber amplifiers," *Photonics Technology Letters, IEEE* , vol.2, no.10, pp.714-717, Oct 1990.

[9] C.R. Giles, and E. Desurvire, "Modeling erbium-doped fiber amplifiers," *Journal of Lightwave Technology*, vol. 9, no. 2, pp.271-283, Feb 1991

[10] Thorlabs. Tools of the Trade. Brochure. Caldwell, N.J.: Author, 2007. Catalog V 19. Thorlabs. Apr. 2007. Accessed on 17 Mar. 2009 <http://www.thorlabs.com/images/Catalog/Vol19.pdf>.

[11] Eiselt, Michael, Mark Shtaif, Robert W. Tkach, Felton A. Flood, Sergey Ten, and Douglas Butler. "Cross-phase modulation in an L-Band EDFA". IEEE Photonics Technology Letters. IEEE, Vol. 11 No. 12 Dec 1999. 1575-1577.

[12] K. Hsu, Calvin M. Miller, J. Thomas Kringlebotn, Elizabeth M. Taylor, Janet Townsend, and David N. Payne, "Single-mode tunable erbium:ytterbium fiber Fabry-Perot microlaser," *Opt. Lett*. 19, 886-888 June 1994.

[13] Shikii, Shigeru, Akira Sasaki, Mikiya Suzuki, Toru Ito, and Yukihiro Ozeki. "EDFA for SCM Transmission Systems". Oki Electric Industry Co., Ltd. Tokyo, Japan: Minato-Ku, 1996. 1-2.

[14] E. Desurvire and M. N. Zervas, "Erbium-Doped Fiber Amplifiers: Principles and Applications", *Phys. Today* 48, 56 (1995), DOI:10.1063/1.2807915

[15] G.E. Town; Sugden, K.; Williams, J.A.R.; Bennion, I.; Poole, S.B., "Wide-band Fabry-Perot-like filters in optical fiber," *Photonics Technology Letters, IEEE* , vol.7, no.1, pp.78-80, Jan 1995

[16] C. E. Lee, H. F. Taylor, A. M. Markus, and E. Udd, "Optical-fiber Fabry-Perot embedded sensor," *Opt. Lett.* 14, 1225-1227 Nov 1989.

[17] K. Lee, "Fiber fabry-perot interferometer (FFPI) sensor using vertical cavity surface emitting laser (VCSEL)," Ph.D. dissertation, Texas A&M University, College Station, 2005.

[18] C.E Lee.; Gibler, W.N.; Atkins, R.A.; Taylor, H.F., "In-line fiber Fabry-Perot interferometer with high-reflectance internal mirrors," *Journal of Lightwave Technology*, vol.10, no.10, pp.1376-1379, Oct 1992.

[19] C.E. Lee, R.A. Atkins and H.F. Taylor, "Performance of a fiber-optic temperature sensor from –200 to 1050 °C, " *Optic Letters*, vol. 13, pp 1038-1040, November 1998.

VITA

Justin Keith Taylor received his Bachelor of Science degree in electrical engineering from Texas A&M University in 2006. He entered the Photonic Signal Processing program at Texas A&M University in January 2007 and received his Master of Science degree in electrical engineering in May 2009. His research interests include optical communication and fiber optic sensors.

Inquiries should be addressed to:

Department of Electrical Engineering

c/o Christi Madsen

Texas A&M University

College Station, TX 77843-3128